EVALUATION TECHNIQUES FOR DETERMINING DAMPING MECHANISMS ON TITANIUM PLATES

THESIS

Kyle S. Allen, Lieutenant, USAF
AFIT/GAE/ENY/05-M01

DEPARTMENT OF THE AIR FORCE
AIR UNIVERSITY

AIR FORCE INSTITUTE OF TECHNOLOGY

Wright-Patterson Air Force Base, Ohio

APPROVED FOR PUBLIC RELEASE; DISTRIBUTION UNLIMITED

The views expressed in this thesis are those of the author and do not reflect the official policy or position of the United States Air Force, Department of Defense, or the United States Government.

AFIT/GAE/ENY/05-M01

EVALUATION TECHNIQUES FOR DETERMING DAMPING MECHANISMS ON TITANIUM PLATES

THESIS

Presented to the Faculty

Department of Aeronautics and Astronautics

Graduate School of Engineering and Management

Air Force Institute of Technology

Air University

Air Education and Training Command

In Partial Fulfillment of the Requirements for the

Degree of Master of Science in Aeronautical Engineering

Kyle S. Allen, BS

Lieutenant, USAF

March 2005

APPROVED FOR PUBLIC RELEASE; DISTRIBUTION UNLIMITED

AFIT/GAE/ENY/05-M01

EVALUATION TECHNIQUES FOR DETERMINING DAMPING MECHANISMS ON TITANIUM PLATES

Kyle S. Allen, BS
Lieutenant, USAF

Approved:

//signed//

_____ _____

Prof. Anthony N. Palazotto (Chairman) date

//signed//

_____ _____

Dr. Richard Cobb (Member) date

//signed//

_____ _____

Dr. Peter J. Torvik (Member) date

Abstract

High cycle fatigue (HCF) is the single largest cause of component failure for all modern military gas turbine engines. Hard coatings, such as magnesium aluminate spinel, have been found to provide significant damping properties. Past studies have had difficulties isolating the contributions of these hard coating damping layers from other damping mechanisms.

This study explored techniques for assessing the contribution of different damping mechanisms on titanium plates during vibration testing. The study investigated 2nd bend and 2-stripe modes. Two different specimen sizes were tested in both a clamped-free-free-free and free-free-free-free condition. Specimens were tested at varying pressures. Increases in pressure caused linear peak modal frequency downshifts for both modes of interest for both specimen sizes, and for both boundary conditions. Increases in damping were also seen with increases in pressure for bare plates for the two-stripe mode for both boundary conditions.

The clamped boundary condition contributions on the system damping were also investigated. Increases in the stiffness of the cantilevered clamp in the clamped-free-free-free condition were shown to have limited affect on plate damping.

Acknowledgments

My efforts throughout this research project were elevated by men and women of incredible intelligence tempered with patience and accommodation. Tommy George and Brian Runyon offered advice, encouragement, and unlimited guidance every day of this study. Without them, this effort would have been a fruitless journey full of far more frustrations. I can not say how much both their help and friendship has assisted me to this point in my academic career. I thank you.

My thesis committee was continually open with their guidance. Dr. Palazotto was repeatedly patient and encouraging. Dr. Cobb, you were a welcomed source of alternative reasoning. Despite your overwhelming schedule, you lent excitement to the project and performed a significant amount of data reduction. Dr. Torvik, your expertise in the field of damping is undeniable. Your intelligence is matched only by your willingness to give constructive and timely feedback. I thank you all.

Thank you Chuck Cross for sponsoring this study. The entire TEFF lab was of enormous help, especially during the fabrication of the pressure vessel. Your technical understanding and willingness to help was both needed and appreciated. Additionally, Chris Miser was helpful in the construction of the pressure vessel. He produced all of the technical drawings. I thank you.

I truly believe that all of my academic success during this study was due to the support of the people that I have met. I value you all as friends. You are all amazing people, and I am in your debt.

Table of Contents

Page

List of Figures

Figure Page

List of Tables

Table Page

THE EVALUATION OF DAMPING MECHANISMS ON TITANIUM PLATES

I: Introduction

Fatigue

High cycle fatigue (HCF) is not only the single largest cause of component failure for United States Air Force (USAF) fighter engines, but also for all modern military gas turbine engines (4). Unfortunately, failures can not be isolated to one specific type of component, engine, or even manufacturer. In 1995 an USAF committee was formed to investigate the root causes for these failures and recommend a new tack for research and development to lessen the failures due to HCF (14). This committee produced a comprehensive technology improvement plan for HCF research (6).

Fatigue is defined as the failure of material due to cyclic stress loading that is below the material's ultimate stress. Fatigue can occur under two scenarios, low-cycle fatigue (LCF) and the above mentioned high-cycle fatigue (HCF). Typically, 10,000 is the number of cycles that separates LCF from HCF (4). LCF failures have historically been overcome through the implementation of damage tolerant design requirements and retirement-for-cause philosophy. Hence, HCF now dominates as the primary cause of fatigue failure.

HCF is the consequence of mechanical vibration caused by various excitation sources. Excitation sources are generally separated into the following categories: aerodynamic excitation, airfoil flutter, and acoustic excitation (6). High vibratory responses in turbomachinery blades caused by the aforementioned categories ultimately form the basis of HCF failures. Unfortunately, efforts to eliminate the sources of excitation have proven to be impractical. Thus, efforts have been made to reduce these failures by attenuating the resonant peak responses of turbine blades.

Damping

A modal response, also named a resonant response, occurs when loading, dictated by the operational loading environment, is coincidental with the resonant frequency of the blade. Avoidance of these coincidental frequencies would thus eliminate the HCF troubles encountered (18). The implementation of this ideal is not feasible for the vast majority of loading conditions since these coincidental frequencies occur throughout the design operating envelope. To help prevent and/or lessen these HCF failures, a variety of methods have been investigated to increase damping for certain damaging modal responses.

Damping is the conversion of mechanical energy into heat (7). Damping reduces the oscillations of a material during cyclic motion. One can classify damping as either passive, active, or a hybrid of the two. Because accurate measures of system damping are difficult to determine analytically, damping properties are usually found experimentally.

Measuring the extent to which the damping mechanism limits the amplitude of peak resonance, directly measuring the energy absorption, and measuring reductions in

structural vibrations due to damping are three basic methods for determining the damping (7). The first method of measuring damping employs the use of forced harmonic vibration through base excitation. This process, commonly referred to as the half-bandwidth method, is the predominate technique for measuring damping for plate excitation.

Damping layers and dry friction dampers are two methods used to attenuate resonant peak responses within acceptable levels (18). Blade-to-ground, blade-to-blade, and shroud dampers are all examples of dry friction dampers. However, dry friction dampers have been shown to be ineffective in damping higher frequency responses. Consequently, damping layers are the most productive means for damping high frequency vibratory responses (18).

Mag Spinel Coating

Ceramic coatings are one form of passive damping layers. Ceramic materials dissipate energy through internal friction within the applied coating and between the coating and the bonded surface. Magnesium aluminate spinel ($MgO+Al_2O_3$) is a hard coating found to have significant enough damping to be of interest to the HCF community (4). It is applied to a specimen via an air plasma spray. Prior testing has shown that mag spinel is both a strain and modal dependent damping coating. The damping of the coating increases with increases in strain within the specimen. The amount of damping is dependent upon the mode of vibration the coated specimen is under. For these reasons, mag spinel is a so-called non-linear damping agent.

Second bend mode, and two-stripe or 1st chordwise, represent two modes of interest for turbine engine blade investigation. These two modes occur within the frequency range of interest to the turbine engine community. Thus, these two modes were selected as the modes of interest for all of the testing performed. The mode shape order is dependent up the geometry of the plate. For a square plate, these two mode shapes correspond to modes 3 and 4. The two mode shapes of interest are shown below Figure 1, which utilizes ANSYS® finite element modeling software. The 2nd bend mode is shown on the left and the 2-stripe mode is shown on the right.

.

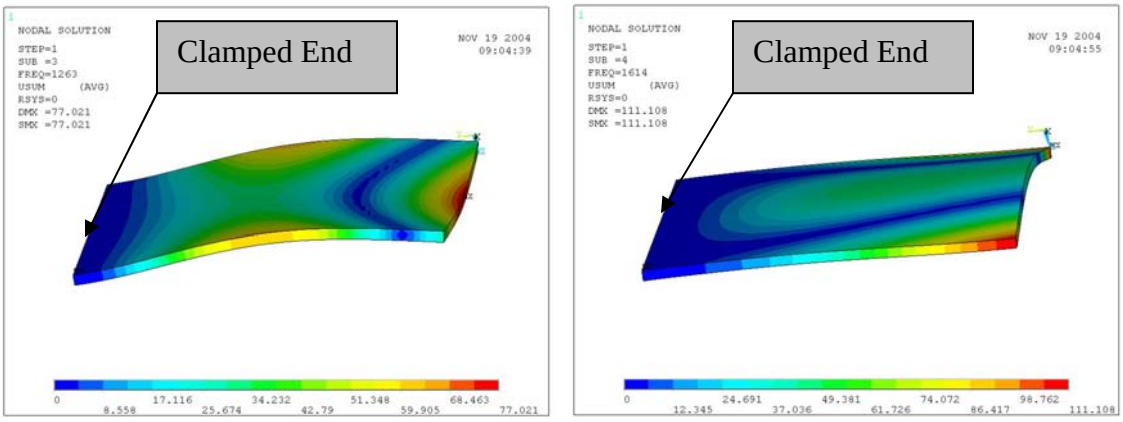

Figure 1. Mode 3 (Left) and Mode 4 (Right) for 4.5" x 4.5" x 0.125" Ti-6Al-4V Plate

Damping Mechanisms

When attempting to classify the amount of damping in a system, isolation to the particular damping mechanism is important. During typical experimentation, material damping, clamping mechanism damping, and air damping (also known as aerodynamic damping) all affect the total damping of the specimen. Air damping is the dissipation of energy into the surrounding air environment during cyclic movement (24). Few studies

have been performed to quantify this damping source and its contribution to total system damping. Dissipation of energy through the clamping mechanism is magnified by the support method. Past efforts have been made to reduce the effects of clamping mechanism damping when classifying the damping contribution of mag spinel hard coatings on titanium plates (4). However, little work has been carried out to quantify clamping mechanism damping.

Prior testing to determine damping contributions for mag spinel hard coating has yielded experimental damping results for the bare plate 4.5” x 4.5” x 0.125” geometric configuration of Ti-6Al-4V that were inconsistent with commonly accepted material values (4). Thus, other possible damping contributors need further investigation. In attempting to determine a reliable value for the damping of mag spinel hard coating, it is necessary to isolate all other possible damping mechanisms within the system. The 4.5” x 4.5” x 0.125” specimen size has been chosen for past testing because it has representative modes of current turbine blades in service.

Air Damping

Five different mechanisms are considered as contributors to air damping. The five mechanisms, axial-shear, transverse-shear, transverse-displacement, axial-displacement, and flow-induced oscillation are not all inclusive in applicability in all test scenarios (24). Each mechanism has varying contributions dependent upon the physical geometry of the specimen, the surrounding environment, and the magnitude of the oscillation. As one would expect, the properties of the surrounding medium and the amplitude of the forced vibration significantly effect the contributions of air damping.

For example, a pendulum swinging in air would be significantly more affected by the surrounding medium than a plate vibrating in a vacuum.

Analytical studies have shown that air damping is of concern for plates when classifying the damping factor (24). Specifically, it is suggested that a vacuum chamber should be incorporated when attempting to quantify the quality factor (Q) values of a damping material. It should be noted here that the damping factor (ζ) and Q have an inverse relationship. The quality factor and the damping ratio are defined later in Chapter I. Specifically, Figure 2 gives a visually representation of the Q measurement. A higher value of Q equates to a lower damping factor.

Axial-shear mechanisms are defined as the vibratory impedance forces contributed by the shear forces acting on both the surrounding medium and the oscillating specimen. This damping mechanism can cause heating of both the structure and the surrounding medium. The friction forces oppose the displacement of the specimen oscillation (24). It should be noted that the specimen's displacement is presumed to be unidirectional.

Stimulated perpendicular motions in the surrounding medium are classified as transverse-shear mechanisms. Past investigations have utilized this mechanism in the development of air film dampers. Ultimate conversion of mechanical energy into heat occurs in the both the surrounding fluid and the specimen (24). The heating of the specimen is amplified if the fluid surrounding the specimen is encapsulated. As the fluid begins to heat, the heat does not dissipate into the surrounding region. Instead, the encapsulated fluid disperses heat to the specimen via conduction. This mechanism is of concern for conditions in which the object under oscillation has openings or air gaps in

which the air is “pumped” in and out of the cavities. Air gaps, as described in the reference, are not contained in the plates under study during this investigation (24). Therefore, this mechanism was assumed insignificant for the plates within this study.

Transverse-displacement is best described as the mechanism that dissipates energy through the creation of traveling air waves running perpendicular to the oscillation of the specimen. Exactly how much energy is dissipated depends, among other things, on the confinement of the medium surrounding the specimen. For example, if the specimen is confined by a pressure vessel, the transfer of energy through the creation of traveling waves during partial pressure or full atmosphere condition may be impacted by the response of the wave reverberations off the inner walls. However, this can be difficult to model analytically, and thus, the majority of studies have been performed using an infinite medium scenario (24).

An axial-displacement damping mechanism is of significance when the specimen’s lateral dimension is large in comparison to the displacement of the oscillations. Such is the case with the plates considered herein. Alternatively, air damping for beams, which represent long slender geometries, is dominated by an axial-shear mechanism. Essentially, the oscillating specimen may be simplistically modeled as a piston. Just as a piston would push the air, the plate creates traveling pressure waves that move parallel with the path of oscillation. However, differing from a piston, the plate does not present a uniform surface during oscillation. The surface area is dependent upon the mode shape. For this study modes 3 and 4, shown above in Figure 1, represent the modes of interest. Of interest is the observation that the two-stripe mode (mode 4)

presents out of phase oscillations (referencing free end tips to free end center) that could affect the influence of this mechanism (24).

Flow-induced oscillation completes the list of mechanisms that contribute to air damping. This mechanism is only of interest when considering specimens with air flow over its surface (i.e. this is not of interest for testing in motionless air). Dependent upon the flow condition, this interference mechanism can either dissipate energy away from the specimen in the form of damping, or increase oscillation amplitude, thus transferring energy from the surrounding medium to the specimen. Although of interest in the final application, this mechanism was not investigated during this study. All surrounding medium were assumed to be either stationary or of such small velocities to negate their effects (24).

Damping Characterization

To better understand the quantitative contributions of a damping mechanism, it is necessary to pick a method for defining the total amount of damping within a system. Multiple methods exist for quantifying damping. The half-power bandwidth method is one method for quantifying damping.

The half-power bandwidth method measures the change in amplitude over a frequency range. As a sine sweep is performed, the response of the specimen is recorded. The variations in velocity are then compared to the frequency at which they occurred. Figure 2 is a physical representation of the half-power bandwidth method (12).

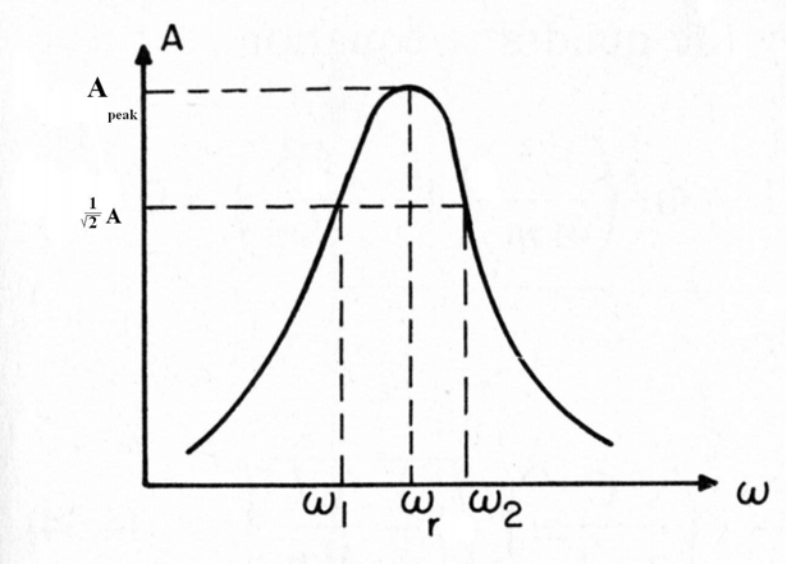

Figure 2. Half-Power Bandwidth Method (12)

The frequency at which the peak frequency occurs is labeled ω_r. The lower and upper frequencies are represented by ω_1 and ω_2, respectively. These are the points at which the amplitude of the excited specimen reaches a magnitude of .707 of the maximum. From these values the damping ratio is then calculated, as shown below.

$$\zeta = \frac{\Delta\omega}{2\omega_r} \quad \textbf{(1)}$$

where

ζ = damping ratio
$\Delta\omega$ = bandwidth ($\omega_2 - \omega_1$)
ω_r = resonant frequency

The quality factor (Q) is often used within the damping community to describe the amount of damping within a system. The damping ratio and Q are inversely related. Thus, an increase in damping is represented by a decrease in the Q value. The relationship is shown below.

$$\mathbf{Q} = \frac{1}{2\zeta} \tag{2}$$

Some sources also refer to the loss factor (η) as an evaluation of the system damping name (4). For reference, the loss factor relationship to damping ratio and quality factor is shown below.

$$\eta = 2\zeta = \frac{1}{Q} \tag{3}$$

Strain Relationships

Finite element analysis (FEA) reveals stress, strain, and displacement relationships at different locations on the plate for different modes. Using FEA results, locations of maximum strain are found and numeric relationships between maximum strain and displacements at the measurement location are determined. The velocity-strain relationships for both modes are linear and are shown for the bare square plate specimen below in Figure 3.

The point of maximum strain is different for modes 3 and 4. For mode 3, the location of the maximum strain occurs at the center of the root of the specimen. For mode 4, the maximum strain occurs at the center of the tip of the specimen. However, in this study, the velocity is measured .1" from the plate tip and .7" from the side of the plate. For this reason a relationship is developed between measured velocity and the maximum strain for each mode. The relationship gives a relative strain for a given displacement.

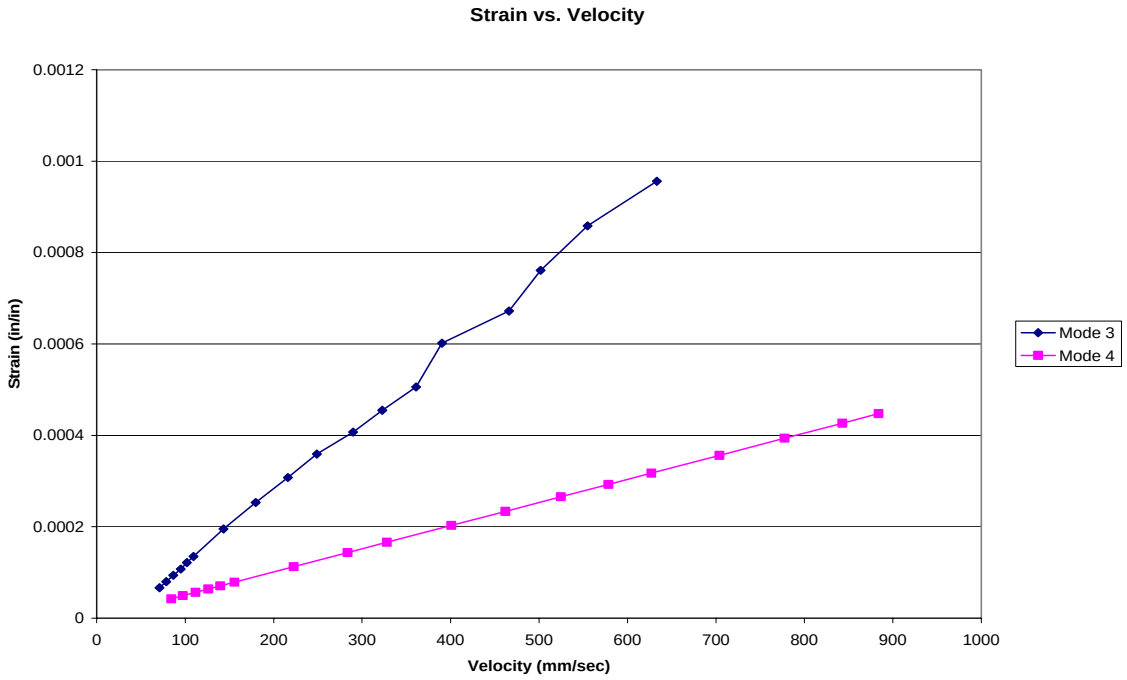

Figure 3. Strain vs. Velocity for Modes 3 and 4

It should be noted that the coated specimen has the same mode shape as the uncoated specimen. For this reason, all strain relationships derived for the bare plate can also be applied to the coated plate to define interface strain.

The laser vibrometer used during testing measured the velocity of the plate. Using the relationship given below, one can then derive the displacement of the tip (4).

$$\delta = \frac{v}{\omega} \qquad \textbf{(4)}$$

where

δ = displacement
v = measured velocity
ω = frequency, in radians/sec

It is also important to understand the units of the frequency. The below equation relates *f*, given in Hertz (cycles/sec), and ω, given in radian/sec. The results in this study are given in Hertz. It is necessary to convert to ω in order to determine the maximum strain.

$$f = \frac{\omega}{2\pi} \tag{5}$$

The maximum strain during a sine sweep test occurs at the largest tip velocity. Hence, all maximum strains are found at the resonant peak of the sine sweep performed. In this investigation, strain was proportional to displacement. Therefore, one can determine the maximum strain for a given velocity at the tip of the plate during the resonance. Using the strain-displacement relationship derived from FEA code, the maximum strain is found. Past strain gauge testing performed by Blackwell verified the strain-displacement relationship used in this study (4).

Finally, all percent differences shown throughout this study are given using the relationship shown below.

$$\%\ \text{Diff} = \frac{HighValue - LowValue}{HighValue} * 100\% \tag{6}$$

Related Work

Several attempts have been made to quantify hard coatings' damping contributions in various geometric configurations. A magneto-mechanical coating has been shown to dramatically increase the damping of a Hastelloy X beam (18). In

addition, mag spinel hard coating has also been shown to attenuate forced peak modal frequency responses (18). Non-linear responses corresponding to increasing forced inputs have shown a decrease in peak frequency response for beams. This decrease clearly showed strain dependence for the mag spinel coating (18).

Testing has revealed that there is an optimization process necessary in order to find the most beneficial application of the mag spinel coating to specimen. Spraying distance, spraying angle, substrate temperature, and coating rate all affected the damping characteristics of mag spinel hard coating (16). Variations in applications methods caused differences of greater than 60% change in damping rates.

Analytical attempts to classify the damping properties of mag spinel using modeling and simulations have yielded varying results. While general trends for the coating characteristics and analytical results were found to be similar, certain frequency and amplitude levels were difficult to model. In addition, dependence on specimen type yielded errors in experimental versus analytical results. Difficulties in modeling strain-dependent coatings lead to significant variations in measured values (15). The analytical model only attempted verification for one mode, the 2^{nd} flexural mode (15). Thus, significant advances in analytical models are needed before accurate damping properties can be derived without significant experimentation.

The most applicable prior testing, performed by Blackwell, found that for 4.5” x 4.5” x 0.125” Ti-6Al-4V mag spinel coated specimens showed strain softening, defined as the decrease in modal frequencies with increase in strain, with increasing forced base excitation. Shen found similar results (18). Results from Blackwell’s testing indicated an increased Q value of 16% and 63% for modes 3 and 4, respectively, at 10 micro-strain

and 31% and 82% for modes 3 and 4, respectively, at 500 micro-strain. All damping increases were found by comparing the responses of bare plates to mag spinel coated plates (4). Unfortunately, bare plate testing yielded inconsistent material damping values perceived as high by the HCF turbine engine test community (4). Thus, values of increased material damping for mag spinel coating were found to be unreliable. It should be noted that the same undamaged specimens used during the Blackwell investigation were used for this study.

Early experimental studies in air damping determined that air damping contributions dominated over other damping mechanisms for specimens with relatively large area to mass ratios, such as thin plates (20). Air damping as large as one magnitude greater than structural contributions resulted. Air damping displayed a linear dependence on pressure and a non-linear dependence on amplitude of oscillation (20). In accordance with these findings, Baker et. al also found that air damping had a drag force proportional to dynamic pressure for transversely vibrating thin beams (2). Decrements of free decay (another measure of air damping) for the beams were shown to be a function of the air density of the surrounding medium.

Analytical studies of the vibration of plates examined the modal frequencies for varying plate geometries under varying pressures and surrounded by varying mediums. Barton found that the frequency shifts for a plate of close approximate dimensions to this study displayed a 3% frequency downshift for mode 3 when changing from a vacuum to 1 atmosphere condition (10). A near zero degree phase shift was found for mode 4 (10).

Finally, recent experimentation performed by Tarnopolsky, et. al attempted to classify damping of oscillating plates in flows parallel to the direction of displacement.

The experiment used only bare brass plates of extremely small dimensions that simulated the oscillation seen during frequency resonances of reeds in woodwind instruments. Again, it was found that aerodynamic damping (air damping) of plates in stationary air varied linearly with absolute pressure. However, it was seen that the air damping contribution was small in comparison to the material damping of the brass specimens. In addition, vibrating specimens in moving air flow at one atmosphere saw air damping vary linearly with flow velocity (20).

Objective of Thesis

The objective of this investigation was to experimentally determine the effect of air damping and the clamping condition damping on Ti-6Al-4V test specimens during vibration testing. Air damping quantification was undertaken by comparing the responses of uncoated titanium plates under varying pressures. The experiment isolated the 2nd bend mode and 2-stripe mode for two specimen sizes. The first, a 4.5” x 4.5” x 0.125” specimen in a free-free-free-clamped condition, included both a mag spinel coated plate and an uncoated plate. The second, a 4.5” x 9.5” x 0.125” in a free-free-free-free condition, will include only an uncoated plate. The investigation quantified the influence of air pressure and the clamped boundary condition on the resonant response of the titanium plates.

Current Approach

This section gives a broad overview of the testing that occurred. Chapter III delineates the exact procedures for all testing. Chapter IV then examines the results of this testing.

This investigation compared the responses of mag spinel coated and uncoated titanium plates under varying pressures. The plate geometry was initially chosen to approximate the aspect ratios of modern turbine engine blades within the compressor section (4). In addition, comparisons between prior testing were needed. Thus, the same undamaged specimens used during Blackwell's testing were utilized during this investigation.

Two experimental setups were used in determining the effects of air damping on the system damping. The electrodynamic shaker testing investigated modes 3 and 4 (2^{nd} bend, 2-stripe) for a square plate in a clamped-free-free-free boundary condition. The magnet excitation section of testing studied similar mode shapes as the shaker testing for a rectangular plate. These similar mode shapes corresponded to modes 4 and 7 for a larger specimen in a free-free-free-free boundary condition. The specimen specific geometries are shown below in Figure 4 and Figure 5 for the two test setups.

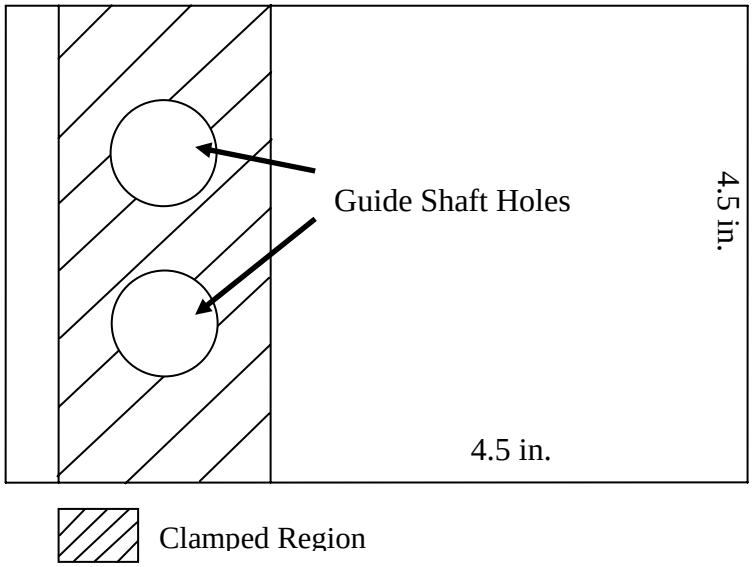

Figure 4. 4.5” x 4.5” x 0.125 Ti Test Specimen

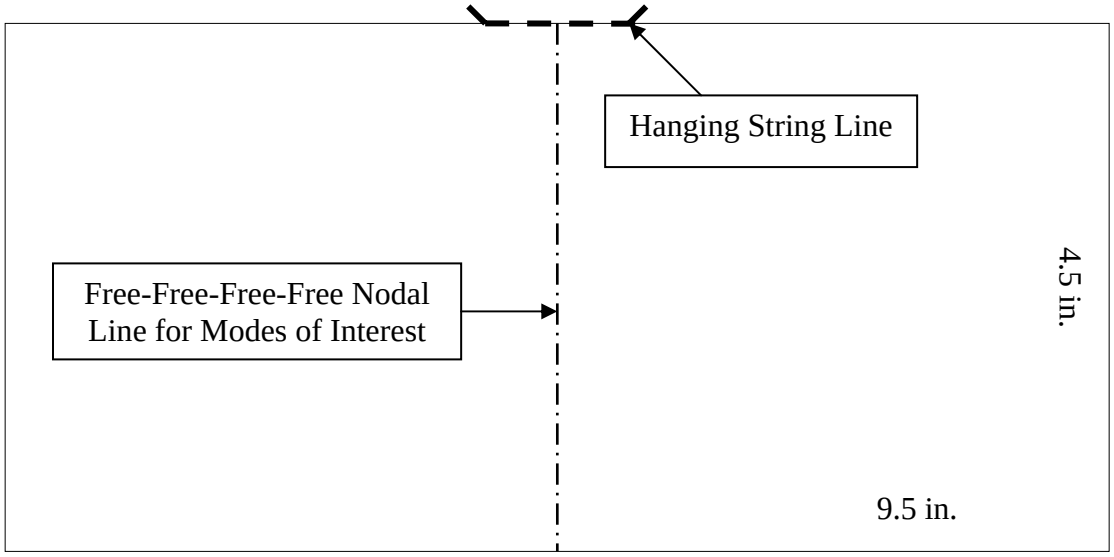

Figure 5. 9.5” x 4.5” x 0.125” Ti Specimen

The first test setup consisted of a 4.5” x 7” x 0.125” in Ti-6Al- 4V specimen secured between blocks and placed on an 18,000 lb electrodynamic shaker located in the Turbine Engine Fatigue Facility (TEFF). The effective test section was 4.5” x 4.5” x 0.125” for this free-free-free-clamped condition and will be referred to as such for the remainder of study. The constraint blocks created a cantilevered boundary condition

similar to the operating conditions within a gas turbine engine. A pressure vessel built to attach to the shaker head was then utilized to alter the atmospheric condition surrounding the specimen. Varying pressures were implemented in order to isolate the effects of air damping for both the coated and uncoated specimens. This setup is shown below in Figure 6.

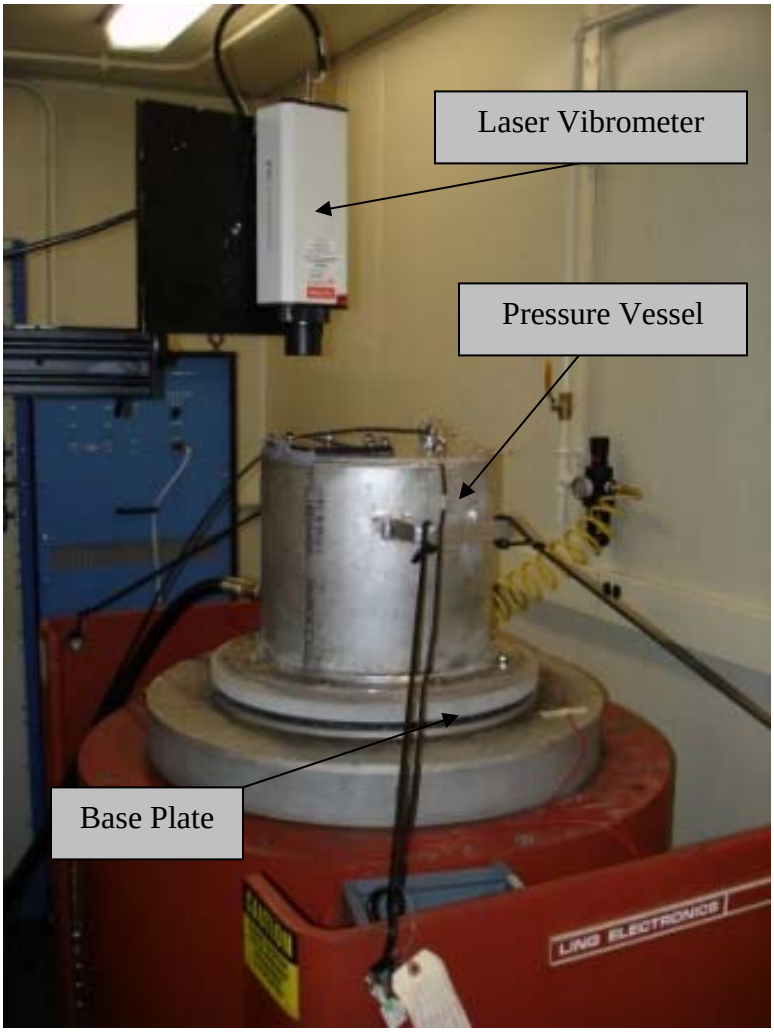

Figure 6. Test Setup for Shaker Head Testing

The specimen was then subjected to sinusoidal frequency down sweeps at constant base excitations. The surrounding pressure was then altered and the specimen was again subjected to identical loading conditions. A laser vibrometer was used to

accurately measure the velocity of the specimen tip. The damping was determined using the half-power bandwidth method for this section of testing. Values for peak strain were determined with the aid of finite element modeling. Testing used both the coated and uncoated plates. This testing was conducted at the Turbine Engine Fatigue Facility, AFRL/PRTS, Wright-Patterson AFB, OH. A more in-depth description of this testing is given in Chapter III.

In an effort to eliminate the possible effects of boundary restraint damping, a free-free-free-free setup was used for a 9.5" x 4.5" x 0.125" Ti-6Al-4V bare specimen. This size was chosen in order to more accurately demonstrate the same mode shapes as was seen for modes 3 and 4 excitation for the 4.5" x 4.5" x 0.125" specimen. Finite element models were used to verify mode shapes for both specimen sizes. Additionally, a scanning laser vibrometer was used to verify the finite element modeling for the 4.5" x 9.5" x 0.125" specimen. See the results of plate modeled using the finite element program ANSYS® in Figure 7 below.

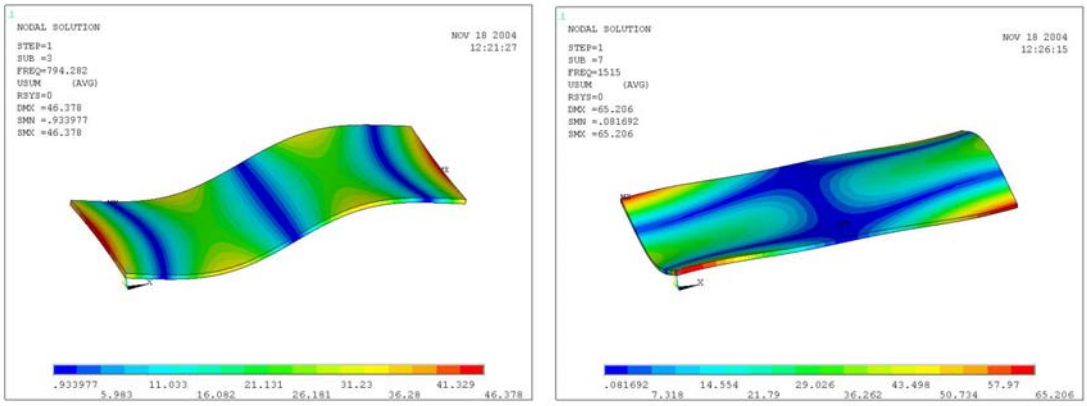

Figure 7. Mode 4 (Left) and Mode 7 (Right) for 4.5" x 9.5" x 0.125" Ti-6Al-4V Plate

During the free-free-free-free condition, a center node line formed during plate excitation that simulated a perfectly constrained cantilevered condition. Thus, the boundary condition damping was essentially eliminated. The specimen was hung on a string that was taped to the top edge of the specimen and secured inside a pressure vessel approximately 6 ft. in height and 3 ft. in diameter. This testing included only one bare plate specimen. A coated plate was not used during this section of testing. Magnetic tip excitation was used to excite the modal frequencies of interest (2^{nd} bend and 2-stripe). The excitation levels applied to the specimen were very low, and hence the measured strains were low. This test setup is shown below in Figure 8.

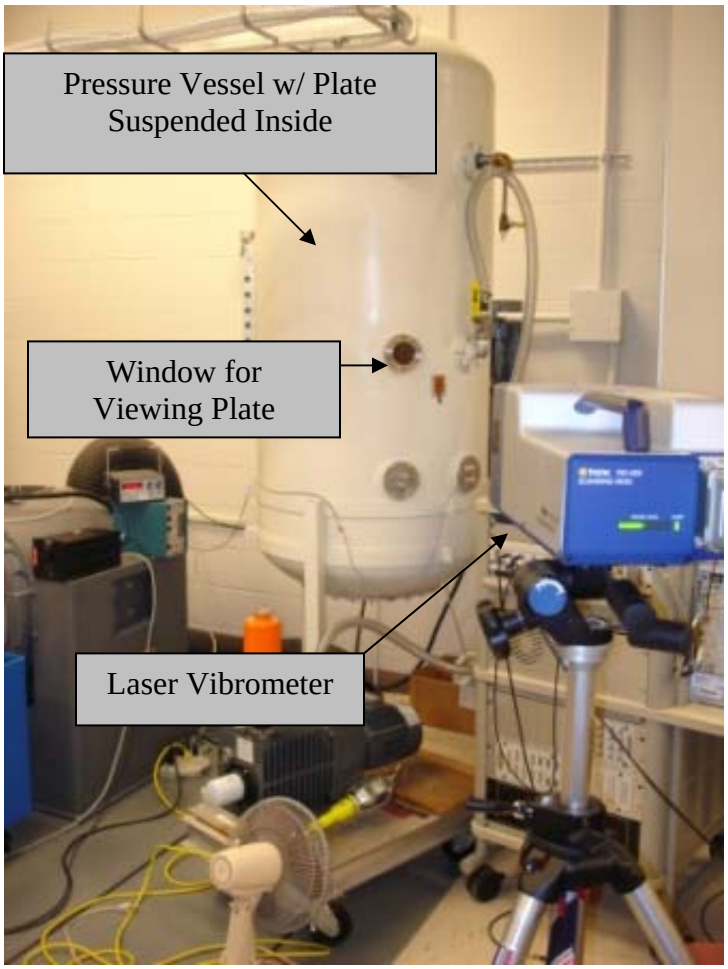

Figure 8. Test Setup for Magnet Testing

Similar to shaker head testing, the specimen was subjected to varying excitations at varying pressures. The damping for the bare plate was determined using an Eigensystem Realization Algorithm (ERA) (5).

All free-free-free-free testing was performed in the Aeronautics Lab at the Air Force Institute of Technology (AFIT) on Wright-Patterson Air Force Base (WPAFB), Ohio.

II: Finite Element Analysis and Pressure Vessel Design

This chapter evaluates the modal natural frequencies for the bare titanium specimens. In addition, it was necessary to design and fabricate a pressure vessel and a base plate that could be used for partial pressure testing with the electrodynamic shaker. This chapter details both the fabrication and analysis for the pressure vessel and the base plate.

Test Specimens

The testing included three test specimens, two of which had the same geometry. The uncoated and coated Ti-6Al-4V specimens are shown below in Figure 9. The specimens were 4.5" x 7" x 0.125" Ti-6Al-4V annealed plates. The effective section was 4.5" x 4.5" x 0.125". The excess was used to secure the plate within the test fixture. A 0.5 in. tail overlapped the backside of the test fixture during testing. The two plates studied were labeled TI (coated) and T4 (bare). These specimens were used prior during Blackwell's testing. Blackwell performed further exact dimension measurements (4).

All test specimens were cut from the same piece of 0.125 in. titanium sheet using a 55,000 psi water jet. The mag spinel coating was applied to both sides of the plate using an air plasma spraying process in which the mag spinel powder is applied to the substrate (Ti-6Al-4V plate) using a high temperature plasma gas (4). The mag spinel coating formed a material thickness layer of 0.01 in. on each side of the plate.

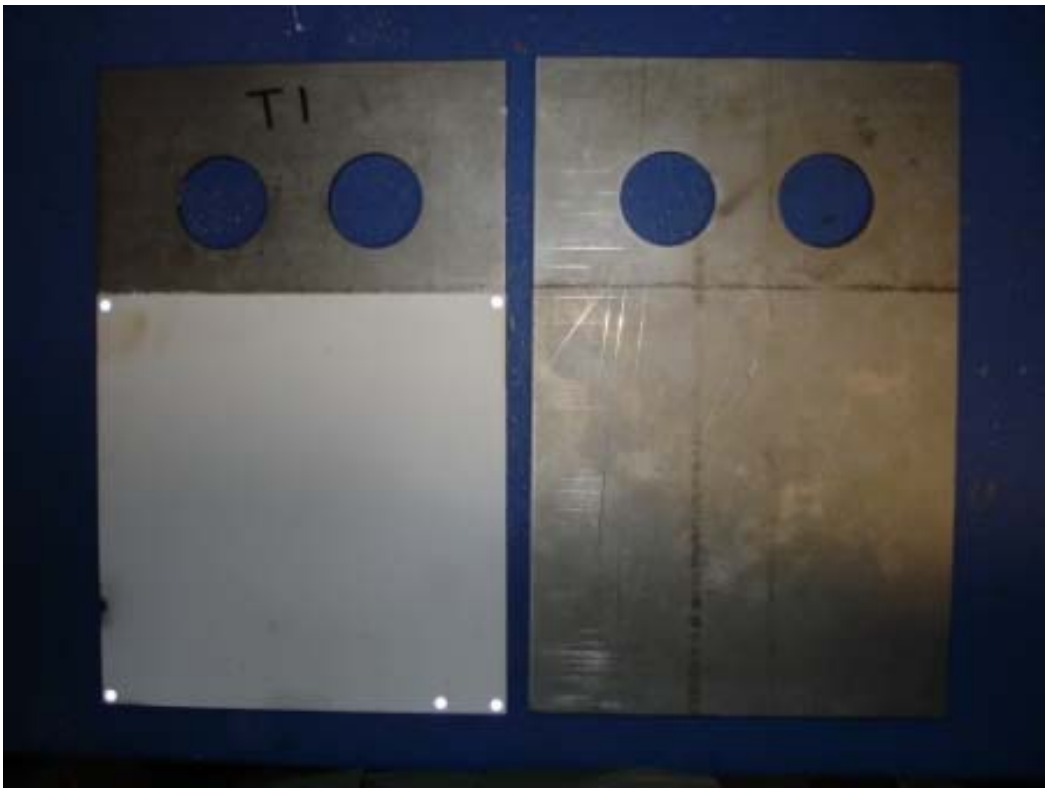

Figure 9. Coated (Left) and Uncoated or Bare (Right) Ti-6Al-4V 4.5” x 4.5” x 0.125” Specimens

The second test specimen, the free-free-free-free test configuration in Figure 10, was again cut from the same sheet of titanium as the first two samples. The specimen measured 4.5” x 9.5” x 0.125”.

Figure 10. 4.5” x 9.5” x 0.125” Uncoated Ti-6Al-4V Plate

Finite Element Analysis

Plates subjected to cyclic loading condition oscillate. The magnitude and shape of the oscillation of the plate vary dependent upon the frequency of the loading condition. The peak of these oscillations will occur at certain frequencies. The frequencies that correspond to these peaks are referred to as the natural modal frequencies, or simply modal frequencies. There exist multiple ways for determining the modal frequencies of a system.

One modal frequency is differentiated from another by the corresponding physical shape a specimen forms when excited at that resonant frequency. These shapes are defined by the node lines around which the plates translates. The plate oscillation about these node lines is reduced by a damping force. At minimum, the specimen will have

some inherent damping within the material. This material damping is minimal for bare specimens. The node lines for the first five modes of a square plate in a clamped-free-free-free condition are shown below in Figure 11.

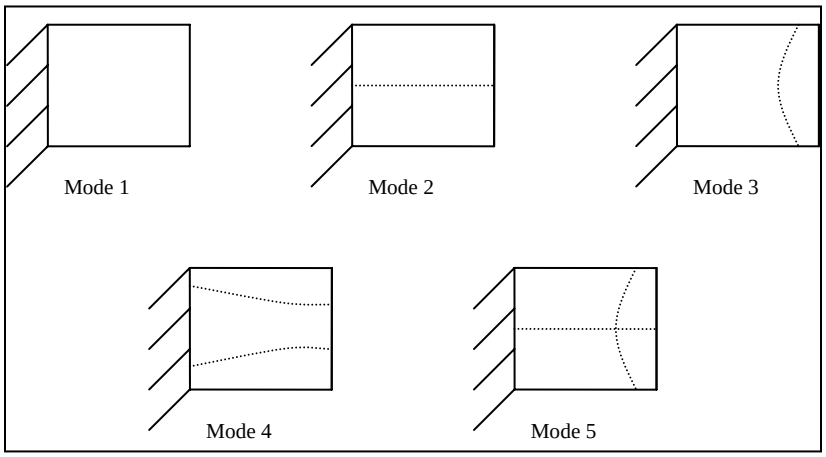

Figure 11. Node Lines for Square Plates in Clamped-Free-Free-Free Condition (4)

Titanium Plate Modeling

For the purpose of this investigation, finite element modeling was chosen as one method for determining the modal frequencies. All FEA done utilized the software program ANSYS®. ANSYS® also functioned as both a pre and post processor.

All test specimens were cut from the same sheet of Ti-6Al-4V. The actual square bare specimen had an average thickness of 0.127". The 9.5" x 4.5" x .125" bare specimen had an actual average thickness of 0.1265". However, the nominal value of 0.125" for thickness was used for all finite element modeling. This difference in nominal versus actual thickness values could cause slight differences in modal frequencies for the model versus the actual testing. Table 1 depicts the material property values used for the finite element code.

Table 1. Material Properties for Ti-6Al-4V (MIL-HDBK-5CD-ROM)

Property	Ti-6Al-4V
Modulus of Elasticity (E)	1.65×10^7 lb/in^2
Poisson's Ratio (ν)	0.33
Density (ρ)	.160 lb/in^3

'Solid 45' elements were chosen to model the plates. Choosing appropriate element types is important in the modeling process. In this case, the plate nature of the specimen assumed was accurately modeled using a solid 8 noded brick element. The solid 45 element has nodes at each corner of the cubic shaped element. The same mesh densities were used for both geometries tested (9.5" x 4.5" x 0.125" and 4.5" x 4.5" x 0.125"). Each element had a length of .1" and a through the thickness height of .042".

Total element count was 12,825 and 6,075 for the larger and smaller specimen respectively. The total nodal count was 17,664 and 8,464 for the larger and smaller specimen, respectively. A convergence study was performed in order to ensure a sufficient amount of elements were used. The element number was doubled until there was less than a 1% change in a modal frequency between incremental models. The modal frequencies for the clamped-free-free-free plate are shown below in Table 2. All frequencies listed within this study are given in Hertz (Hz).

Table 2. 4.5" x 4.5" x 0.125" Modal Frequencies

Mode Number	Frequency (Hz)
1	207.76
2	498.62
3	1263.2
4	1613.9
5	1818.6

The first five mode shapes for the square specimen in the clamped-free-free-free condition are shown below in Figure 12. Again, the two modes of interest were modes 3 and 4. The shading denotes the relative displacement of the plate. All figures display the relative sum of the displacements in all directions. The node lines are the areas showing zero relative displacement.

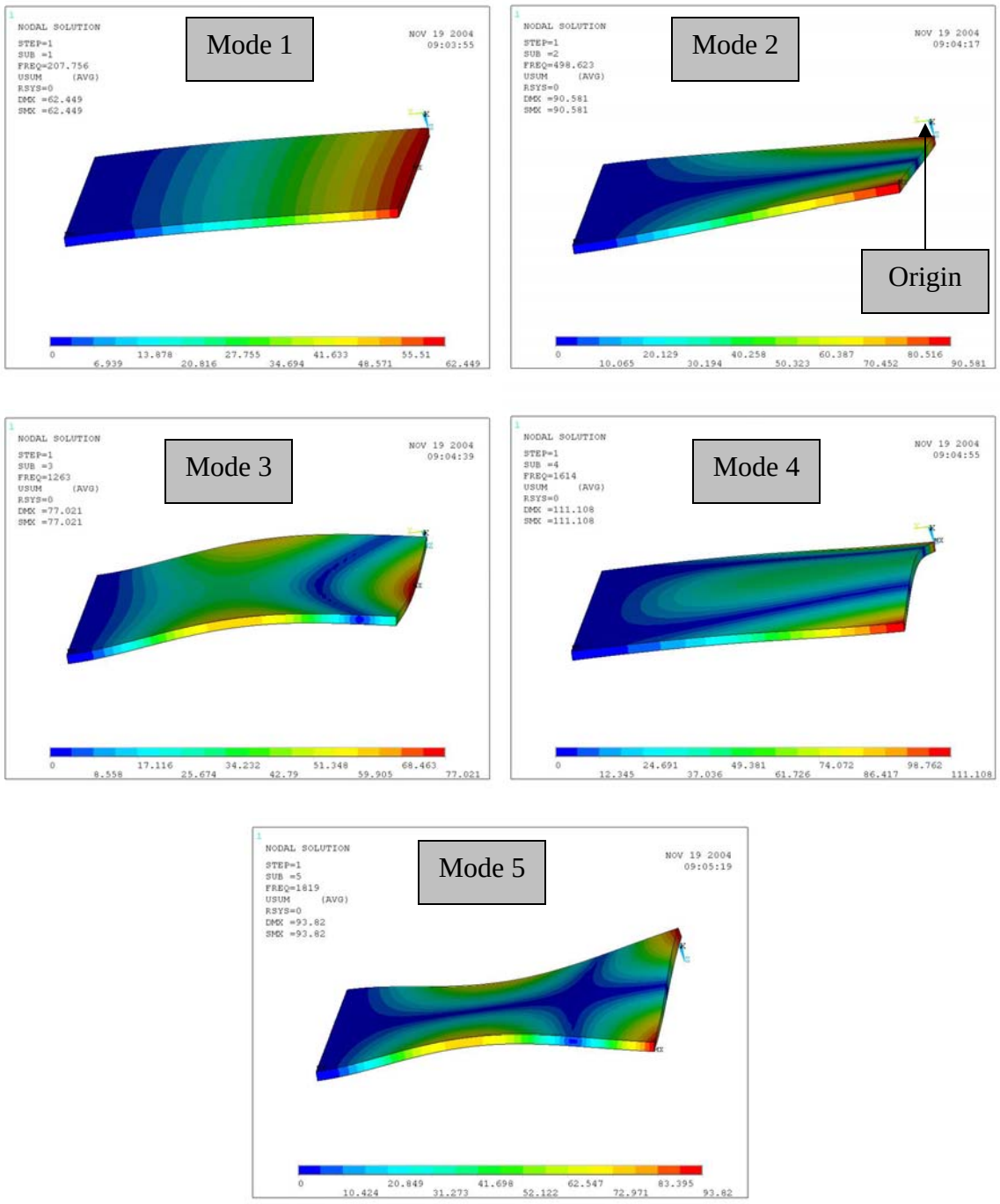

Figure 12. First Five Modes for 4.5” x 4.5” x 0.125” Plate in Clamped-Free-Free-Free Condition

The modal frequencies for the free-free-free-free plate tested are shown below in Table 3. Due to the nature of the new geometry and boundary conditions, certain modal

frequencies not prevalent in Table 2 were seen. The free-free-free-free boundary condition had additional mode shapes that were not seen in the clamped-free-free-free condition. For this reason, it was necessary to match approximate mode shapes with the mode shapes of interest. Specifically, mode 4 for the 4.5” x 4.5” x 0.125” specimen had a different mode shape than mode 4 for the 9.5” x 4.5” x 0.125” specimen.

Table 3. 9.5" x 4.5" x 0.125" Modal Frequencies

Mode Number	Frequency (Hz)
1	285.78
2	366.17
3	794.28
4	802.17
5	1303.5
6	1381.9
7	1514.7
8	1595.2

It was important to determine which modal frequencies for the larger plate had similar mode shapes to modes 3 and 4 of the smaller plate. The first eight modes for the 9.5” x 4.5” x 0.125” plate are shown below in Figure 13 and Figure 14. In this case, mode 3 (794.28 Hz) and 7 (1514.7 Hz), have roughly the same mode shapes as the 2nd bend and two-stripe for the smaller specimen, respectively.

In comparison to the square plate, additional modes were seen due to the altered boundary conditions and different plate geometry. The close proximity of modes 3 and 4 was important to note. In actual testing, the modes could reverse order. Therefore, it was necessary to verify the mode shapes before partial pressure magnet excitation testing.

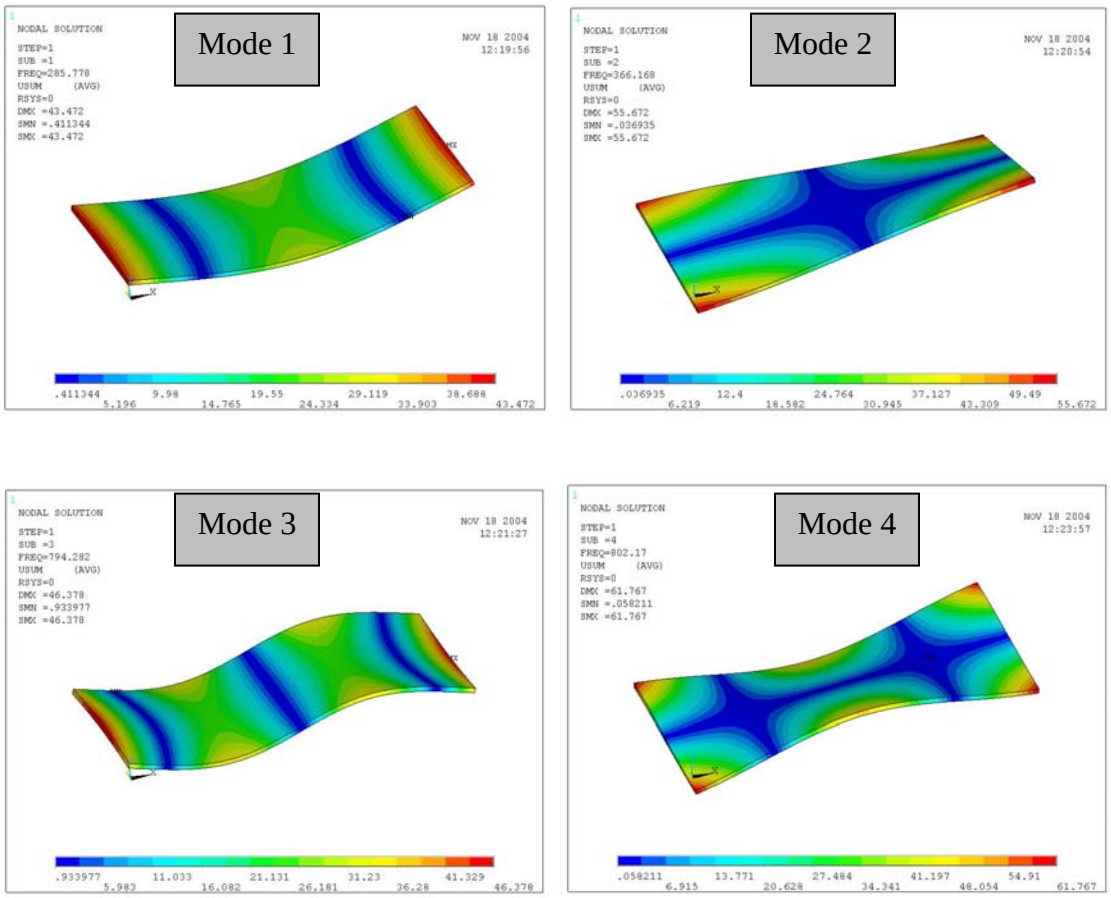

Figure 13. Modes 1 through 4 for 9.5" x 4.5" x 0.125" Plate

It is important to note, although intuitively obvious to some readers, that these modes were only the modes that fell around the frequency range of interest. In general, the range of interest was 0 - 2,000 Hz. This was true for both specimen sizes. This range was chosen in order to ensure the inclusion of the 2nd bend and two-stripe modes within the range of interest. There are many additional mode shapes that occur at higher frequencies. However, these higher and more complex mode shapes are not of interest during this study.

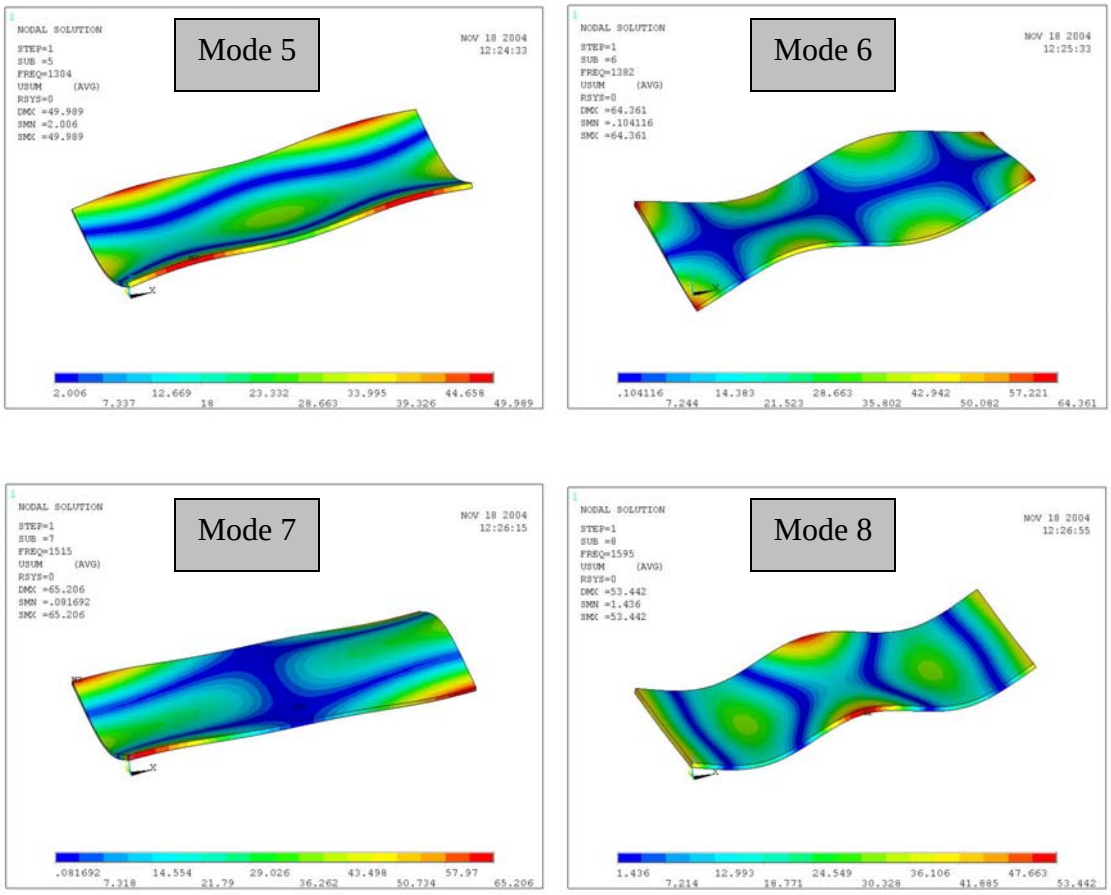

Figure 14. Modes 5 through 8 for 9.5” x 4.5” x 0.125” Plate

Modal Verification

In order to verify the mode shapes from FEA results with actual experimental mode shapes the 9.5” x 4.5” x 0.125” Ti-6Al-4V specimen was excited in a free-free-free-free boundary condition using a speaker. A scanning laser vibrometer was used to measure the deflection of the titanium plate at each modal frequency for the first eight modes. Table 4 below compares the modal frequencies predicted by the finite element modeling with the actual experimental values found during testing. The modal frequencies found during FEA match closely with experimental values. However, the close proximity caused the FEA resulting modes 3 and 4 to be crossed in comparison to

experimental testing. Mode 4 (2.71% difference) and mode 7 (1.31% difference) were the two modes of interest during this study.

Table 4. Modal Frequencies for 9.5" x 4.5" x 0.125" Titanium Plate

Mode Number	Frequency (Hz)			
	FEA	Exp Vacuum	Exp 1 Atm	% Difference (FEA vs. Vacuum)
1	285.78	293.6	292.9	2.74%
2	366.17	364.7	364.1	0.40%
3	802.17	802.1	800.7	0.01%
4	794.28	815.8	814.2	2.71%
5	1303.5	1325	1323	1.65%
6	1381.9	1392.7	1390.4	0.78%
7	1514.7	1534.5	1532	1.31%
8	1595.2	1643.4	1640.3	3.02%

The mode shapes for the titanium plate in the free-free-free-free condition are shown below in Figure 15. The modes are matched with the same mode shapes from the finite element analysis. The dark areas shown on the scanning laser vibrometer results indicate the area where the plate was suspended using tape. It is important to note that the laser vibrometer only scanned half of the plate. As one can see, the mode shapes are symmetric about the midsection.

The mode 3 from finite element analysis corresponded to the mode 4 from the experimental excitation. Mode 7 from finite element analysis corresponded to mode 7 for the experimental excitation. All references to the 2nd bend mode made within Chapter IV and V refer to it as mode 4.

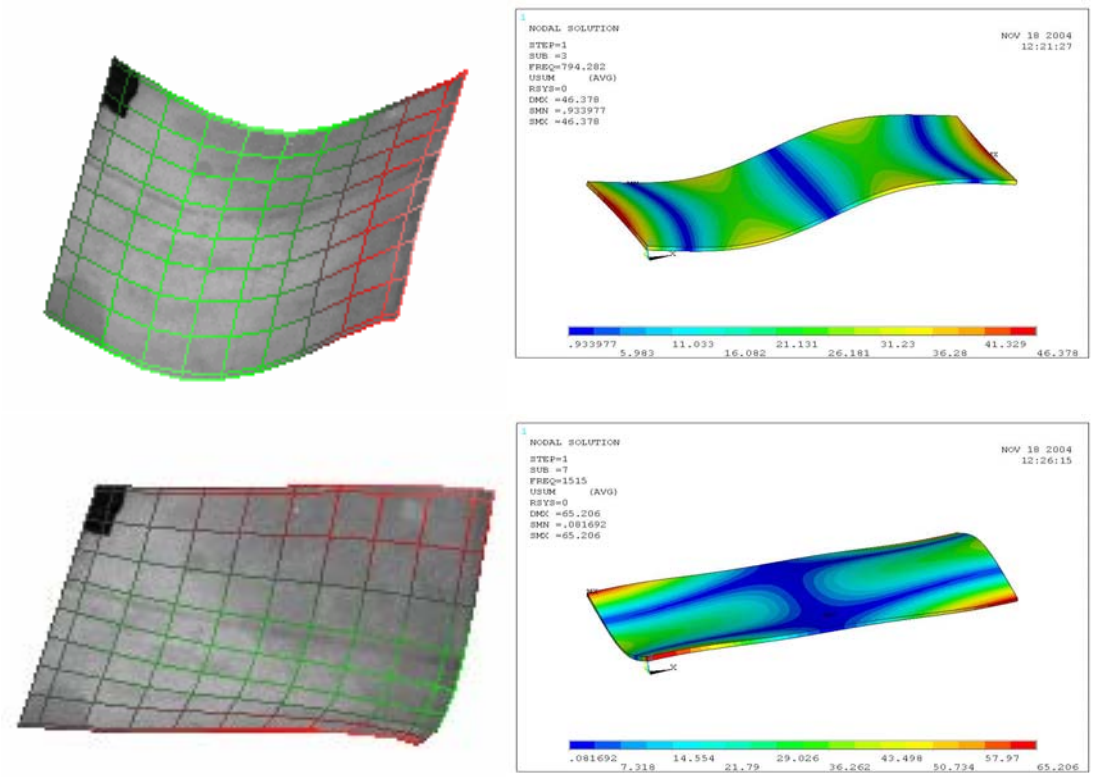

Figure 15. Laser Vibrometer and Finite Element Mode Shape Analysis

Pressure Vessel Design

The design process for the pressure vessel presented the greatest fabrication difficulties within this study. The pressure vessel was manufactured out of 6061-T6 aluminum. Total mass of the system was of primary concern. Achieving high g loads on the specimen with large masses attached to the shaker head presented difficulties. The total system, to include vessel, base plate, and blocks weighed 77 lbs.

The pressure vessel consisted of a ½" wall thickness aluminum cylinder welded to a 5/8" aluminum hoop flange, a 5/8" aluminum lid welded to the opposing end of the cylinder, and an acrylic window secured to the top of vessel via eight screws. The hoop flange secured the vessel to the shaker head for all partial pressure testing. The window

atop the cylinder was necessary for the recording of velocity data, using a laser vibrometer, during the sinusoidal down sweeps. Also atop the vessel was a rubber stopper which, when drilled, allowed for the transfer of readings (either accelerations or temperature) from partial pressures inside the vessel to the full atmosphere conditions outside the vessel. Detailed technical drawings are shown in Appendix A: Technical Drawings for Pressure Vessel.

The vessel was sealed to the shaker head using an existing 8 bolt pattern. Vacuum grease and a rubber gasket were applied between the pressure vessel and shaker head. RTV was used to seal both the rubber plug atop the vessel and the specimen viewing window. Figure 16 below demonstrates the aforementioned details.

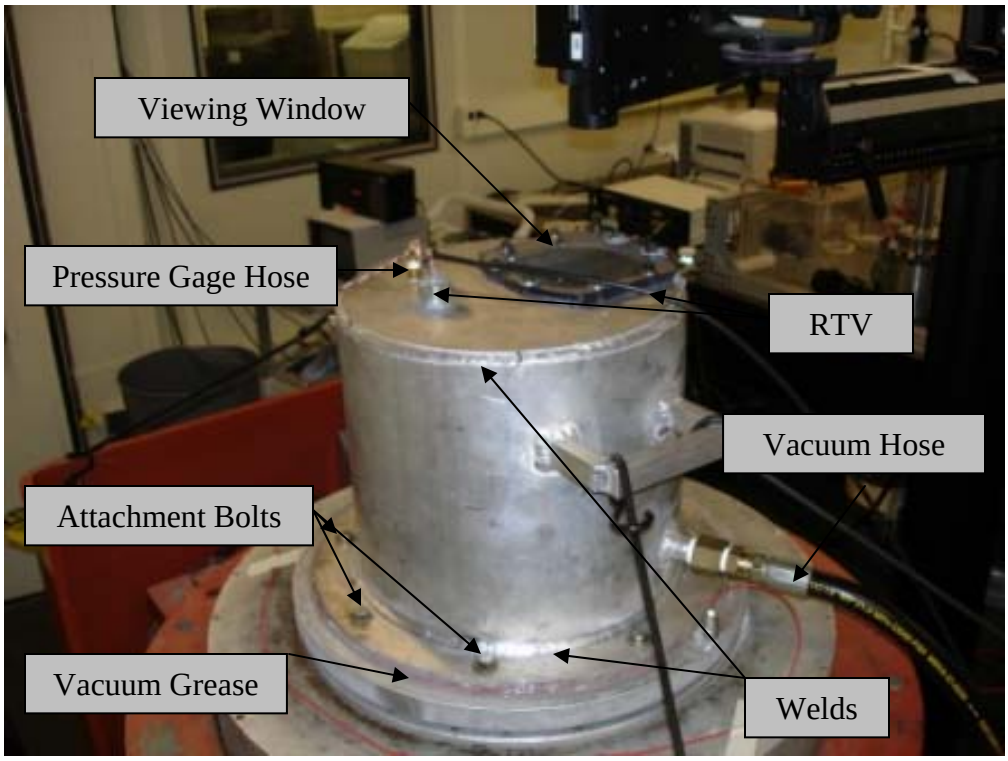

Figure 16. Pressure Vessel

One small addition occurred at the end of the design process. Welded handles were added to the vessel to aid in the movement of the vessel on and off the shaker head. Unfortunately, one modal frequency of the handles was coincidental with a plate mode. The solution for this problem is addressed further in the testing anomalies section of Chapter III.

Pressure Vessel Finite Element Analysis

This section explains the finite element analysis needed to determine the modal frequencies and mode shapes of the pressure vessel. Finite element analysis was done prior to fabrication of the pressure vessel to ensure that there were no modal interference issues between the pressure vessel and the specimen within the frequency range of interest. A top hat design, using a cylinder and bottom flange, was chosen in order to best secure the vessel to the shaker while also incorporating longitudinal stiffness of a cylinder, thus preventing longitudinal modal interference during testing. The vessel also needed to withstand near vacuum conditions.

The FEA models included a lid, viewing window, and cylinder. The models did not include the vacuum pump attachment, signal feed plug, or pressure gage attachment. The models also did not include handles, which were added at the end of fabrication. The handles did present modal interference issues.

Table 5 displays all the material properties for both the 6061-T6 Aluminum used to construct the vessel cylinder and top and the acrylic properties used for the window.

Table 5. Material Properties for 6061-T6 Al and Acrylic (11)

Property	6061-T6 Al	Acrylic
Modulus of Elasticity	1.0×10^7 lb/in^2	4.27×10^4 lb/in^2
Poisson's Ratio (ν)	0.3	0.3
Density (ρ)	.100 lb/in^3	.0403 lb/in^3

Solid 92 elements were used to model the vessel. The element has a pyramidal shape with a total of 10 nodes per element. This element was utilized because it allowed for the painless joining of circular shapes, specifically, the lid and cylinder of the pressure vessel. When modeling the pressure vessel, 19,703 elements and 39,084 nodes were used. A convergence study was performed in order to ensure a sufficient amount of elements were used. The mesh density was doubled until the modal frequency variation changed less than 1% between runs.

Multiple FEA models were run with varying geometries. For modeling purposes, it was assumed that the pressure vessel was perfectly clamped at the base. The base was assumed to be perfectly rigid. Restrictions on the electrodynamic shaker dictated that the mass of the vessel was of major concern. Thus, many refinements were made in efforts to reduce weight. Original models had a lid made completely of acrylic. FEA results showed significant deflections in the lid in the vacuum condition. These deflections were assumed to greatly affect the laser vibrometer readings. In addition, a significant amount of modal interference was found with solid acrylic lid models. Models that had thick enough acrylic lids were found to be unfeasible.

Initial studies of thinner cylinder pressure vessel designs (not shown here) yielded interfering modes. The modes of interference had axial deflections in their mode shapes. These axial deflections were thought to dramatically effect the sine sweep testing. For

this reason, the walls of the vessel were thickened and thus, the pressure vessel became more rigid. Further finite element analysis was performed. Only the final design of the vessel is shown within this document. The FEA results are shown below in Table 6.

Table 6. Pressure Vessel Modal Frequencies

Mode Number	Frequency (Hz)
1	577.33
2	935.64
3	1120.3
4	1123.2
5	1167.6
6	1398.8
7	1466.1
8	1621.6
9	1658.2
10	1674.6

It was found that the bare plate specimens that would be tested with this pressure vessel had modal peaks of interest (Mode 3 and Mode 4, shown in Table 2) at approximately 1263 and 1614 Hz. For this reason, the mode shapes of the vessel were important for identifying possible interference issues. As one can note from the aforementioned table, there exist a few potential interference frequencies of interest. Specifically, modes 9 and 10 fall very close to the two-stripe mode for the square plate. Below, Figure 17 demonstrates possible interfering modes. The figure corresponds to modes 5, 6, 8, and 9 from the above table.

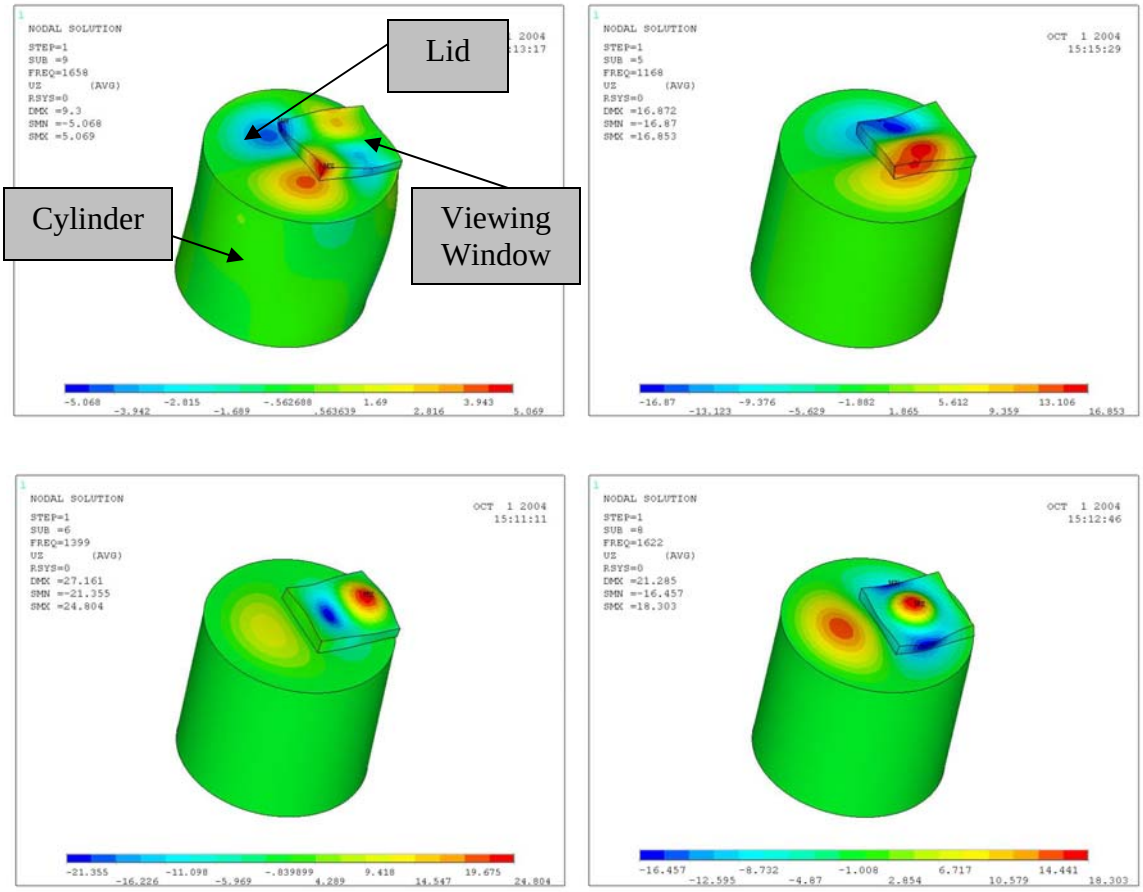

Figure 17. Four Modes of Interest for the Pressure Vessel

The figure shows the mode shapes of the vessel by displaying the displacement sum. Thus, it indicates the places of greatest deflection for the mode shape. As one can see, the cylinder section of the vessel remains rigid. Great deflections in the cylindrical section of the vessel may have posed difficulties during testing. However, motion isolated to the lid section was not expected to cause interference issues. All pressure vessel mode shapes in the frequencies range of interest (below 2,000 Hz) showed deflections isolated to the lid of the vessel similar to Figure 17. The cylinder section of the vessel was extremely stiff. Therefore, all deflections associated with the cylinder

section were seen at frequencies much greater than 2,000 Hz and thus, were not of concern for this study.

Additionally, the stress and deflection of the vessel under maximum pressure was of interest. Near vacuum conditions would induce approximately 14.7 lb/in^2, therefore this value was used as a distributed load on all exterior vessel surfaces in a static condition. The results are shown below in Figure 18.

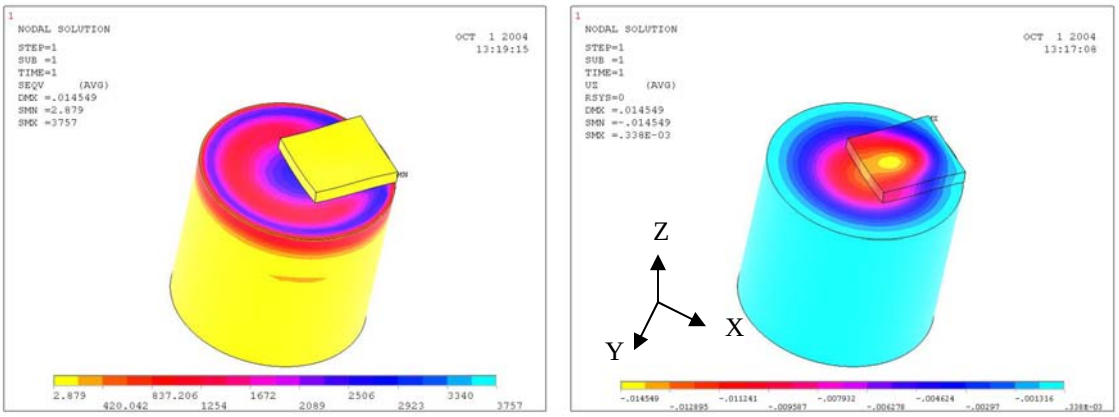

Figure 18. von Mises Stress (Left) and Z Displacement (Right) Under Static Maximum Pressure Loading

Maximum von Mises stress levels of under 4,000 lb/in^2 in the above figure are far below the yield strength of 40 ksi for 6061-T6 Al (11). Again, the maximum stress seen by the viewing window is also far below the yield strength of 8 ksi for acrylic (11). The above figure also illustrates the Z displacement of the vessel subjected to 14.7 lb/in^2 surface loading. A displacement of .015" near the center of the top of vessel is insignificant in its possible effects on testing.

Base Plate Design

As seen below in Figure 19, preexisting base plates did not allow for a sealed attachment of a pressure vessel that would completely enclose the specimen during partial pressure testing. The specimen extended beyond the circumference of the initial base plate shown.

Figure 19. Initial Test Setup with Old Base Plate

Hence, a 1" piece of aluminum was manufactured to have a diameter of 20" and matched the existing bolt pattern of the 18,000 lbs. electrodynamic shaker. The diameter of each bolt through hole was .375". Each of the 16 holes was equally spaced around two circles with radii of 4" and 8". Due to the extremely constrained condition of the base plate during testing (16 bolts), modal interference of the base plate was not initially considered and hence, no finite element models were created. The fabricated base plate is shown below in Figure 20.

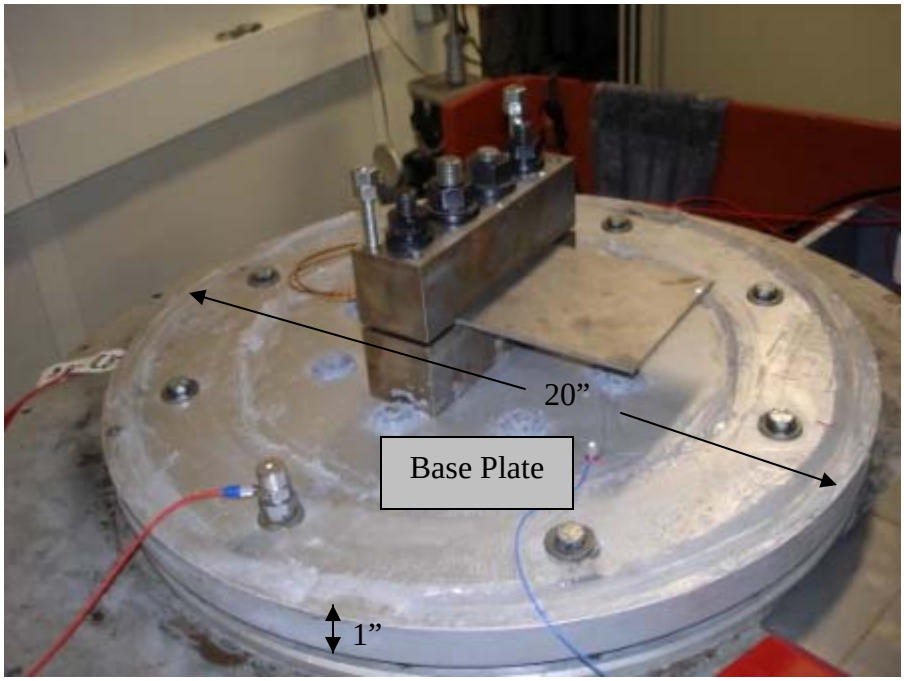

Figure 20. Fabricated Base Plate

III: Test Setup and Procedures

This chapter outlines the procedures used to obtain the vibration data. Figure 21 below breaks the tests up into reference sections for ease of understanding. Data sets that produced unusable data are shown as white boxes. The reasoning for this is explained within this chapter. The comparison testing for the uncoated and coated square specimen is shown in blue. The data collected is presented within Chapter IV.

The testing was divided into two major sections: testing employing the electrodynamic shaker and testing using magnetic excitation in a stationary pressure vessel. The shaker testing subjected the specimen to a clamped-free-free-free condition. Alternatively, the magnet excitation used a stationary pressure vessel and subjected the specimen to a free-free-free-free condition.

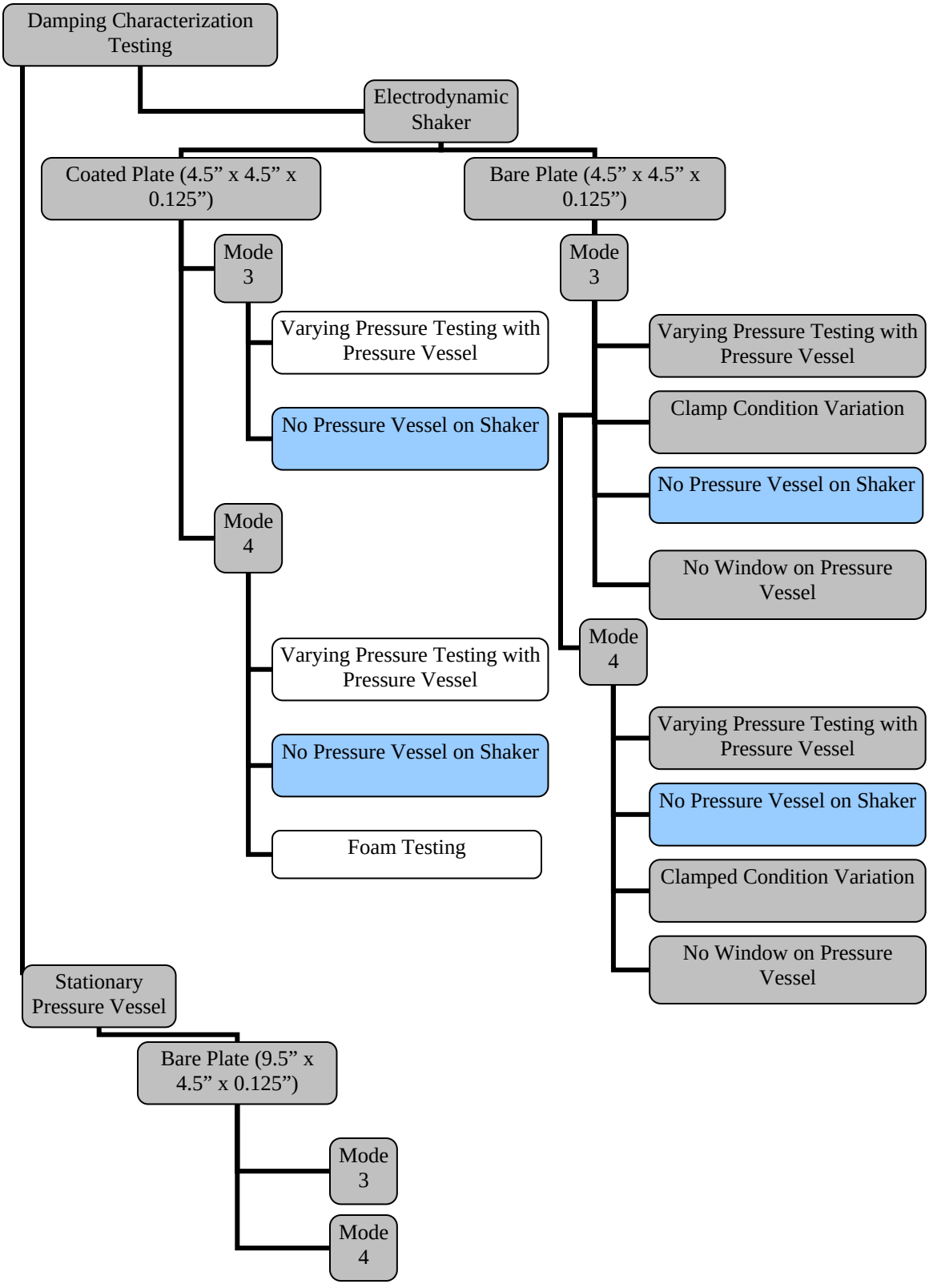

Figure 21. Test Structure

Employment of the Electrodynamic Shaker Testing

The test setup used to execute all TEFF (Turbine Engine Fatigue Facility) testing utilized an 18,000 lb electrodynamic shaker combined with an Unholtz-Dickie PC based software package as a controller. Due to the non-linear material characteristics of the mag spinel hard coating, all sine sweeps were performed from the highest to the lowest frequency within the range of interest, also labeled down sweeps. Although frequency sweeps for the coated plates yielded asymmetric velocity curves with respect to the peak frequency, the half-bandwidth method was used to determine all Q values for all testing performed within the TEFF. This method of determining Q was used during past testing (4).

Sinusoidal base excitations were applied to the specimen at a constant force quantified as g level. The velocity of the specimen of the tip was measured using a laser vibrometer. The velocity of the tip was plotted versus frequency. The amount of force applied to the specimen was then altered and the sinusoidal test repeated. The frequency range of the sweep was dependent upon the mode of interest. All of the testing was performed at a 5 Hz per minute down sweep rate in order to appropriately capture the true peak resonant responses of the specimen (22). All base excitation was kept constant throughout each sine sweep. All testing was carried out from lowest to highest g load to minimize possible high strain memory effects in the mag spinel coating would cause errors in the results. All maximum strains were kept under 750 micro-strain for both the coated and uncoated plates. Research has shown that excessive strain on the mag spinel

coating may cause permanent damage to the coating on the plates and hence alter follow-on test results (26).

Test Fixture

The test fixtures used to secure the first set of coated and uncoated specimens were originally created in order to closely model the true clamped condition and limit the amount of slipping the specimen would see during testing (4). The specimen was secured over two bushings as shown below in Figure 22.

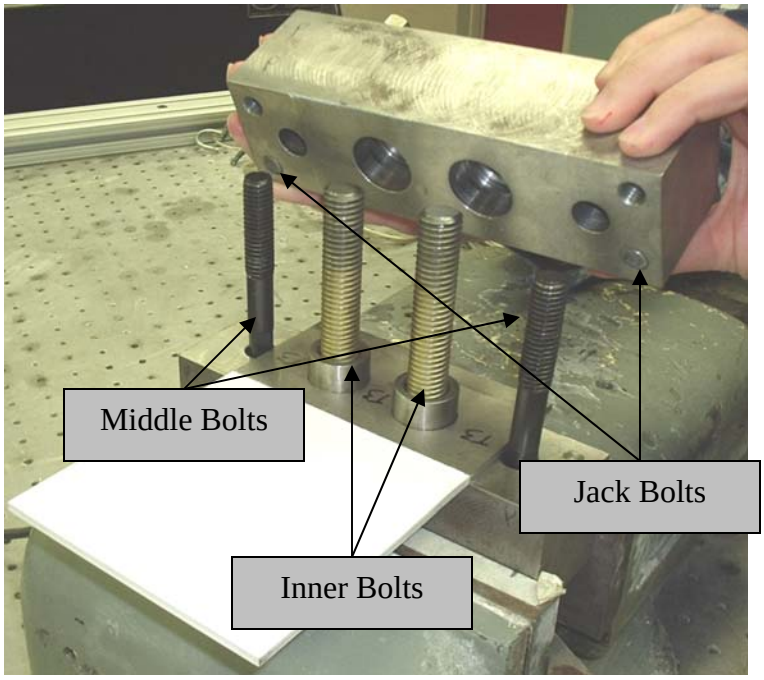

Figure 22. Constraint Blocks (4)

A total of six bolts (3 pairs) secured the plate between the blocks. The innermost bolts (with a torque equal to 125 ft.-lbs.) secured the titanium plate within the steel blocks. The middle bolts (with a torque setting of 100 ft.-lbs.) fastened the entire fixture to the aluminum base plate. Finally, the outermost bolts, also referred to as jack bolts, (with a

torque setting of 120 in.-lbs.) were utilized to better clamp the front section of the blocks, and thus create a more secure clamped condition.

Repeatability was of primary concern for all experimentation. For this reason, all data within a data set was taken without removing the plate from the clamp. Altering the clamp in anyway, especially the torque of the bolts that secure the plate, significantly alters the test results. This issue will be addressed further in the Clamp Condition Variation Testing section of this chapter.

Data Collection Location

Below, Figure 23 demonstrates the position measured by the laser vibrometer on the 4.5" x 4.5" x 0.125" specimen. This location was chosen in order to best measure velocities for both modes of interest. A measurement location near a nodal line creates difficulties. If the laser collects velocity measurements along nodal lines, velocities can be extremely low (by definition). Large gradients occur close to nodal lines. Thus, slight variations in laser vibrometer measurement locations may lead to drastically different velocity measurements. When matching these measurements to finite element code strain ratios, great variations in velocity directly correspond to large shifts in peak strain measurements. The point of measurement coincided with the point measured in past studies.

It has been demonstrated that there is no mode shape difference between the uncoated and coated specimens when they are excited in mode 3 or mode 4 (4). For this reason, the location of measurement was kept constant throughout testing for both the

coated and uncoated specimens. The point measured was located 0.7 in. from the long edge and 0.1 in. from the short edge of the specimen.

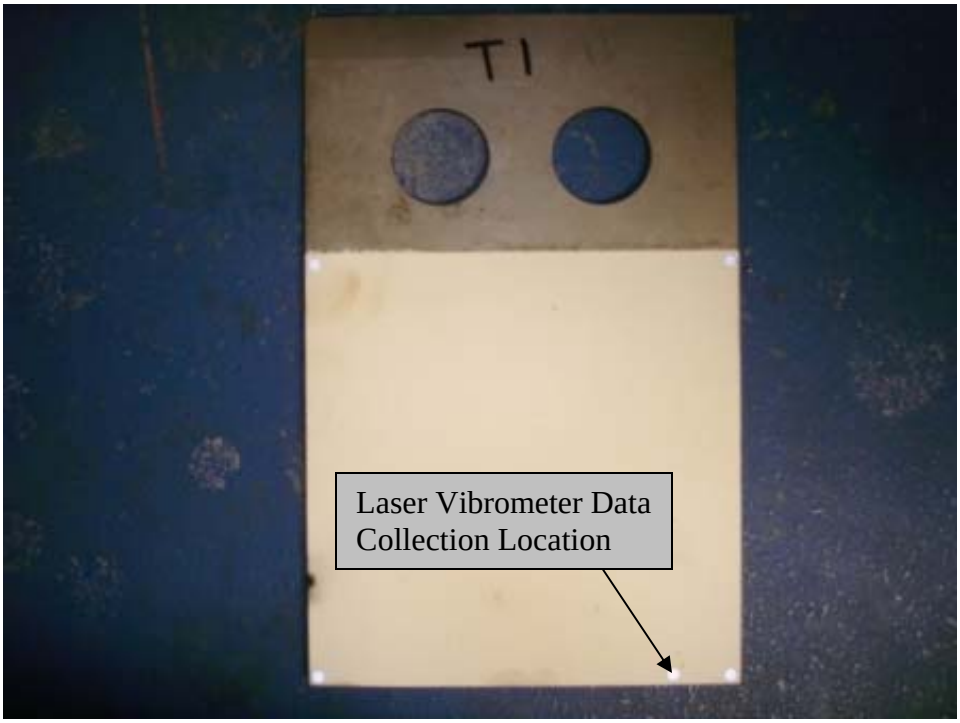

Figure 23. Laser Vibrometer Data Collection Location on Specimen

Full Atmosphere Testing

Initial baseline testing was performed in order to ensure that the current test approach yielded analogous results for damping found during prior testing for both the coated and uncoated specimens. The maximum strain values were taken from Blackwell's testing and runs were carried out to simulate past conditions (4). The bare specimen was compared to the coated specimen. This testing was performed for both mode 3 and mode 4. The Q values were then compared to Blackwell's results (4).

The base excitation force was altered incrementally. From these varying sine sweeps, velocity versus frequency graphs were created. An example of the bare plate testing is shown below in Figure 24.

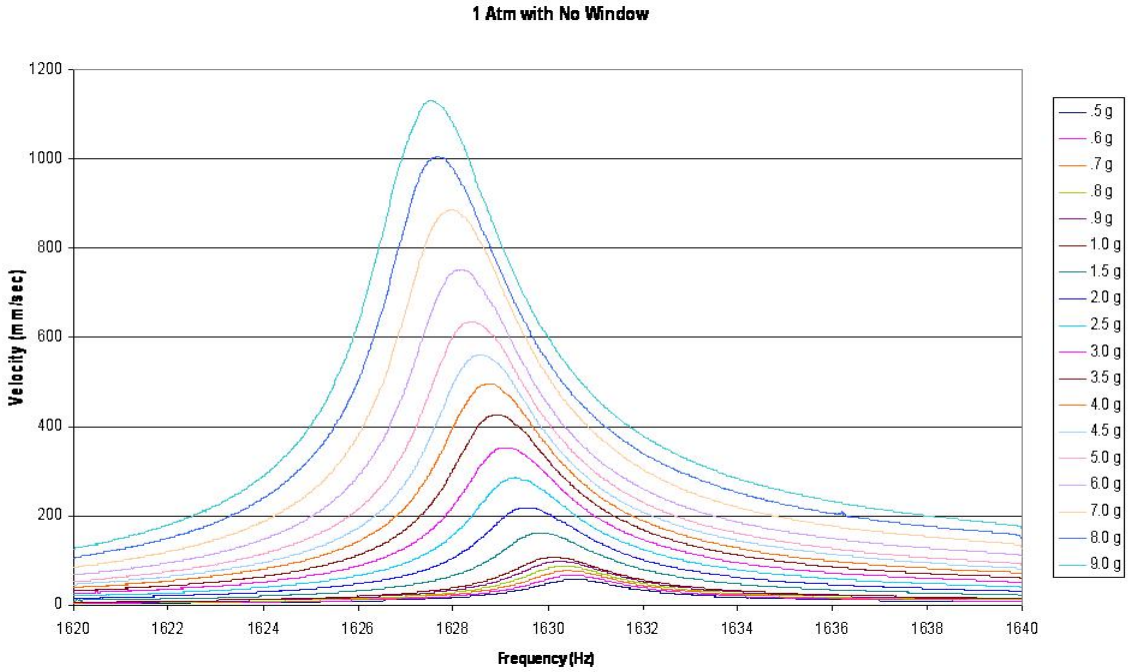

Figure 24. Bare Plate, Mode 4, No Window on Pressure Vessel

The frequency range of the sweeps was altered for each mode. The exact range of interest varied not only based upon the mode shape, but also the test specimen. Different frequency ranges were tested for the coated versus uncoated plates, but all frequency ranges corresponded with either mode 3 or mode 4. Due to the strain dependent layer of the hard coating on the specimen, the frequency range was shifted as the forced base excitation was increased.

In order to capture the half-power bandwidth frequencies needed to determine Q for the coated plate, the frequency range of the sine sweep was altered. The modal frequencies of interest were higher for the coated plate compared to the bare plate. There

was also more material damping associated with the coated plate. Hence, larger sine sweeps were needed in order to capture the full frequency needed to determine Q. The down sweep range was both raised by approximately 50 Hz and doubled to 40 Hz. Table 7 below illustrates the various sine sweeps performed and the base excitation level at which they were performed.

Table 7. Full Atmosphere Test Matrix

	Bare Plate		Coated Plate	
	Frequency Sweep Range			
Base Excitation Level (g)	Mode 3 (1230-1250 Hz)	Mode 4 (1620-1640 Hz)	Mode 3 (1270-1320 Hz)	Mode 4 (1650-1710 Hz)
0.5	X	X	X	
0.6	X	X	X	
0.7	X	X		
0.8	X	X	X	
0.9	X	X		
1	X	X	X	X
1.2			X	
1.5	X	X	X	
2	X	X	X	X
2.5	X	X		
3	X	X	X	
3.5	X	X		
4	X	X	X	X
4.5	X	X		
5	X	X	X	
6	X	X		X
7	X	X	X	
8	X	X	X	X
9	X	X	X	
10				X
15				X
20				X
25				X
30				X
35				X
40				X
45				X
50				X

Partial Pressure Testing

In order to demonstrate the effects of air damping, partial pressure testing was performed. A vacuum pump was used to evacuate the air inside the chamber. The chamber was fastened to the shaker head via 8 bolts. Air was emptied from the chamber down to approximately 0.003 atm (atmospheres). Three sine sweeps of 1g, 5g, and 9g were then performed at the same 5 Hz/min down sweep rate. Upon conclusion of the three sweeps, the vacuum pump was turned off and the pressure was released to 0.25 atm. The same three sweeps were performed again. The process was repeated for 0.5 atm, 0.625 atm, 0.75 atm, 0.875 atm, and 1 atm conditions. The test setup is shown below in Figure 25.

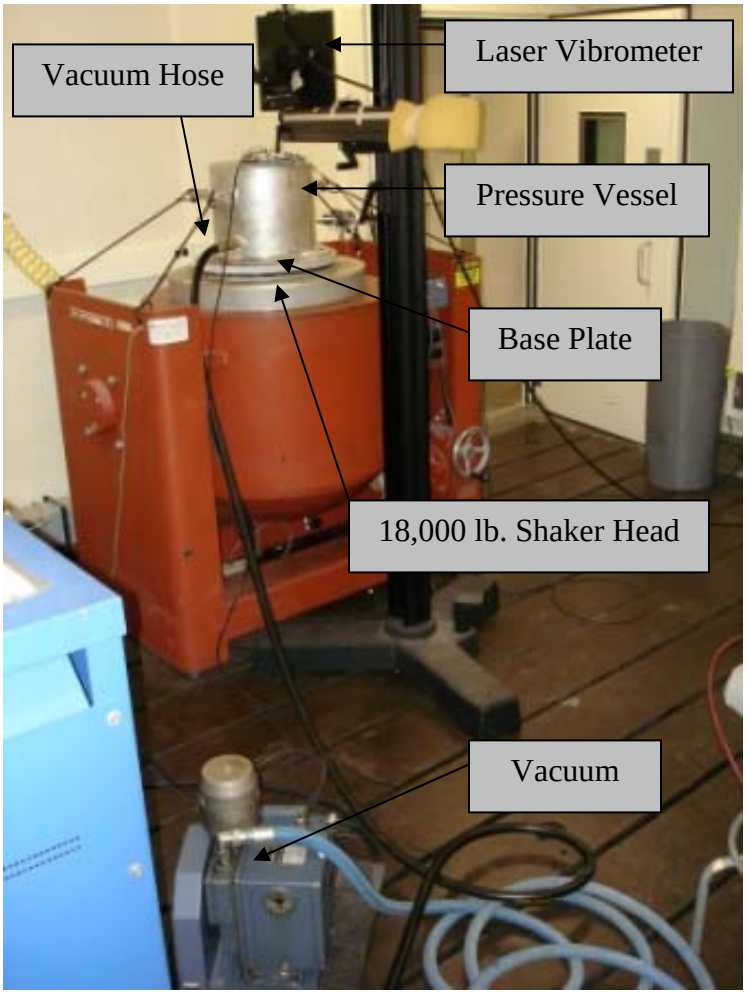

Figure 25. Partial Pressure Test Setup

Table 8 below illustrates the pressures and base excitation levels that were included in the partial pressure testing for the bare plate specimen.

Table 8. Partial Pressure Test Matrix

Bare Plate, Mode 3 & 4 = X	Pressure (atm)						
Base Excitation Level (g)	0.003	0.25	0.5	0.625	0.75	0.875	1
1	X	X	X	X	X	X	X
5	X	X	X	X	X	X	X
9	X	X	X	X	X	X	X

Clamp Condition Variation Testing

Despite the use of specially designed blocks, the accuracy of the perfectly clamped condition was still questioned. For this reason, this study included testing to determine if the boundary was perfectly clamped. Torque settings of the constraint bolts were varied and sine sweeps were run. So as to not cause permanent deformation, the highest torque setting tested corresponded with the material elastic limits for the bolts. Identical sinusoidal sweeps were run at each torque setting and Q was calculated. The Q values were then compared to evaluate the possible damping created by the clamping condition.

The torque settings of 125 ft.-lbs. (inner bolts), 100 ft.-lbs. (middle bolts), and 125 in.-lbs. (jack screws) were used as a baseline. Figure 26 below denotes the location of these bolts.

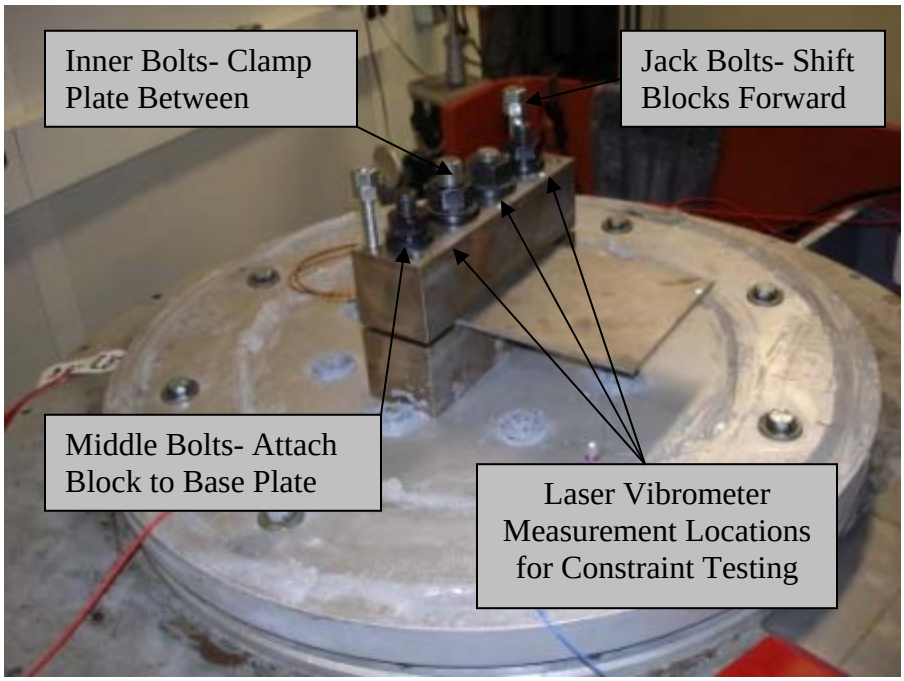

Figure 26. Bolt Locations

The torque on the bolts was varied at 75%, 87.5%, 100%, 112.5% and 125% of the baseline torques. Three sine sweeps were run at each torque setting. Table 9 below illustrates the various test scenarios for the clamp condition variation testing. The results are discussed in Chapter IV.

Table 9. Clamp Condition Variation Test Matrix

	Torque: First Number = Inner Bolts (ft-lbs), Second Number = Middle Bolts (ft-lbs), Third Number = Jack Bolts (in-lbs)				
	90, 75, 93.75	105, 87.5, 109.375	120, 100, 125	125, 112.5, 140.625	150, 125, 156.25
Mode 3					
.5g	X	X	X	X	X
3.0g	X	X	X	X	X
6.0g	X	X	X	X	X
Mode 4					
1.0g	X	X	X	X	X
5.0g	X	X	X	X	X
9.0g	X	X	X	X	X

Additionally, the velocity at three points along the top of the constraint blocks was measured during a sine sweep at a base excitation level. This was done at three different base excitation levels. The tests were performed for both modes 3 and 4. The constraint block velocity measurement locations are denoted above in Figure 26. The responses were then compared to determine the uniformity of the constraints during testing.

Ping Testing

After the occurrence of some testing anomalies, additional modal evaluation of the base plate was desired. Ping testing was performed on the base plate in order to properly evaluate the possible modal interference. A PCB voltage type accelerometer was secured to the base plate and the plate was impacted (pinged) with a hammer. The response was measured and a sample graph is shown below in Figure 27. For this particular figure, the test was performed with the pressure vessel in place and with the specimen in the blocks.

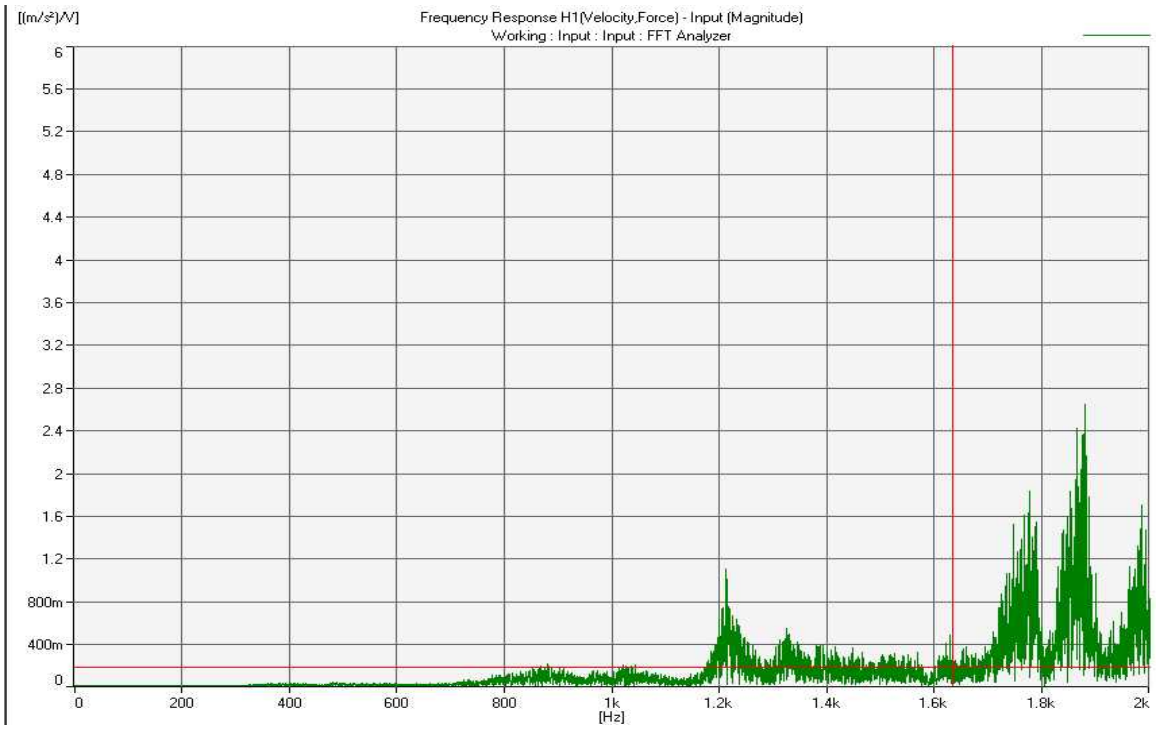

Figure 27. Base Plate Frequency Response

The amount of impact created by the striking of the hammer on the base plate was not measured. Therefore, the amount of forced input created by the hammer was unknown. Thus, the amplitude of the peaks cannot be compared between different response graphs. A peak response as demonstrated by the vertical axis in the graph will vary from graph to graph. The frequency location of the peaks was the primary focus of this investigation. The testing configurations were varied with the following deviations: with/without pressure vessel, with/without specimen in the constraint blocks, with/without bungee cords attached to the pressure vessel. Further discussion of the ping testing results is given in Chapter IV.

Control Accelerometer Location

As was mentioned in the last section, the design of the base plate presented difficulties with modal interference issues. The location of the control accelerometer was kept constant throughout the vast majority of testing. This location was approximately half way between two bolt holes on the outer 2" radius of the base plate. This location is shown below in Figure 28.

During the partial pressure coated plate testing, large base excitations were difficult to achieve. To address possible errors in the control accelerometer, all accelerometers were crossed checked with the laser vibrometer. After verification of the accuracy of the control accelerometers, further investigations found that the modal interferences of the base plate were too large to overcome with the control accelerometer's current location. For this reason, the accelerometer was moved to an attachment point atop a pressure vessel connection bolt. This is location is demonstrated in Figure 28 below. The only testing that occurred with the control accelerometer at this second location included: partial pressure testing using the coated plate and foam testing (which also used a coated plate). Despite the new location of the control accelerometer, the high base accelerations needed during these two portions of coated plate testing caused significant interference with the base plate. Due to these base plate interferences, neither of these data sets were valid.

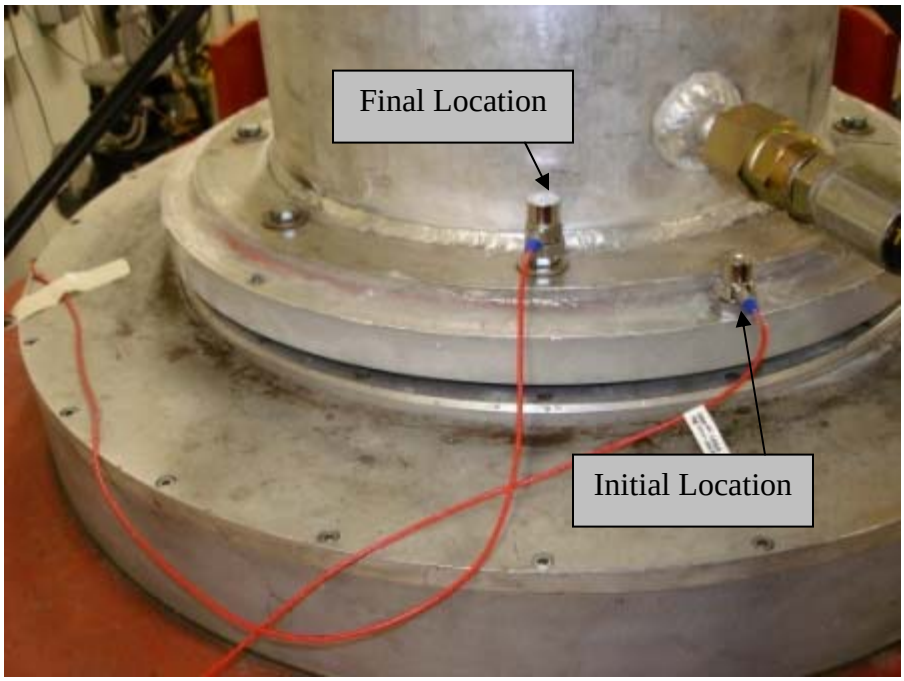

Figure 28. Control Accelerometer Locations

The most dramatic implication of altering the control accelerometer location was the variation in base excitation. The control accelerometer measured acceleration was dependent upon its location on the base plate. Altering the location of the control accelerometer also altered the perceived excitation for the same base excitation.

For example, a 9 g base excitation for a coated plate at .5 atm was not directly comparable to a 9 g base excitation for an uncoated plate at .5 atm.

If the base plate interfered with the consistency of the base excitation, strain and damping levels measurements were invalid. This was the case for partial pressure testing using the coated plate and for the foam testing. A problem occurred when the base plate interference caused an inconsistent base excitation over a frequency sweep. For example, the experimenter performed a 9 g base excitation sweep from 1250 to 1230 Hz using the coated specimen at .5 atm. The base excitation should have been 9 g's throughout the

sweep. The test was invalid because the specimen was not excited at 9 g's throughout the sweep. The entire frequency sweep must have the same base excitation. If the control accelerometer was greatly affected by the modal interference of the base plate, a constant base excitation was not possible. Further explanations, to include how to recognize if this interference was occurring, are given in Chapter IV under the Base Plate Interference Results section.

Accelerometer Mounted on Specimen Tip

Concerns surrounding the accuracy of the laser vibrometer when shooting through an oscillating acrylic window were addressed with the addition of an accelerometer on the tip of the test specimen. The accelerometer with a reflective decal mounted atop was glued to the tip of the uncoated plate. The laser vibrometer measured the velocity readings from this location. The results of these measurements are compared in Chapter IV. Figure 29 below displays this setup.

Figure 29. Verification Accelerometer Location

Thermocouple

A thermocouple was added during later phases of testing. There were repeatability issues during testing. Tests that were run in the beginning of the day were repeated and the end of the day. There was a shift in peak frequency between the morning and evening tests for these "bookend" tests. One conjecture was that the temperature of the room changed over the course of the day due to the operation of the shaker. The room temperature varied as much as 20 deg F over the period of an eight hour day. This temperature variation slightly affected the modulus of elasticity for the specimen. The modulus decreased with an increase in the specimen temperature. A

change in modulus directly affected the modal frequency. The effect of heat addition on titanium is shown in Chapter IV.

The thermocouple was spot welded to the top of the blocks. This is shown below in Figure 30 in a top down view of the constraint blocks.

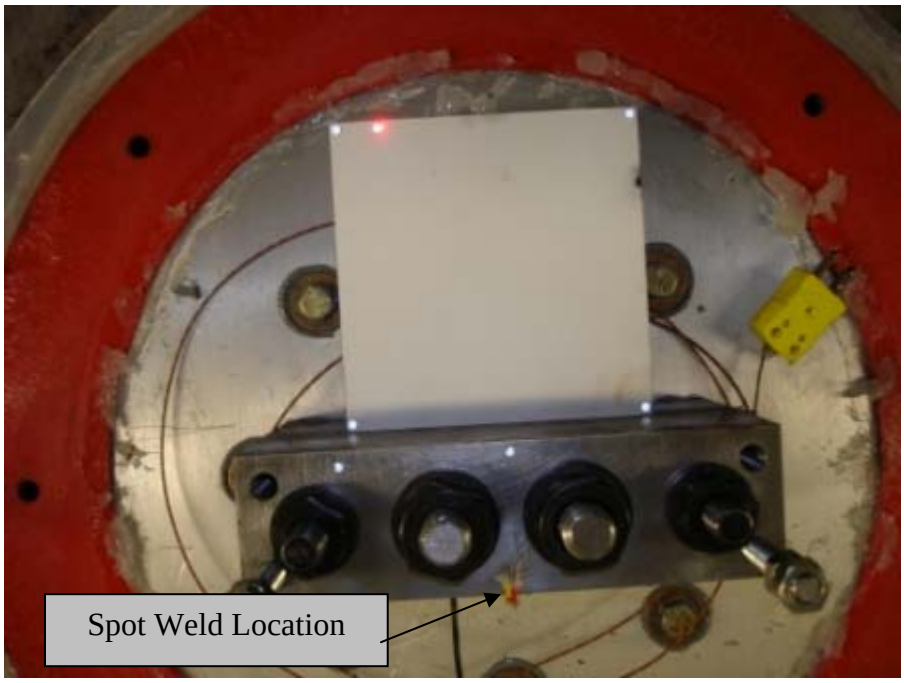

Figure 30. Thermocouple Location

Pressure Wave Testing

Due to constraints on air flow during partial pressure testing imposed by the pressure vessel, pressure wave excitation was deemed of possible interest. Specifically, it was found analytically that the half-wavelength for air near the frequencies of interest for modes 3 and 4 was approximately the same in length as the distance between the plate specimen and the base plate (25). The boundary constraints on air flow imposed by the boundary of the pressure vessel further accentuated the concern of interference during testing.

In order to determine the affects of the addition of the pressure vessel on the shaker head, sine sweeps were performed with the vessel on the shaker head and the viewing window removed. The Q values, peak resonant frequencies, and strain levels were then compared between the full atmosphere condition with and without the pressure vessel. This comparison was done for both the coated and uncoated plates. Figure 31 below shows the setup for testing without the viewing window and a bare plate specimen.

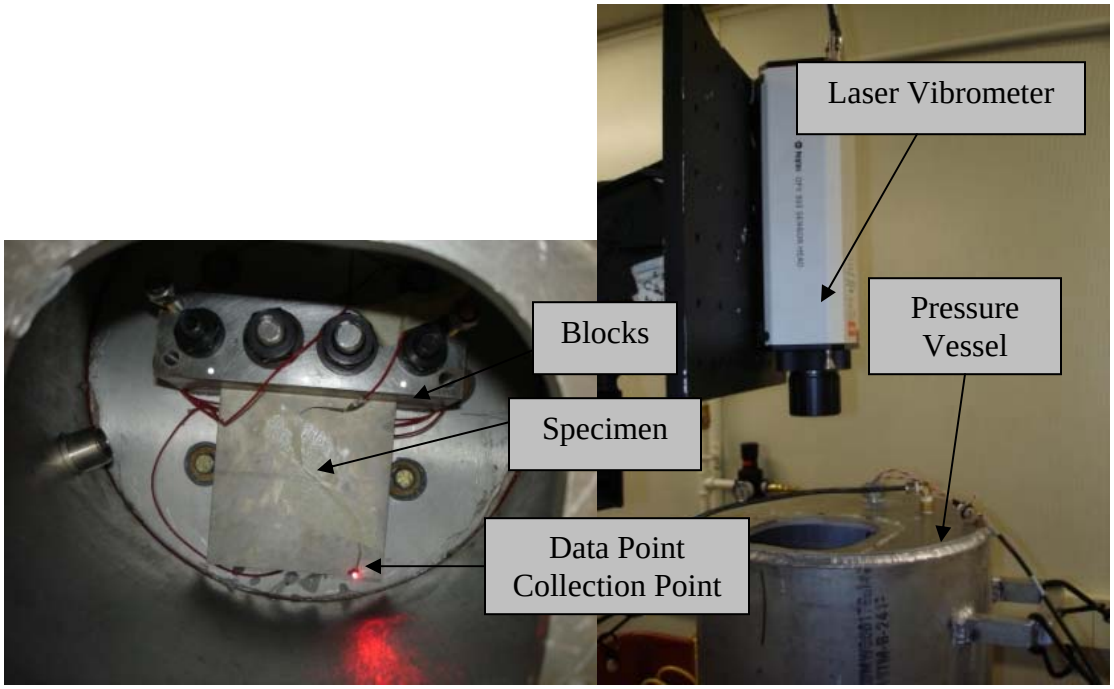

Figure 31. No Viewing Window on Pressure Vessel. Top Down (Left) and Vertical (Right)

In order to address the possible pressure wave interference issues, foam was secured under the specimen to break up any possible acoustic excitation caused by the air within the vessel. Tests were then run at varying base excitation levels and at varying pressures. Figure 32 depicts the location of the foam under the plate.

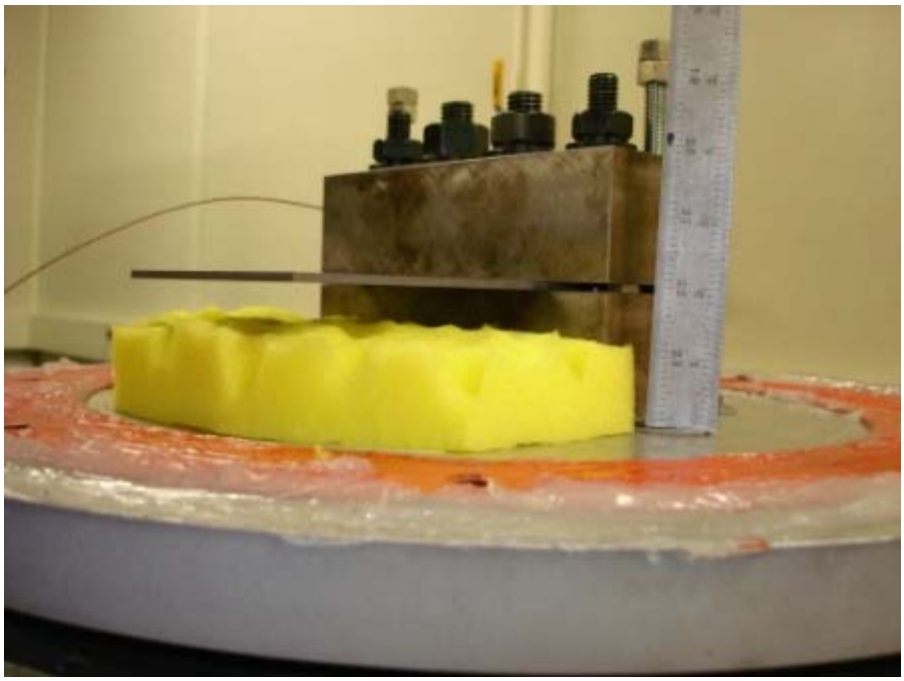

Figure 32. Foam Testing Setup

Bungee Cables

Bungee cords were added to the pressure vessel setup in order to restrain the handles. The four cords were attached both to the supports of the electrodynamic shaker and to the handles of the pressure vessel. Modal frequencies of the pressure vessel handles were found to be coincidental with the modal frequencies of the specimen. This in turn, prevented the electrodynamic shaker from accomplishing peak excitation levels needed for testing. Restraining the handles moved the modal frequencies out of the range of interest for modes 3 and 4 of the test specimens. The addition of bungee cables had no affect on the test results. The setup is shown below in Figure 33.

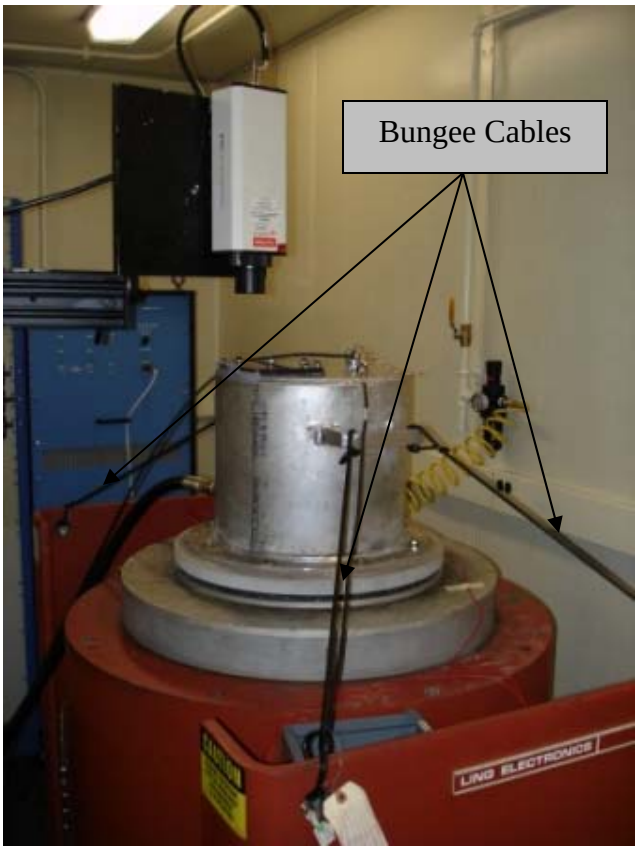

Figure 33. Bungee Cord Attachment Points

Magnet Excitation using a Stationary Pressure Vessel

In an attempt to isolate and quantify air damping, additional testing was executed for a plate in a free-free-free-free boundary condition. By subjecting a specimen to this boundary condition, damping due to the clamp was eliminated. Thus, the effects of air damping were easily isolated.

The testing, performed at the Aeronautics Laboratory at The Air Force Institute of Technology, utilized a large, stationary pressure vessel approximately 6 feet tall and 3 feet in diameter.

Partial Pressure Testing

The specimen was hung inside the chamber by a string. Magnet excitation was used to excite the specimen within the pressure vessel. Cobalt discs were attached to both sides of the specimen using wax. A magnet was placed in close proximity to the discs. The magnets excited the plate using alternating charges. Figure 34 displays the mounted position of the titanium plate within the pressure vessel. The first photograph is taken from the bottom of the vessel, looking directly up towards the ceiling of the vessel. The second photograph demonstrates the placement of the magnet excitation on the specimen.

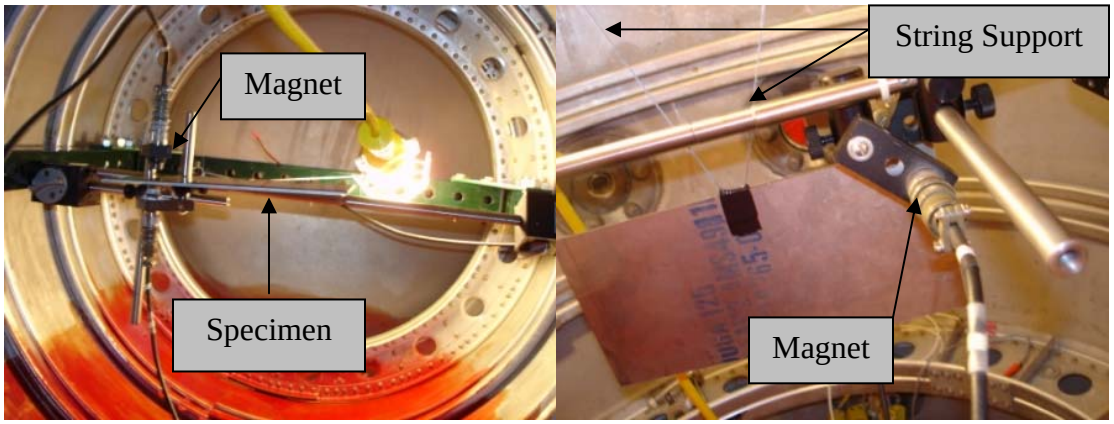

Figure 34. Magnet Excitation Pressure Testing

The laser vibrometer mounted outside of the pressure vessel utilized a small window in the side of the vessel to take measurements. The magnet excitation signal was fed from the computer to the magnets through an air tight connection plate in the wall of the pressure vessel. A chirp signal was induced by magnetic excitation and the response of the plate was measured. One hundred chirps were performed at each pressure. The response signals were then averaged. The chirps covered a frequency range of 0 - 2000 Hz. Therefore, multiple different modal peaks were identified.

The physical setup is shown below in Figure 35.

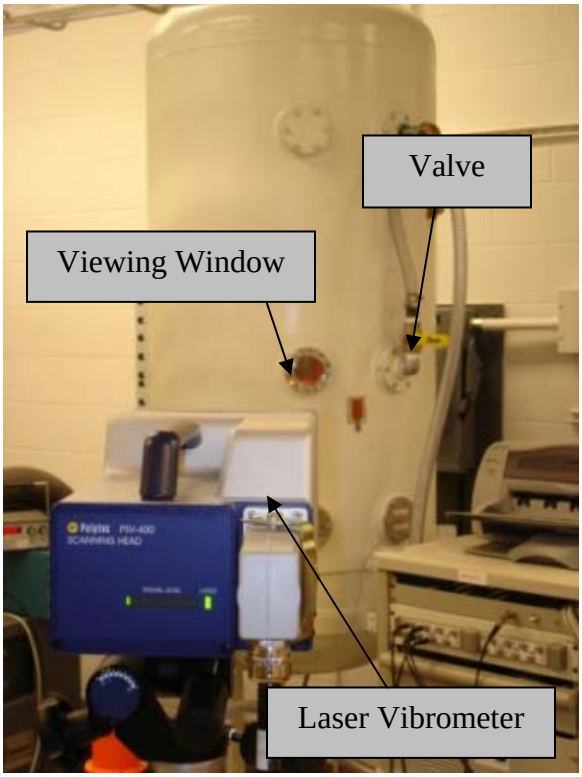

Figure 35. Stationary Pressure Vessel Test Setup

Each set of chirp data was collected at a particular pressure. The data was collected for seven different pressures that ranged from near vacuum to full atmospheric condition. The level of excitation voltage was kept constant throughout testing. Limits of the free-free-free-free magnetic excitation setup prevented high strain testing. For this reason, strain levels and damping characterizations were not compared to electrodynamic shaker data.

Velocity versus frequency graphs were created and an eigensystem realization algorithm was used in order to determine the damping of the bare plate (5). An example of the results from the chirp testing is shown below in Figure 36. The velocity results are graphed in dB. The two modes of interest are marked appropriately. Each peak

represents a mode. In the diagram, mode 3 falls very close to mode 4. The mode shape verification performed ensured that mode 4 was the mode of interest.

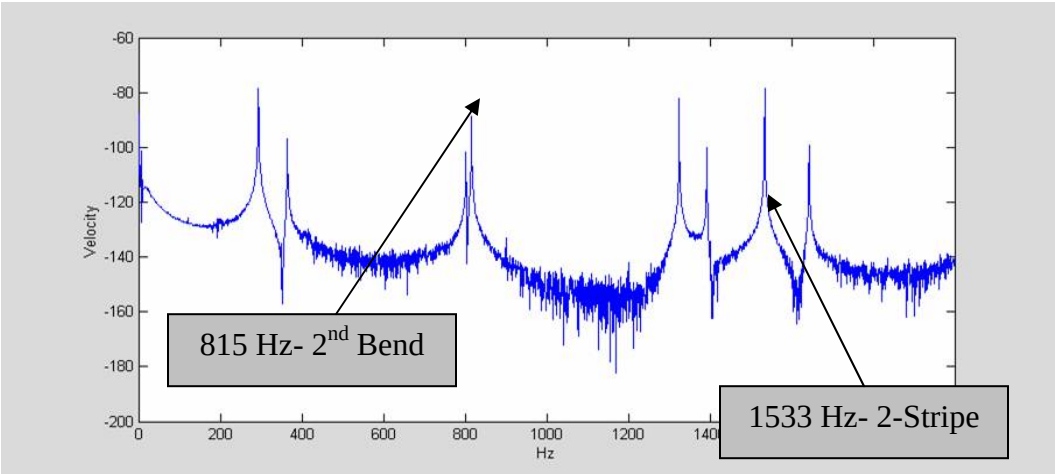

Figure 36. Stationary Pressure Vessel Results

The exact location of velocity measurement on the plate was not recorded during this section of testing. Therefore, exact values for strain were not calculated. However, it was known that the levels of strain were very small in comparison to electrodynamic shaker testing.

IV: Results and Discussion

This chapter presents the results from testing both for the electrodynamic shaker testing and the magnetic excitation (stationary pressure vessel) testing. It was found, and will be discussed further within this chapter, that due to base plate interference issues, all test data taken using the coated specimen was invalid. No damping level comparisons were made between magnet excitation and shaker excitation testing. This was due to the significant differences in strain levels between tests.

Changing of control accelerometer locations, discussed further in this chapter, made g level comparison only valid within an individual data set. They are not compared between data sets. However, strain levels versus damping level comparisons were valid between data sets and were investigated accordingly.

Generally, damping levels were compared using a 1/Q value versus strain (in/in). Isolated comparison using Q versus strain (in/in) were used for evaluation of past studies. The relationship between different damping measurements is listed at the end of Chapter I.

Electrodynamic Shaker Testing

Full Atmosphere Testing

Past results were used in order to validate the initial test setup for the electrodynamic shaker testing. As mentioned previously, past studies have yielded Q

values for bare plate titanium that were unexpectedly low (4). Thus, in order to verify the current test setup and also set a baseline for follow-on testing, sine sweeps were run at similar strain levels, using the same constraint blocks, and the same test specimens as Blackwell (4). So that the mag spinel coating was not damaged, all strain levels throughout testing were held below 750 micro-strain.

Figure 37 and Figure 38 are the frequency responses of the bare plate for modes 3 and 4. From these graphs, all other data analysis was performed. Due to modal interferences with the base plate and changes in control accelerometer locations, g levels are not comparable between data sets. G level comparisons are used only within a single data set. Bare plate, mode 3, no vessel is an example of a data set. Each data set is shown as an individual box in Figure 21. All further comparisons utilized similar sine sweep compilations to deduce the needed data.

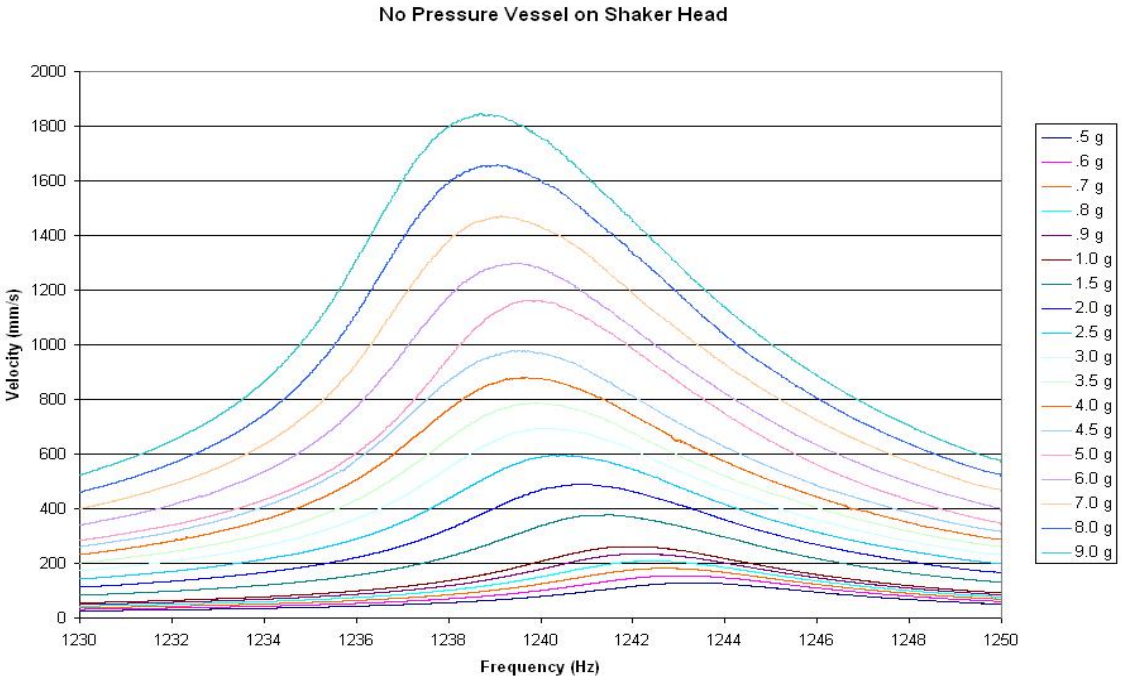

Figure 37. Bare Plate, Mode 3, Frequency Response

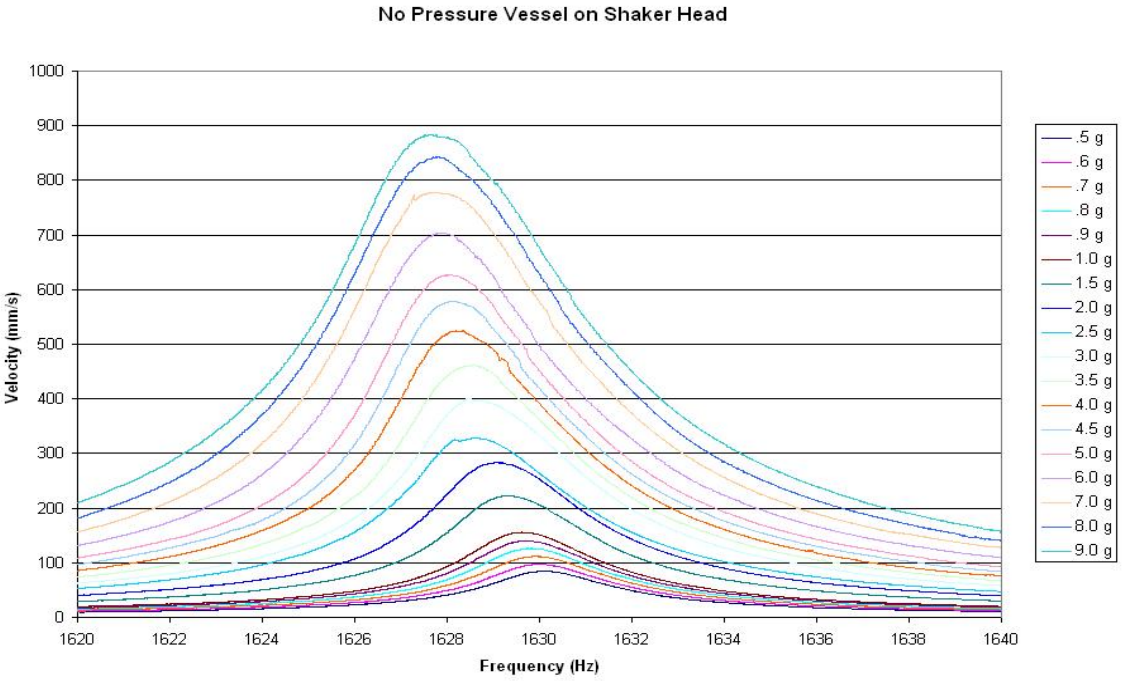

Figure 38. Bare Plate, Mode 4, Frequency Response

Figure 39 and Figure 40 demonstrate overlaid sine sweeps graphs as velocity versus frequency for modes 3 and 4 using the coated specimen.

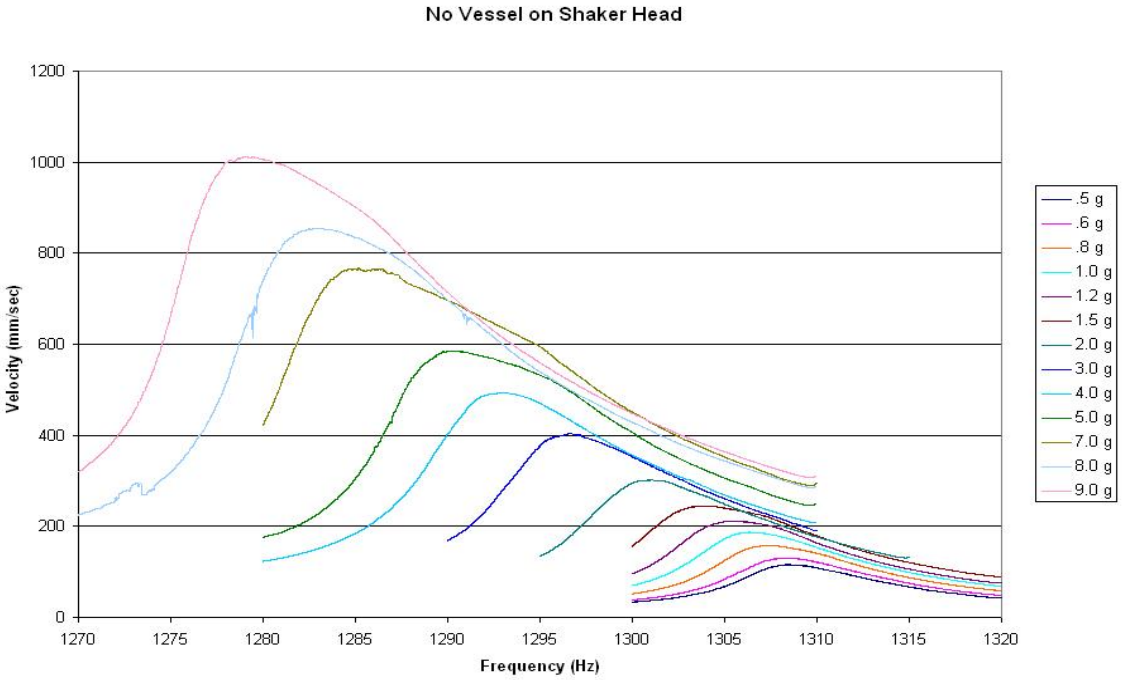

Figure 39. Coated Plate, Mode 3, No Vessel

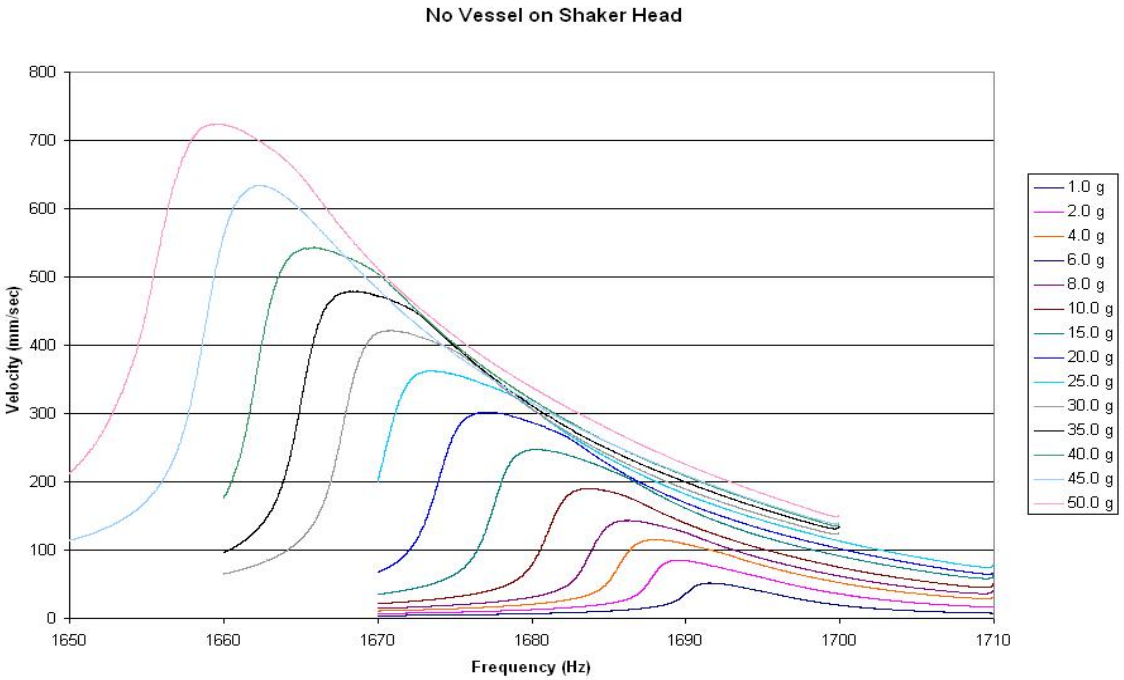

Figure 40. Coated Plate, Mode 4, No Vessel

The Q values versus strain levels compared within this section contrast Blackwell's results with those found during the initial sections of this testing (4). For this study, the same coated (T1) and bare (T4) specimens from Blackwell's results were used.

Figure 41 and Figure 42 below display the results from this study representing modes 3 and 4 for both coated and uncoated plates without the pressure vessel on the shaker head. All graphs reference 1/Q. Therefore, an increase in the vertical axis corresponds with an increase in damping. All relationships between different damping measures are shown at the end of Chapter I. The net difference of the coated and uncoated plates is also displayed.

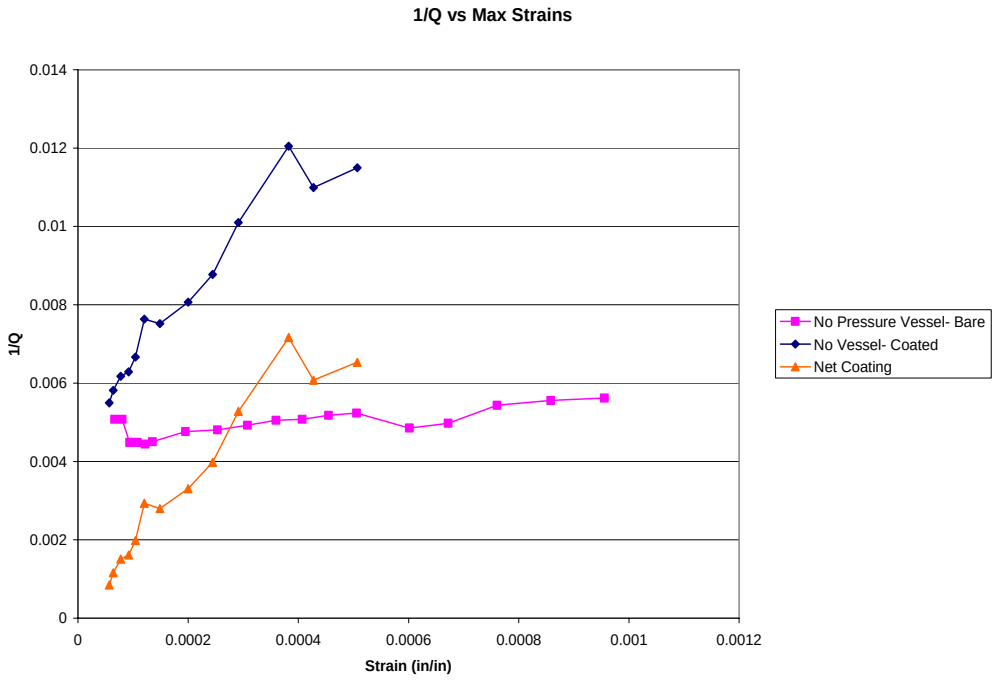

Figure 41. Bare vs. Coated, Mode 3, No Vessel

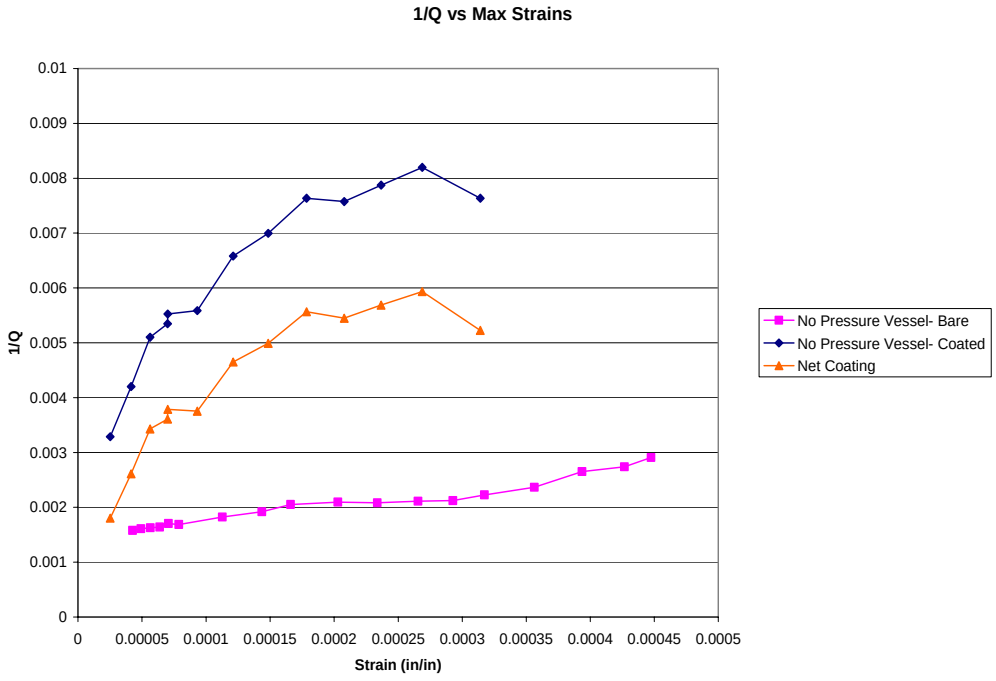

Figure 42. Bare vs. Coated, Mode 4, No Vessel

The difference in damping between the coated and uncoated specimen displays the contribution of the mag spinel coating to the total system loss factor. This difference is shown above with triangular data points. The differences for mode 3 is small at smaller strain levels. The material damping appears to has a greater affect at larger strain levels. For mode 4, the damping associated with the mag spinel coated dramatically increased the total system damping at all strain levels.

Also demonstrated in the above graphs is the general trend of increased damping with increased strain levels. This was expected for the strain dependent mag spinel coating. Alternatively, the increased damping in the bare plate specimens was generally not expected. One possible explanation of this phenomenon is the influence of the clamped boundary condition. If the clamped condition essentially softened with an increase in strain (forced excitation), this would in turn cause the entire system to show a larger damping level.

Table 10 and Table 11 show the tabulated effects of the mag spinel coating. A best fit trend line was added to the bare plate data. From these trend lines, values were taken at specific maximum strain values corresponding to the measurements taken for the coated plate. The difference was found and an increased in damping is displayed in the tables below.

The net damping of the coating material shown in the “Difference (1/Q)” column for mode 3 grows dramatically with increases in strain. The amount of damping associated with the mag spinel coating was minimal at lower strain levels. The specimens showed a peak difference in damping of 59.5%. There was a much more

significant level of damping at all strain levels tested for mode 4. The peak difference showed a 72.4% increase in damping.

Table 10. Bare vs. Coated, Mode 3

Strain (in/in)	Coated	Bare		
	1/Q	1/Q	Difference (1/Q)	% Difference
5.69353E-05	0.005494505	0.004647747	0.000846758	15.41%
0.000064069	0.005813953	0.004653588	0.001160365	19.96%
7.74753E-05	0.00617284	0.004664482	0.001508358	24.44%
9.17207E-05	0.006289308	0.004675938	0.00161337	25.65%
0.000104078	0.006666667	0.004685777	0.00198089	29.71%
0.000120496	0.007633588	0.004698708	0.00293488	38.45%
0.000148797	0.007518797	0.004720625	0.002798172	37.22%
0.000199964	0.008064516	0.004759069	0.003305447	40.99%
0.000244506	0.00877193	0.004791328	0.003980602	45.38%
0.000291084	0.01010101	0.004823889	0.005277121	52.24%
0.000382408	0.012048193	0.00488438	0.007163813	59.46%
0.000427365	0.010989011	0.004912589	0.006076422	55.30%
0.000507133	0.011494253	0.004960204	0.006534049	56.85%

Table 11. Bare vs. Coated, Mode 4

Strain (in/in)	Coated	Bare		
	1/Q	1/Q	Difference (1/Q)	% Difference
2.51973E-05	0.003289474	0.001486373	0.001803101	54.81%
4.15379E-05	0.004201681	0.00158889	0.00261279	62.18%
5.63323E-05	0.005102041	0.001670556	0.003431485	67.26%
7.00155E-05	0.005347594	0.001737526	0.003610067	67.51%
7.00342E-05	0.005524862	0.001737612	0.00378725	68.55%
9.30827E-05	0.005586592	0.001833984	0.003752608	67.17%
0.000121205	0.006578947	0.001928332	0.004650616	70.69%
0.000148582	0.006993007	0.00200161	0.004991397	71.38%
0.000178386	0.007633588	0.002067825	0.005565763	72.91%
0.000207855	0.007575758	0.002126964	0.005448793	71.92%
0.000236721	0.007874016	0.002186215	0.0056878	72.24%
0.000268746	0.008196721	0.002262285	0.005934437	72.40%
0.000314192	0.007633588	0.002407618	0.005225969	68.46%

The data was then plotted logarithmically. Equations for the exponential best fit lines are also shown. Figure 43 corresponds with mode 3 and Figure 44 corresponds with

mode 4. Again, the net difference associated with the contributions of the coating material on the system was much greater for mode 4 than for mode 3.

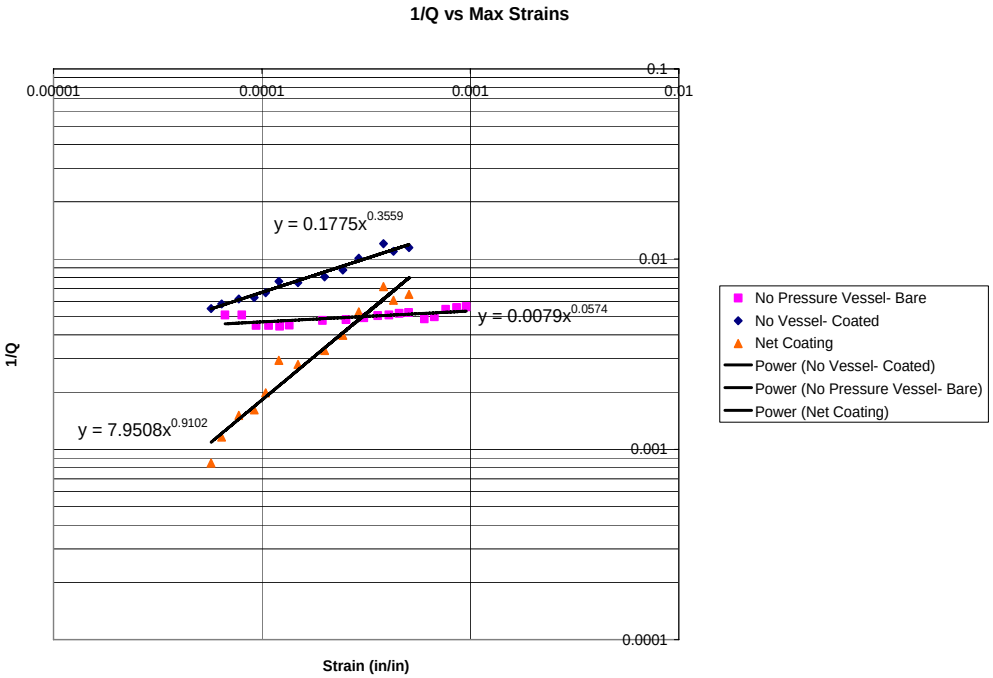

Figure 43. Bare vs. Coated, Mode 3, No Vessel

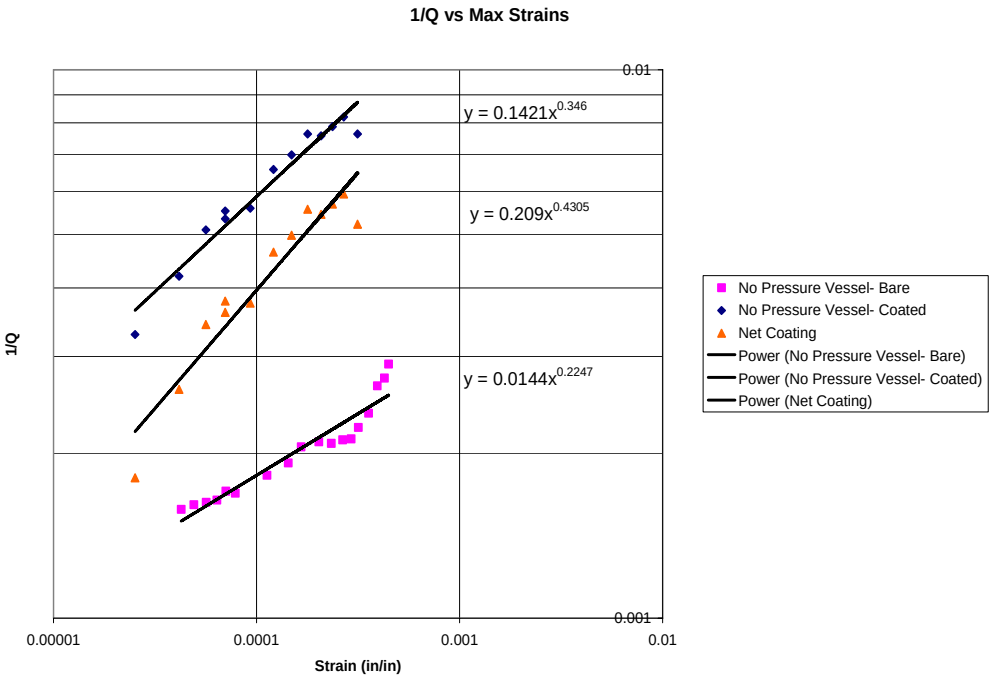

Figure 44. Bare vs. Coated, Mode 4, No Vessel

Table 12 through Table 15 and Figure 45 through Figure 48 below compare the average uncoated and coated plate results from Blackwell's testing to that found during the initial testing in this investigation. It should be noted that exact strain levels were difficult to achieve. The experimenter had to approximate base accelerations in order to achieve approximate strain levels of interest. Therefore, approximate strain levels were compared.

The exact strain levels are shown along with the associated Q value. The Blackwell values were taken from Blackwell's smooth curve fits to his data. It can be seen that damping levels illustrated are very similar to those found by Blackwell. Thus, the initial test setup without the vessel was assumed valid for both modes 3 and 4.

Damping levels for the bare specimen were much higher than expected. Mode 4 compared to mode 3 yielded higher Q values for similar strain levels. Small differences

between bare and coated specimen damping levels results in small amounts of net damping associated with the mag spinel hard coating.

All of the graphs demonstrate damping levels that are slightly lower than Blackwell's data except for the coated plate, mode 4 scenario. Slight variations in damping levels were common. Of primary concern is the observation that damping levels for both specimens were generally higher (lower values of Q) than expected. The same phenomenon was found during Blackwell's testing.

Table 12. Allen vs. Blackwell Results, Bare Plate, Mode 3

	Mode 3- Blackwell		Mode 3- Allen
Strain (in/in)	Uncoated Q	Strain	Uncoated Q
1.00E-05	330.67	6.65E-05	360
2.00E-05	297.34	8.00E-05	361
3.00E-05	279.42	9.37E-05	349
4.00E-05	267.36	1.08E-04	346
5.00E-05	258.37	1.22E-04	337
6.00E-05	251.25	1.35E-04	340
7.00E-05	245.38	1.95E-04	317
8.00E-05	240.41	2.53E-04	320
9.00E-05	236.11	3.08E-04	325
1.00E-04	232.33	3.59E-04	321
1.50E-04	218.32	4.07E-04	320
2.00E-04	208.91	4.55E-04	311
2.50E-04	201.88	5.06E-04	319
3.00E-04	196.32	6.02E-04	311
3.50E-04	191.73	6.72E-04	305
4.00E-04	187.85	7.61E-04	301
4.50E-04	184.48	8.58E-04	294
5.00E-04	181.53	9.56E-04	292

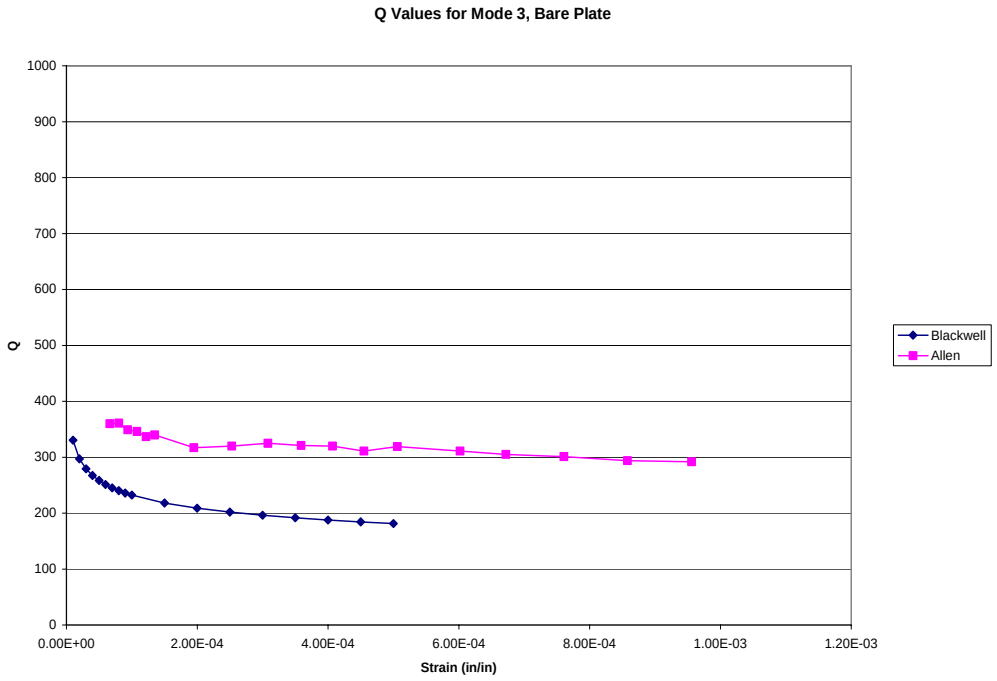

Figure 45. Allen vs. Blackwell Results, Bare Plate, Mode 3

Table 13. Allen vs. Blackwell Results, Bare Plate, Mode 4

	Mode 4- Blackwell		Mode 4- Allen
Strain (in/in)	Uncoated Q	Strain	Uncoated Q
1.00E-05	647.67	4.26E-05	633
2.00E-05	597.39	4.92E-05	621
3.00E-05	569.8	5.65E-05	615
4.00E-05	551	6.38E-05	609
5.00E-05	536.85	7.06E-05	587
6.00E-05	525.56	7.87E-05	592
7.00E-05	516.2	1.13E-04	549
8.00E-05	508.22	1.43E-04	521
9.00E-05	501.29	1.66E-04	487
1.00E-04	495.17	2.03E-04	477
1.50E-04	472.31	2.34E-04	480
2.00E-04	456.73	2.66E-04	473
2.50E-04	445	2.93E-04	471
3.00E-04	435.64	3.17E-04	449
3.50E-04	427.87	3.56E-04	423
4.00E-04	421.26	3.94E-04	377
4.50E-04	415.52	4.27E-04	365
5.00E-04	410.45	4.47E-04	344

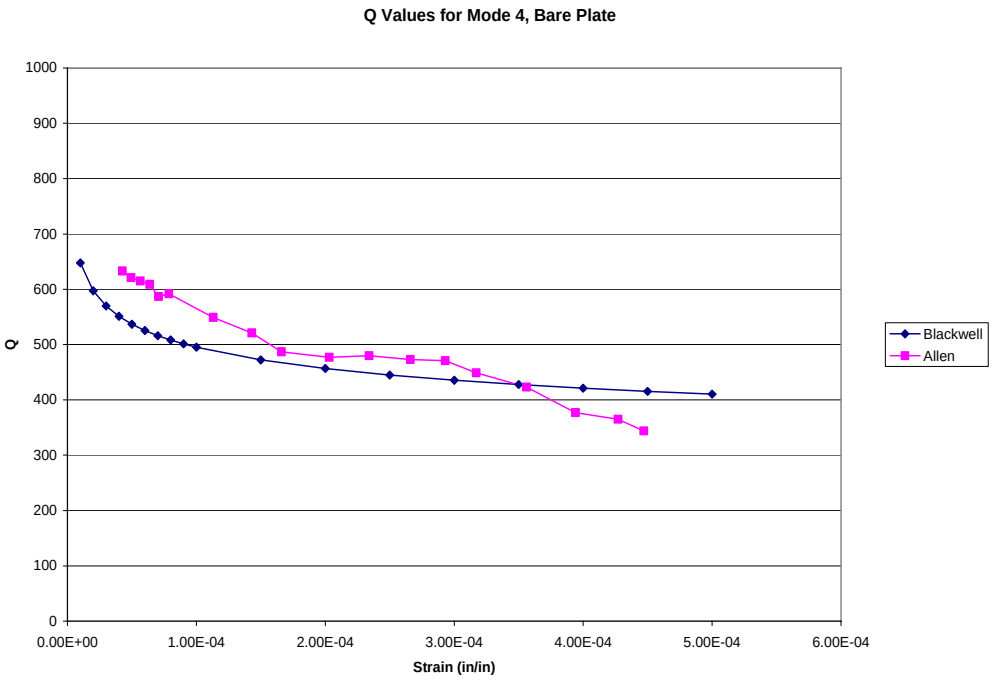

Figure 46. Allen vs. Blackwell Results, Bare Plate, Mode 4

Table 14. Allen vs. Blackwell Results, Coated Plate, Mode 3

	Mode 3- Blackwell		Mode 3- Allen
Strain (in/in)	Coated Q	Strain	Coated Q
1.00E-05	258.28	5.69E-05	197
2.00E-05	228.61	6.41E-05	197
3.00E-05	212.86	7.75E-05	223
4.00E-05	202.36	9.17E-05	223
5.00E-05	194.57	1.04E-04	225
6.00E-05	188.43	1.20E-04	222
7.00E-05	183.4	1.49E-04	210
8.00E-05	179.14	2.00E-04	208
9.00E-05	175.47	2.45E-04	203
1.00E-04	172.25	2.91E-04	198
1.50E-04	160.41	3.82E-04	197
2.00E-04	152.51	4.27E-04	193
2.50E-04	146.65	5.07E-04	191
3.00E-04	142.03		
3.50E-04	138.24		
4.00E-04	135.04		
4.50E-04	132.28		
5.00E-04	129.86		

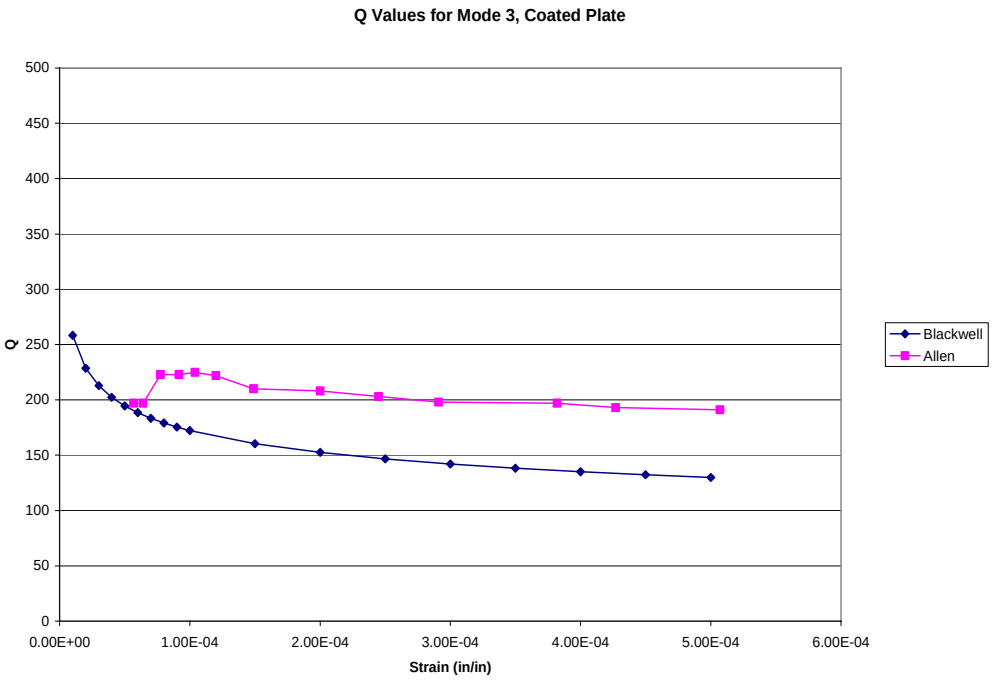

Figure 47. Allen vs. Blackwell Results, Coated Plate, Mode 3

Table 15. Allen vs. Blackwell Results, Coated Plate, Mode 4

	Mode 4- Blackwell		Mode 4- Allen
Strain (in/in)	Coated Q	Strain	Coated Q
1.00E-05	259.52	2.52E-05	304
2.00E-05	208.06	4.15E-05	238
3.00E-05	183.42	5.63E-05	196
4.00E-05	167.97	7.00E-05	187
5.00E-05	157.01	7.00E-05	181
6.00E-05	148.67	9.31E-05	179
7.00E-05	142.02	1.21E-04	152
8.00E-05	136.53	1.49E-04	143
9.00E-05	131.89	1.78E-04	131
1.00E-04	127.9	2.08E-04	132
1.50E-04	113.77	2.37E-04	127
2.00E-04	104.84	2.69E-04	122
2.50E-04	98.47	3.14E-04	131
3.00E-04	93.6		
3.50E-04	89.7		
4.00E-04	86.47		
4.50E-04	83.73		
5.00E-04	81.36		

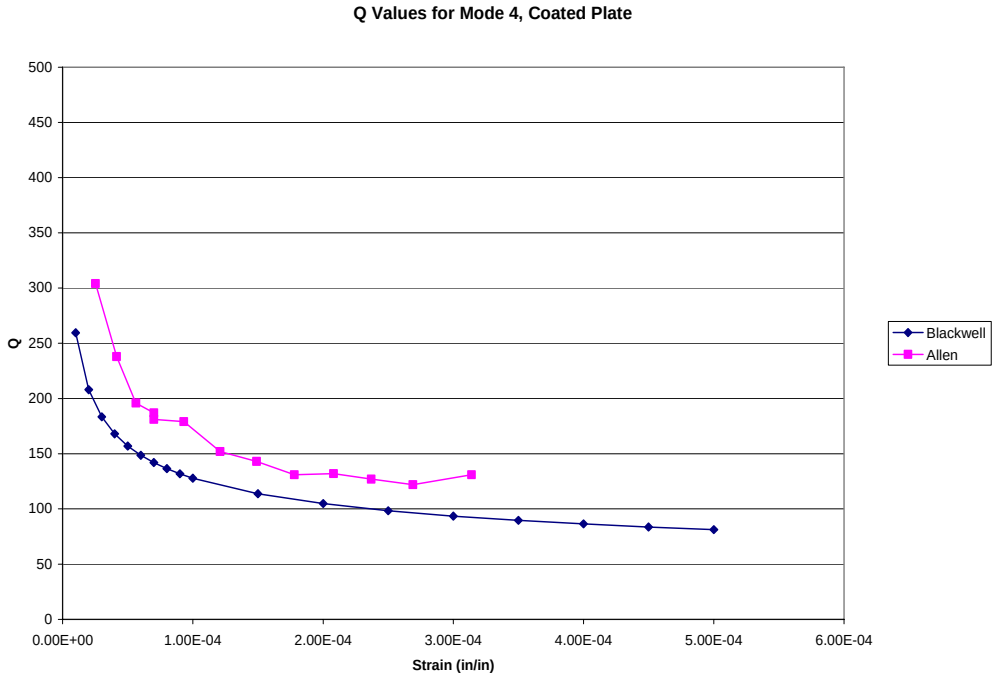

Figure 48. Allen vs. Blackwell Results, Coated Plate, Mode 4

Figure 49 and Figure 50 demonstrate the expected strain softening effect of the mag spinel coating. There was a clear, linear relationship between the peak frequency and the strain level. Thus, as the base excitation was increased, the frequency of the peak decreased. It is important to reiterate that strain was derived from velocity. There was no quantitative relationship between strain and base excitation. This same downshift in peak frequency was not seen for the bare plate specimen.

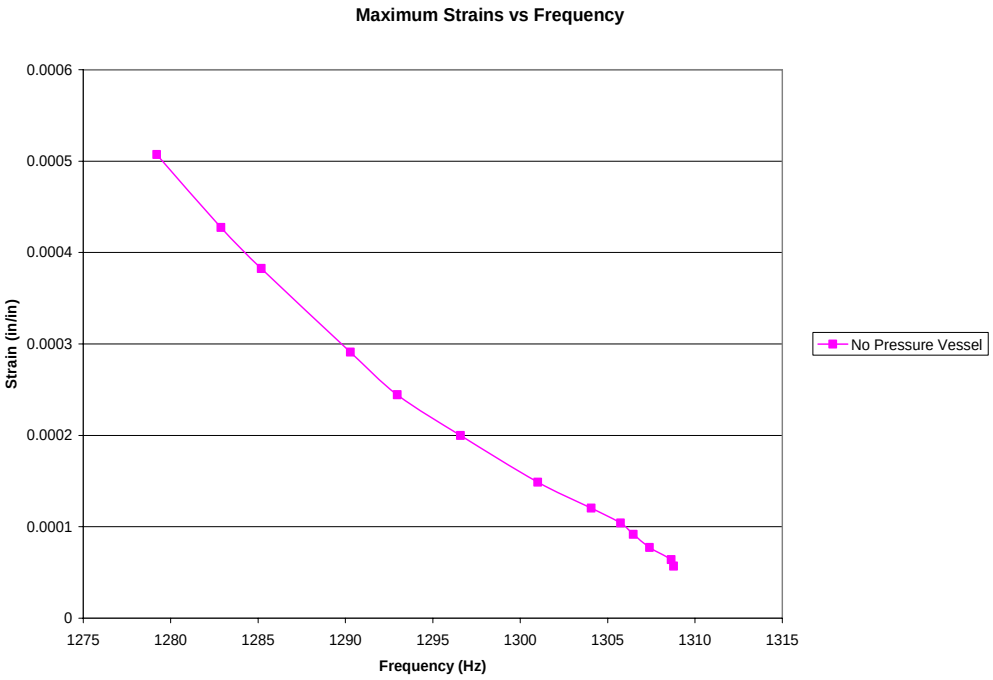

Figure 49. Coated Plate, Mode 3, No Vessel

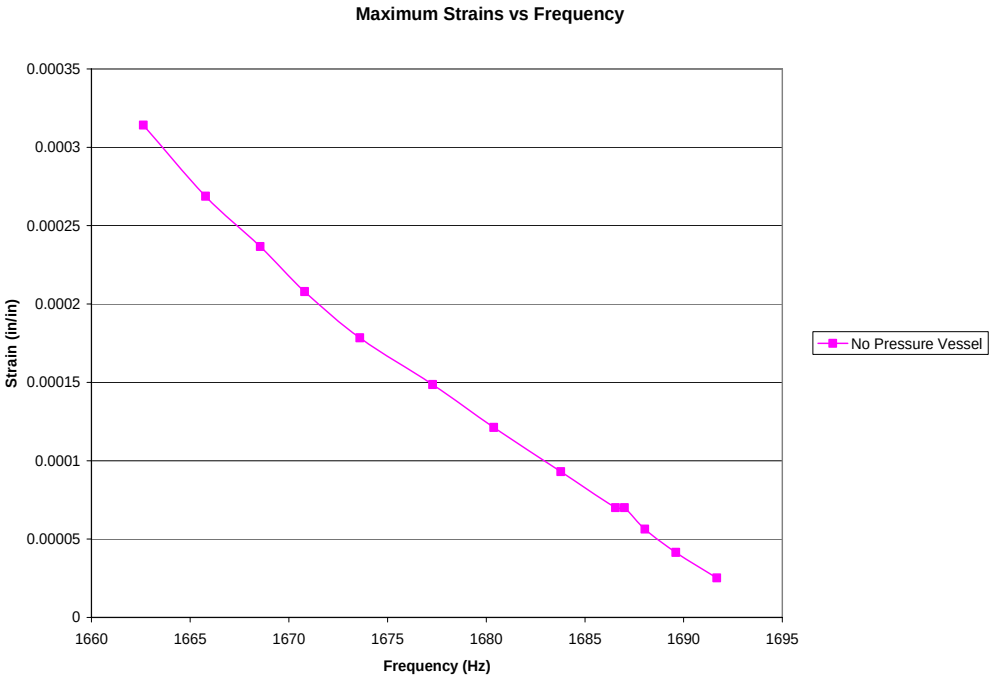

Figure 50. Coated Plate, Mode 4, No Vessel

Partial Pressures

Due to the constraints imposed by the modal interference of the base plate and pressure vessel, the results presented only include testing for the bare plate specimen.

Mode 3

The damping levels versus strain levels are shown below in Figure 51. The figures that correspond to mode 3 display three different base acceleration levels. The three accelerations for mode 3 were 1.0, 5.0, and 9.0 g's. The average difference between the maximum and minimum damping levels under the varying scenarios was 11.7%. However, there was a significant amount of scatter within the data sets. As is demonstrated in Figure 51, no clear trend was present at a specific strain level. No conclusive observation can be drawn other than an increase in damping was seen with an increase in strain.

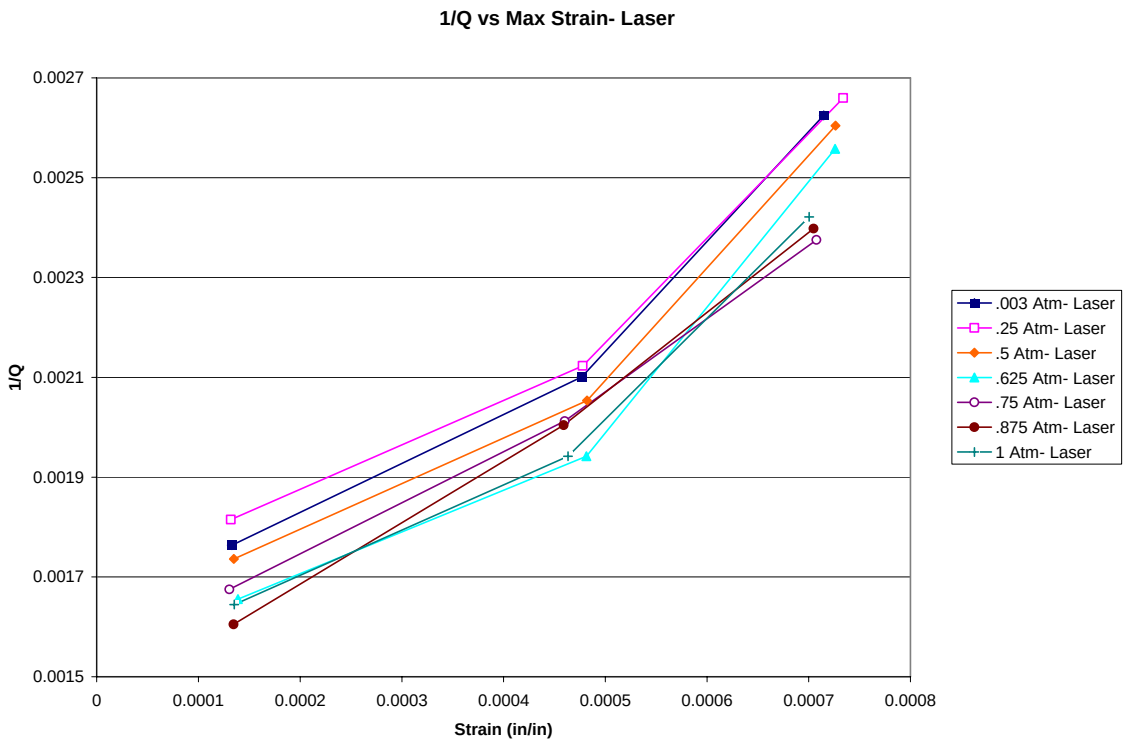

Figure 51. 1/Q vs. Maximum Strain for Bare Plate, Mode 3

Figure 52 clearly demonstrates two trends. The first is the average 0.24% downshift in peak modal frequency between the near vacuum condition and the full atmosphere condition. The intermediate pressures follow the same trend.

Secondly, the peak modal frequencies decreased linearly with increases in strain levels. This held true for all partial pressures. Again, this testing was performed with a bare plate specimen. Therefore, there should be no material damping dependency on strain or frequency.

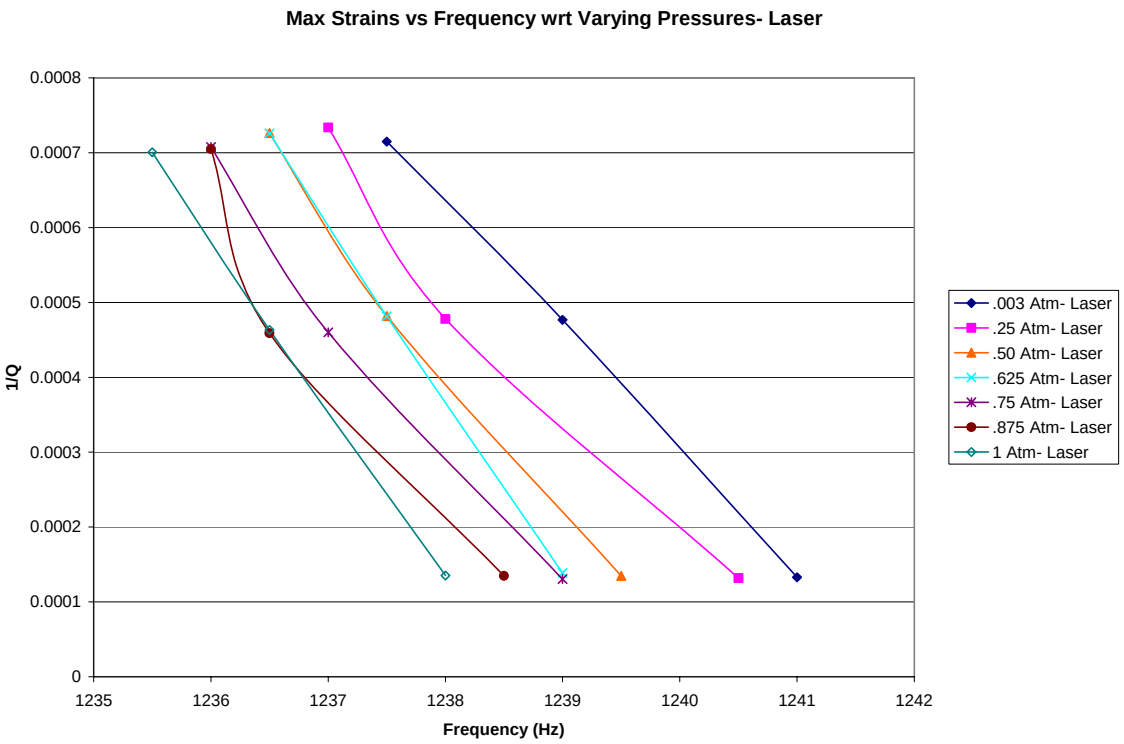

Figure 52. Maximum Strain vs. Frequency for Bare Plate, Mode 3

Mode 4

Much clearer trends in damping are shown below for mode 4 in Figure 53. Testing for mode 4 subjected the specimen to three different base acceleration levels of 1.0, 5.0, and 9.0 g's. There was an average difference of 20.1% in damping for a given strain level between near vacuum and full atmosphere condition. Additionally, this increase in damping trend was demonstrated at the partial pressures. Each partial pressure aligns from near vacuum through full atmosphere in sequence for a given strain level.

The largest changes in damping were between the .875 atm and 1.0 atm. This change accounted for nearly 3/4 of the average 20.1% change in damping.

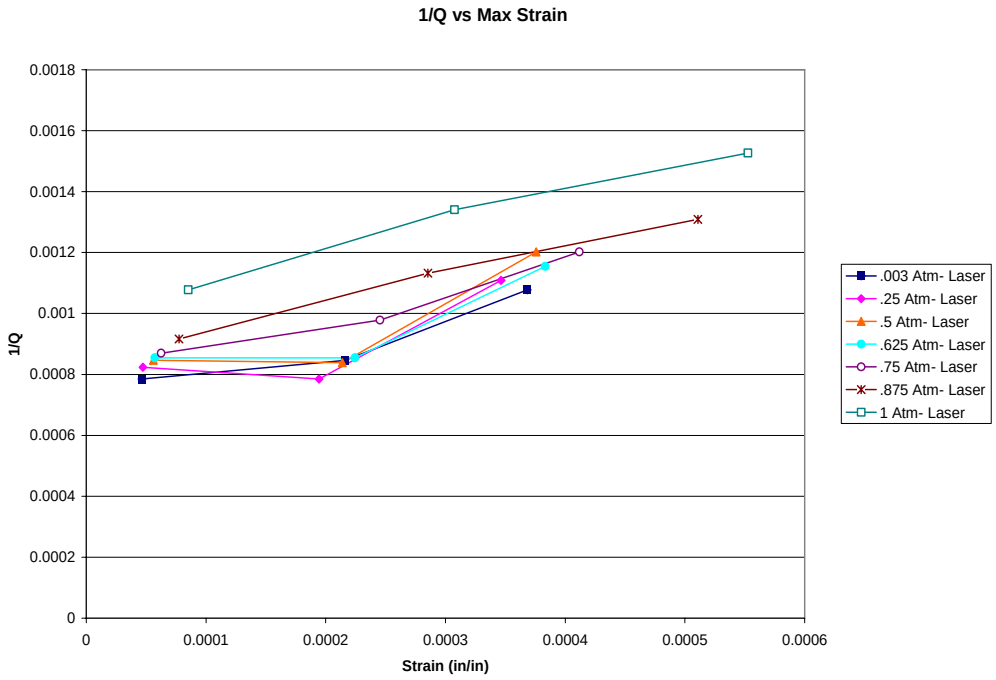

Figure 53. 1/Q vs. Maximum Strain for Bare Plate, Mode 4

In reference to the modal peak frequency, the trends prevalent in mode 3 results were visible for mode 4. Figure 54 demonstrates the average 0.18% difference in peak frequencies between the near vacuum and full atmosphere condition. Again, this trend held true at varying partial pressures as well as at the near vacuum versus full atmosphere.

Also visible is the trend of decreased modal frequency with increased strain. This trend was not as clearly linear as it was for mode 3, but it was generally true for all partial pressures.

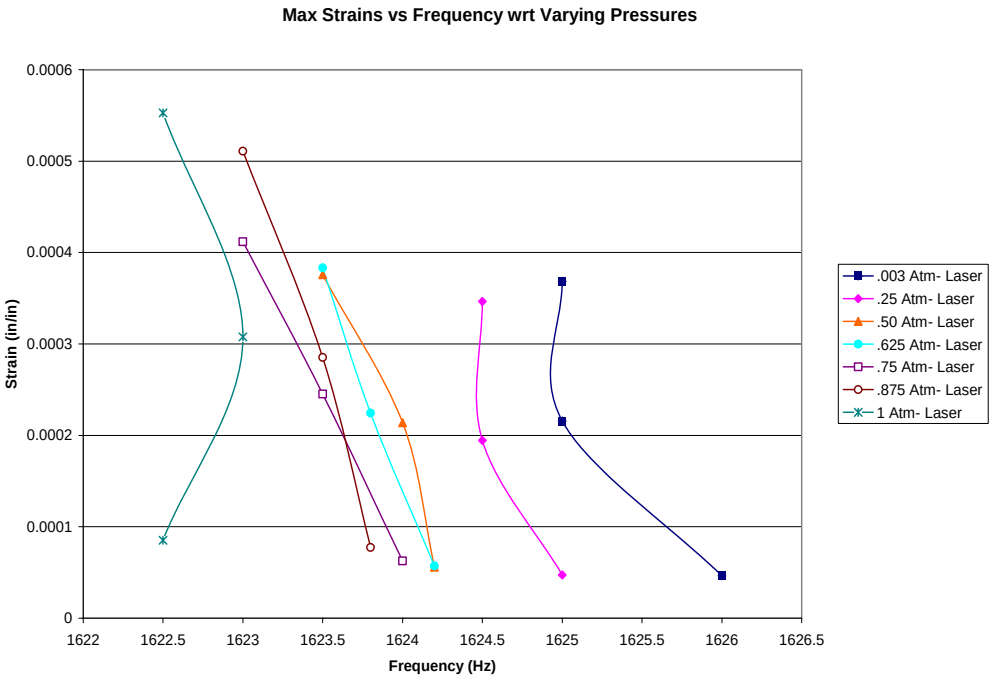

Figure 54. Maximum Strain vs. Frequency for Bare Plate, Mode 4

Clamped Condition Variations

The clamped boundary condition was altered in order to determine the effectiveness of the constraint blocks during various constraint conditions.

Table 16 below lists the Q values for varying torque conditions. This testing was performed in order to estimate the effect of the "softening" of the clamped condition. All tests were performed with a bare plate specimen. The torque values were based upon the normal torque setting of 125 ft-lbs, 100 ft-lbs, and 120 in-lbs for the inner bolts, middle bolts, and jack bolts respectively. The "100%" column in the table represents Q values found at these torque settings. The increases in torques were limited by the material strength of the bolts.

The bare plate yielded low values of Q for all settings. There appeared to be no significant benefit from increasing the torque of the attachment bolts for either mode 3 or 4. However, the larger Q values for mode 4 revealed that perhaps mode shape is of significance when determining the influence of the blocks on the perfectly clamped condition. The 2nd bend (mode 3) presented greater difficulties for the clamp.

Table 16. Torque Testing Table

	75% Torque	87.5% Torque	100% Torque	112.5% Torque	125% Torque	Difference (max vs. min)
Mode 3						
.5 g	110.74	139.7	212.4	183.21	190.74	41.94%
3.0 g	86.81	101	152.48	129.14	136.71	36.50%
6.0 g	94.65	127.05	131.41	167.01	130.87	27.68%
Mode 4						
1.0 g	647.32	593.04	734.23	593.49	623.25	-3.86%
5.0 g	475.07	539.55	510.52	519.32	522.98	9.16%
9.0 g	400.99	447.41	515.16	467.01	482.47	16.89%

Also of interest for the clamped condition was the ability of the blocks to apply a uniform boundary condition. In other words, does the right end of the blocks apply the same forced excitation on the specimen as the middle and left of the blocks? Figure 55 and Figure 56 below demonstrate the response of the blocks when they were measured using the laser vibrometer. The responses are labeled left, middle, and right to denote the approximate location of measurement. The figures represent only one response for mode 3 and one response for mode 4 with 5g base excitation. Responses at varying forced excitation levels are shown in Appendix C: Constraint Block Results. For explanation reasons, a specimen response divided by 100 is overlaid on the block responses.

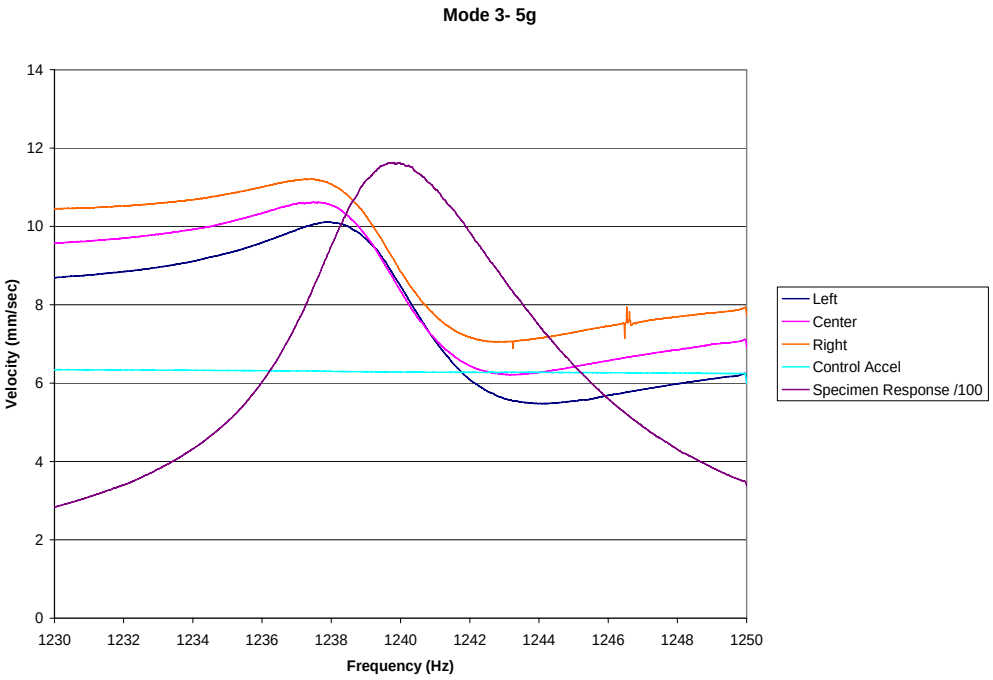

Figure 55. Mode 3, 5g Base Excitation

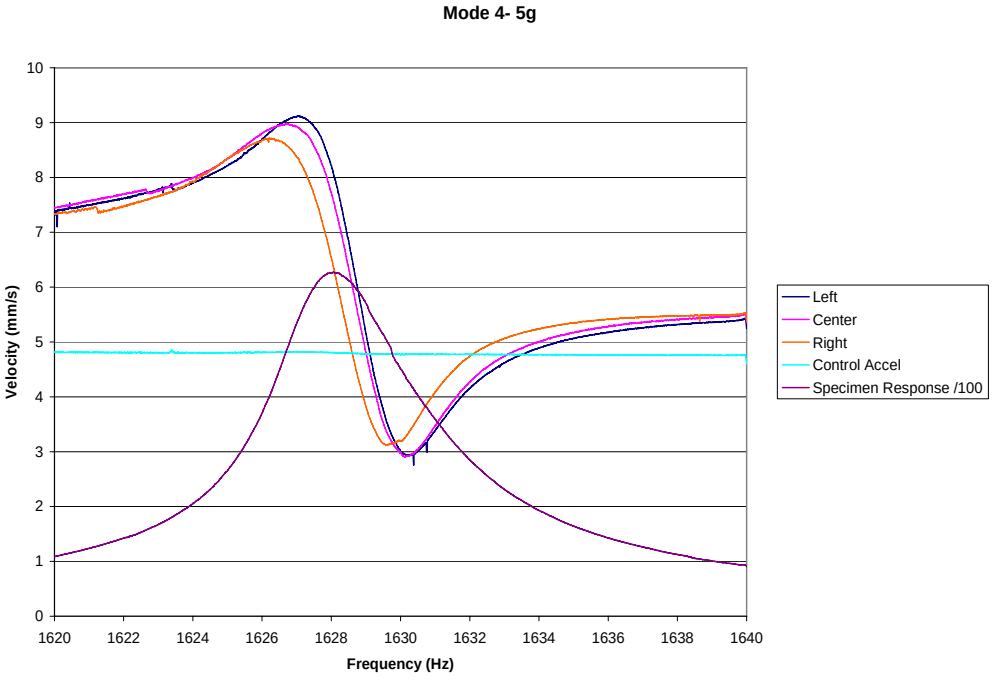

Figure 56. Mode 4, 5g Base Excitation

There is close proximity of the overlaid responses of varying constraint block locations. Thus, the ability of the blocks to clamp the specimen, whether or not it is perfectly clamped, was relatively uniform across the boundary of the plate.

While the control accelerometer stayed at a constant g level throughout the sine sweep, the block acceleration did not. It is important to note that the control acceleration was converted and then graphed as velocity in the above figure. The variation may have been caused by either modal interference of the base plate, as will be discussed in the following sections, or by the modal influence of the specimen.

The test was performed with a specimen within the constraint blocks. Therefore, the mode of the specimen influenced the response of the blocks. The overlaid response was taken from a 5 g test for both modes 3 and 4. The graphed signal was divided by 100. The variations in acceleration corresponded with the modal frequencies of the specimen. Hence, the peaks and dips, which correspond to the overlaid specimen response, signify that the specimen itself had a great influence on the oscillation of the blocks.

However, outside of the range of specimen modal interference, the blocks did not show the exactly same velocities as the control accelerometer. For this reason, the base plate most likely interfered with the system in the frequency range of interest.

Base Plate Interference Results

Ping testing was performed on the base plate. These results are shown below in Figure 57 and Figure 58. These were performed for various test setups. The two most applicable, “No Vessel, Specimen in Blocks” and “With Vessel, with Bungee Cords,

Specimen in Blocks" are shown below. All other ping results are shown in Appendix B: Ping Testing Results.

The bottom of the graph denotes the frequency. The vertical axis denotes the amplitude of the response. Because the impact of the hammer on the base plate was not measured during testing, the amplitudes of response are not comparable between the below graphs. The magnitudes of the frequency peaks are only comparable to other peaks within the same graph. The peak frequency locations in the below graphs denote the modes of the base plate. There were clearly possible interference issues for conditions shown below. Modes 3 and 4 for the specimens are approximately 1230 and 1640 Hz. Therefore, peaks around the frequencies of interest could affect the test results.

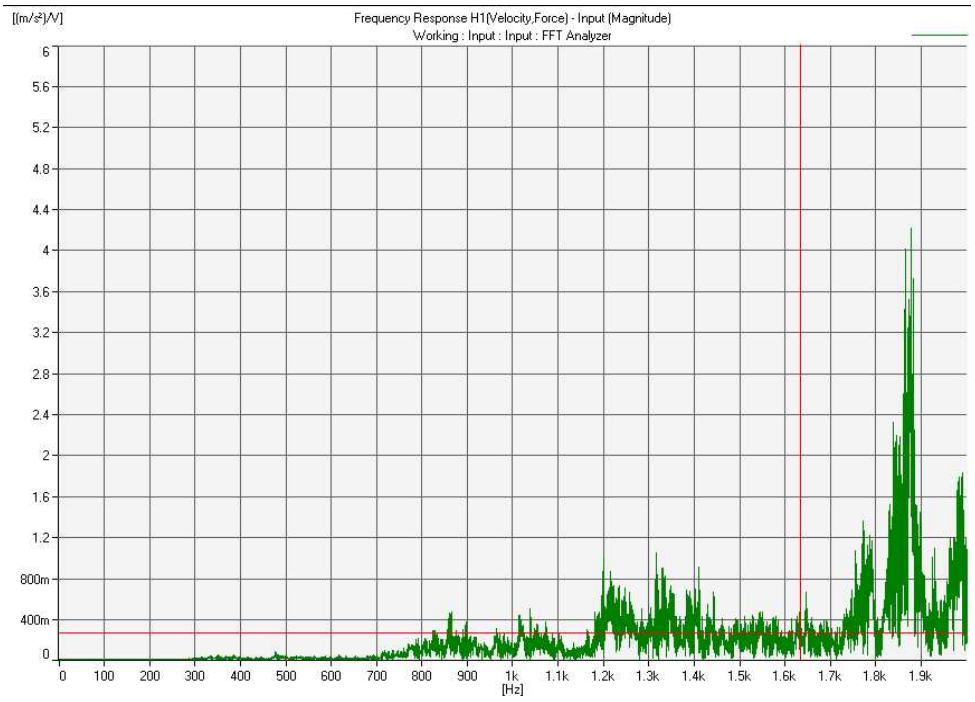

Figure 57. Ping Testing Results with Vessel, without Specimen in Blocks, with Bungee Cords

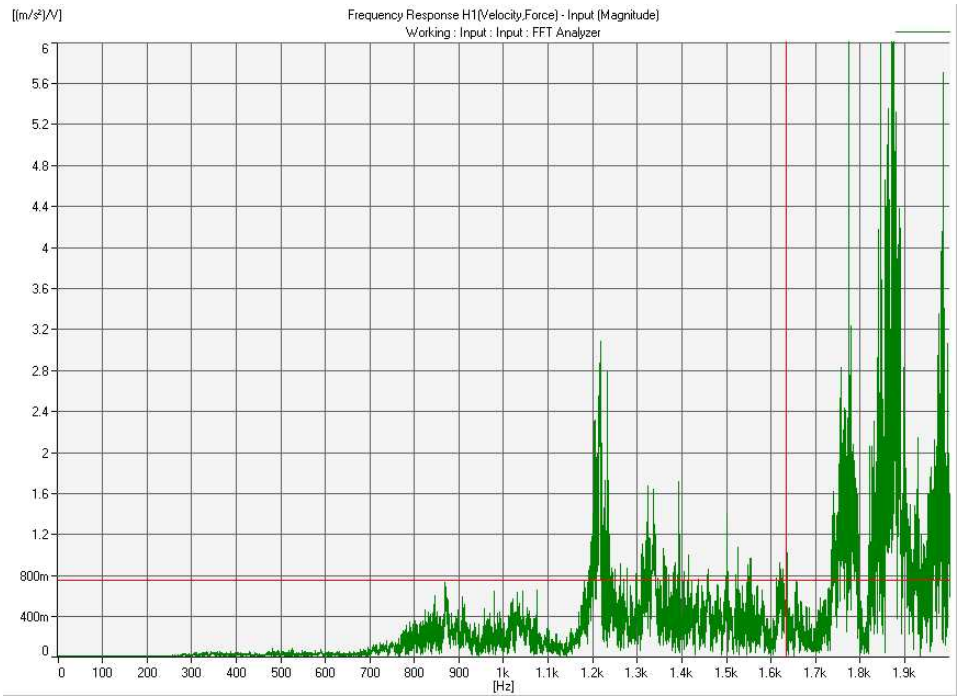

Figure 58. Ping Testing Response with Pressure Vessel, without Specimen in Blocks, without Bungee Cords

Interferences are shown below in Figure 59. The picture of the oscilloscope was taken during a down sweep with the pressure vessel on the shaker head. The overlapping signal shown is the modal interference of the base plate in the response of the specimen during the sine sweep. The signal in the figure with two sine waves combined into one response depicts both the base plate response and the specimen response in the same wave. The smooth and uniform sine wave illustrates the control signal.

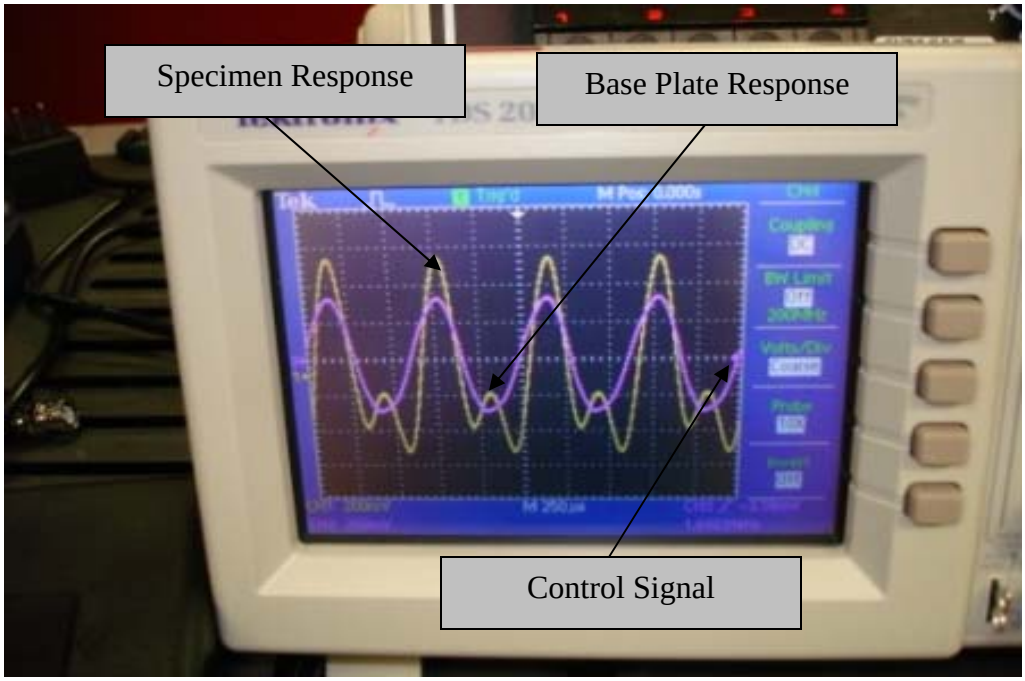

Figure 59. Oscilloscope Output Demonstrating Modal Interference

This interference was only seen in isolated circumstances. Specifically, these were: partial pressure testing using a coated plate and foam testing using a coated plate. When the peak response of the specimen was distinct, there was no serious alteration in the damping, modal frequency, or strain. However, in the limited circumstances demonstrated in both the above figure and Figure 60 below, this interference clearly affected the measured damping. Therefore, test results were not used in all circumstances with possible interference from the base plate. Specifically, interference was seen for the coated plate under varying pressures and foam testing using the coated plate. This is why all comparisons performed at varying pressures used the bare specimen.

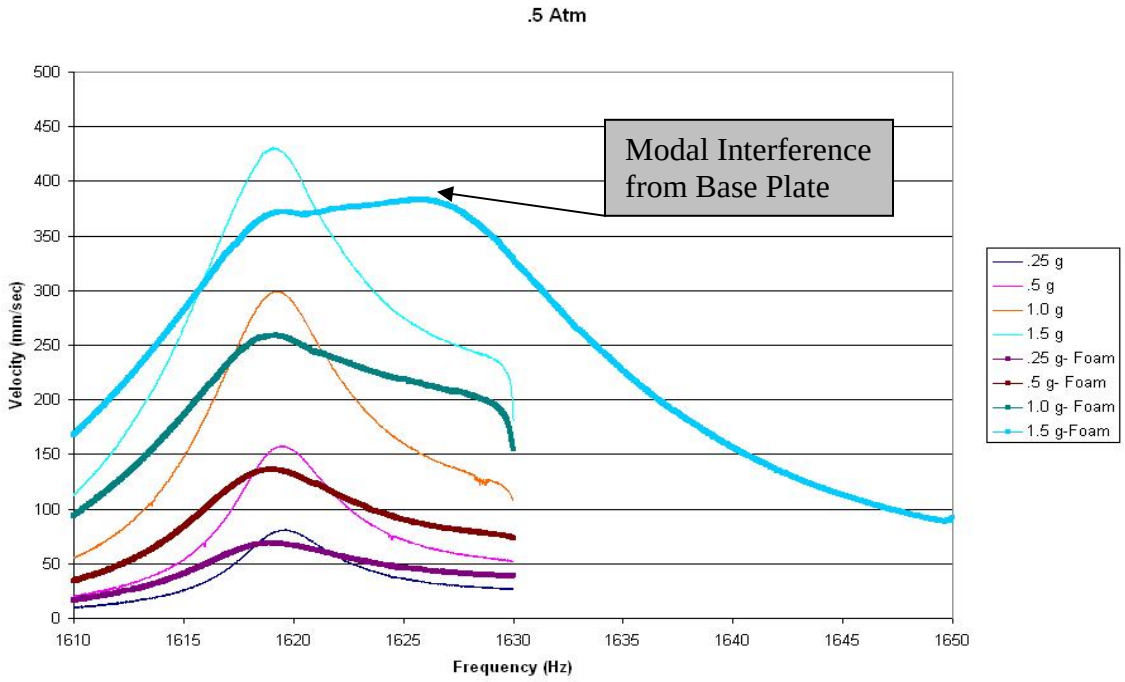

Figure 60. Base Plate Interference

In Chapter III, the location of the control accelerometer was discussed. During certain phases of testing with the coated plate, higher base excitations were desired in order to force certain strain levels in the specimen. In attempting to force higher base excitation in the coated specimen, troubles were encountered with uncontrollable interference with the base plate and pressure vessel. The above figure demonstrates testing that was performed with a mag spinel coated plate tested at .5 atm. The interference increased with amplified base excitation levels.

The location of the control accelerometer was altered in an attempt to alleviate these difficulties. Unfortunately, certain interference issues persisted. Therefore, no useable data was produced from partial pressure testing with the coated specimen. The

interference issues did not impact the validity of damping measurements for the coated plate testing without a pressure vessel.

It is important to note that the location of the control accelerometer was not altered during any single set of testing (as denoted by individual boxes in Figure 21). For this reason, each base excitation level (g level) is valid for comparison only within a data set. For example, comparing a 5 g sweep without the pressure vessel mounted to the shaker head to a .5 atm, 5 g sweep with the pressure vessel mounted to the shaker head is not a valid comparison. For this reason, the comparisons within this study contrast strain levels, damping levels, and peak modal frequency. This is a valid comparison.

Tip Accelerometer versus Laser Vibrometer

The accuracy of the laser vibrometer was verified by attaching a small accelerometer to the bare plate specimen tip. Figure 61 and Figure 62 demonstrate the output from partial pressure testing using the shaker. The figures represent the data measured for both modes 3 and 4. There is a difference between the accelerometer and laser vibrometer readings, which was exacerbated as the base excitation was increased.

In the figures below, the lines with squares at the data points correlate to the laser vibrometer readings. The lines with the triangles at the data points correlate to the accelerometer placed on the tip of the specimen. The accelerations listed in the legend of the figures correspond to the inputted acceleration.

The apparent dramatic rise of strain at pressures near one atmosphere in Figure 62 was also worth examination. Two possible reasons for this rise were the modal interference of the base plate and pressure wave interactions between the vessel and the

specimen. The degree of coupling between the base plate and the specimen response may have been affected by the addition of the pressure vessel. The addition of air inside the vessel allowed for the reverberation of pressure waves with the vessel. This in turn may have caused additional specimen excitation. Additionally, this was not see for mode 3. Therefore, if the pressure wave interference were an issue, it would seem to have had modal dependence.

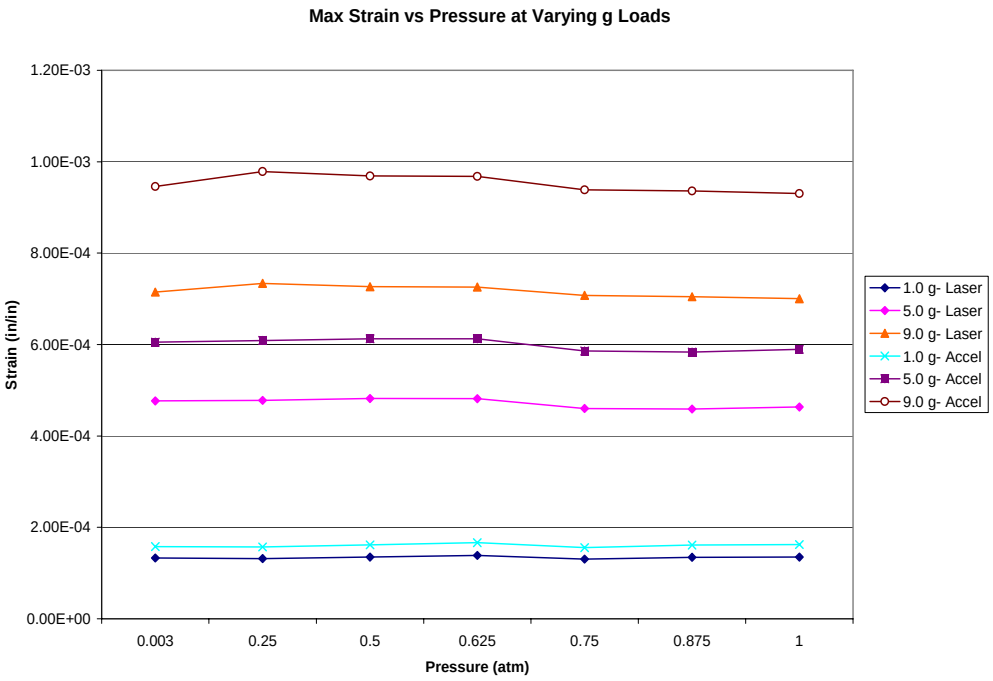

Figure 61. Strain vs. Pressure for Laser Vibrometer and Tip Accelerometer, Mode 3

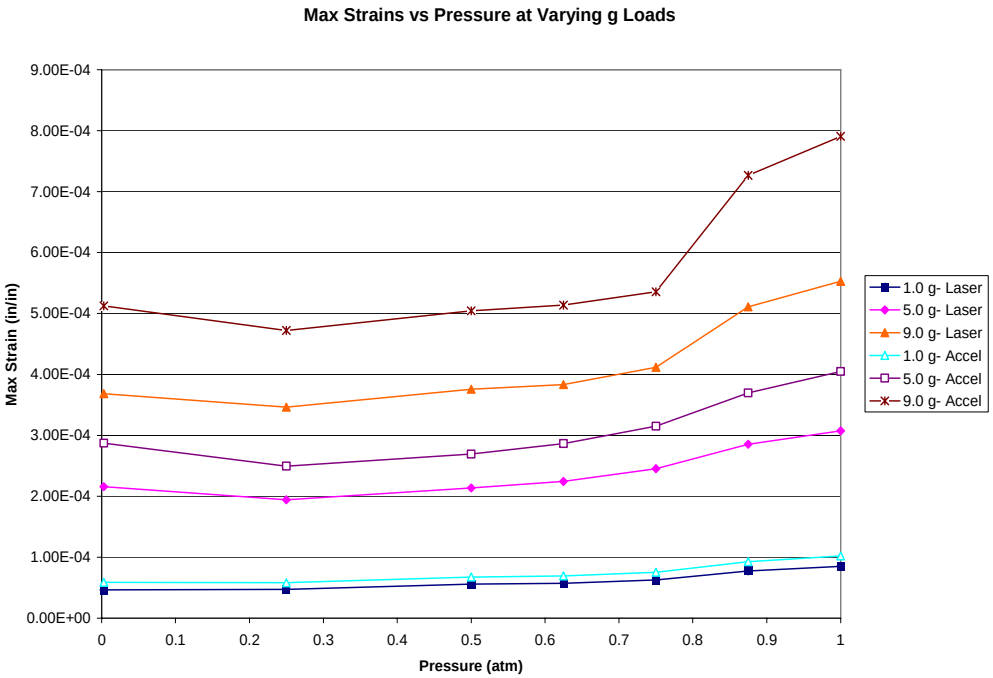

Figure 62. Strain vs. Pressure for Laser Vibrometer and Tip Accelerometer, Mode 4

Table 17 below denotes the differences between the accelerometer and laser vibrometer readings. All differences listed are the averages taken for each base excitation level. It is important to note that all measurements for the laser vibrometer and tip accelerometer were taken concurrently. The difference between the readings increased as the base excitation increased. The trend was true both for modes 3 and 4.

Table 17. Tip Accelerometer and Laser Vibrometer Differences

	1 g Base Excitation	5 g Base Excitation	9 g Base Excitation
Mode 3	16.04%	21.23%	24.42%
Mode 4	18.64%	22.12%	28.11%

The reasoning for these differences included two causes. The first, the accelerometer lost accuracy with increased excitation. Per the manufacturer's specifications, g levels of greater than 500 g's induced errors in measurement. This excitation level is not to be confused with the base excitation. The base excitation is the excitation experienced at the root of the specimen. Alternatively, the data shown in Figure 61 and Figure 62 represents measurements taken from the accelerometer on the tip on the specimen. For both the 5 g and 9 g base excitation tests, the tip acceleration exceeded 500 g's. The error induced measured 2% for every 100 g's above the 500 g threshold.

The second possible reason for the difference deals with the perceived velocity of the laser vibrometer versus the actual acceleration seen by the tip accelerometer. The laser vibrometer only measured the velocity in the vertical direction. However, the tip accelerometer measured both the in-plane and out-of-plane accelerations. The excess accelerations were caused by the out-of-plane translations of the plate established by the mode shape of the specimen during the oscillation. This out-of-plane acceleration was added to the in-plane acceleration for the total acceleration registered by the accelerometer on the tip of the plate.

Temperature Variations

Repeatability was seen as an issue during certain phases of testing. For this reason, different causes were investigated that might influence the results. A thermo-couple was mounted on the blocks to monitor the temperature throughout a day of testing. Bookend sweeps, which repeated the first sine sweeps of the day, were run and the

change in temperature was noted. Figure 63 and Figure 64 below demonstrate a typical change in peak frequency over the course of an 8 hour day of testing. Changes in temperature as great as 20 degrees were witnessed over an 8 hour period. The peak modal frequencies downshifted as much as 1%.

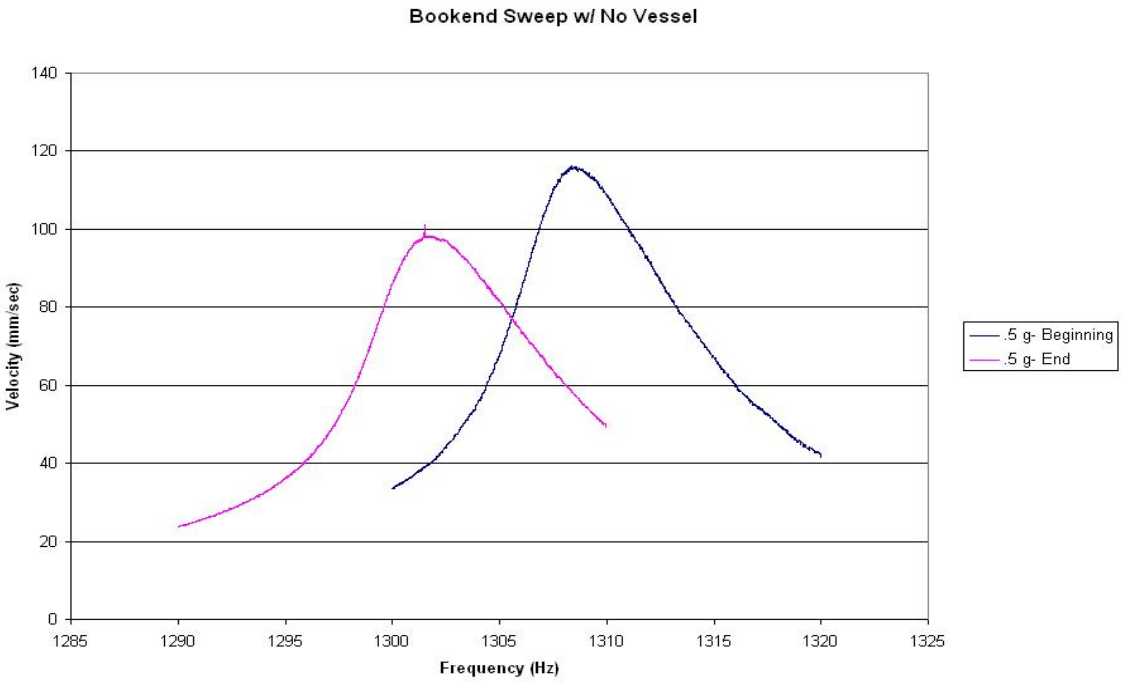

Figure 63. Bookend Sweep for Mode 3

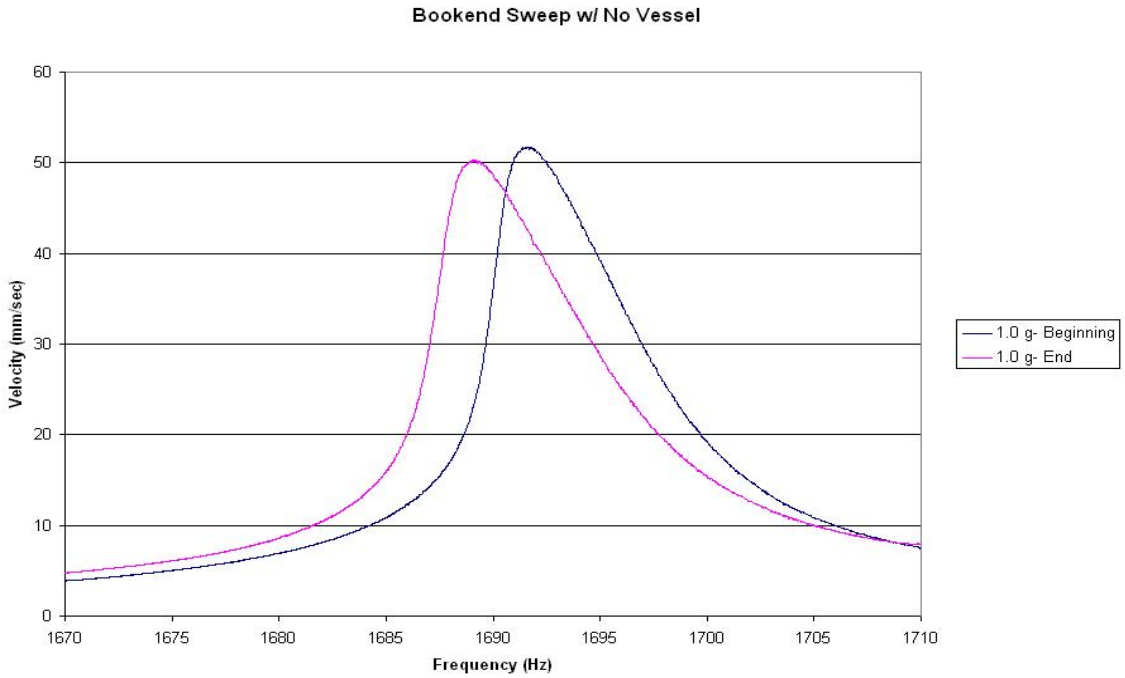

Figure 64. Bookend Sweep for Mode 4

One possible explanation for this frequency shift is the change in the specimen modulus of elasticity. Figure 65 below shows the effect of increased specimen temperature on the modulus of elasticity. An increase in room temperature of 20 degrees may lead to significant enough change in modulus for the examiner to incorporate this when accounting for possible reasoning behind frequency downshifts during testing. From the below figure, a 20 degree shift in temperature equates to an approximate 0.7% change in the modulus of elasticity.

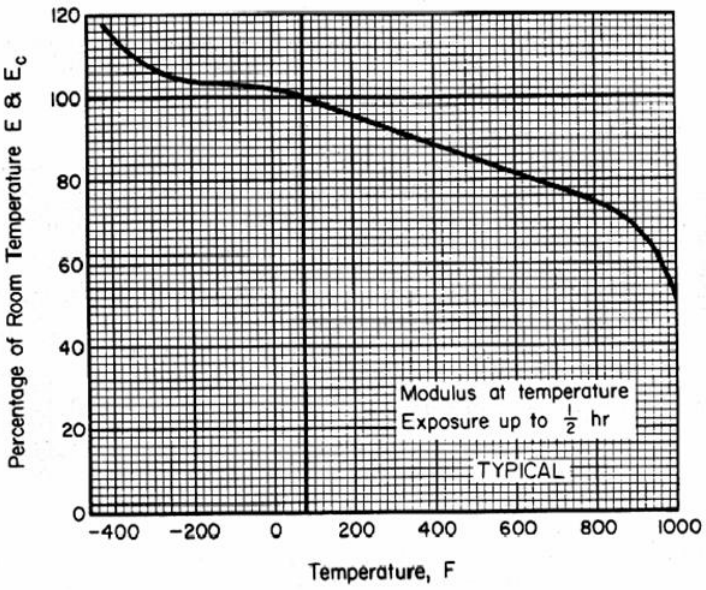

Figure 5.4.1.1.4. Effect of temperature on the tensile and compressive moduli (E and E_c) of annealed Ti-6Al-4V alloy sheet and bar.

Figure 65. Changes in Modulus of Elasticity with Changes in Specimen Temperature (13)

Pressure Wave Excitation

Testing that contrasted excitation of the specimen without the pressure vessel and with the pressure vessel minus a viewing window was performed. The viewing window was removed to alleviate some of the possible pressure wave excitation witnessed by the specimen. The contrasting graphs are shown below in Figure 66 and Figure 67.

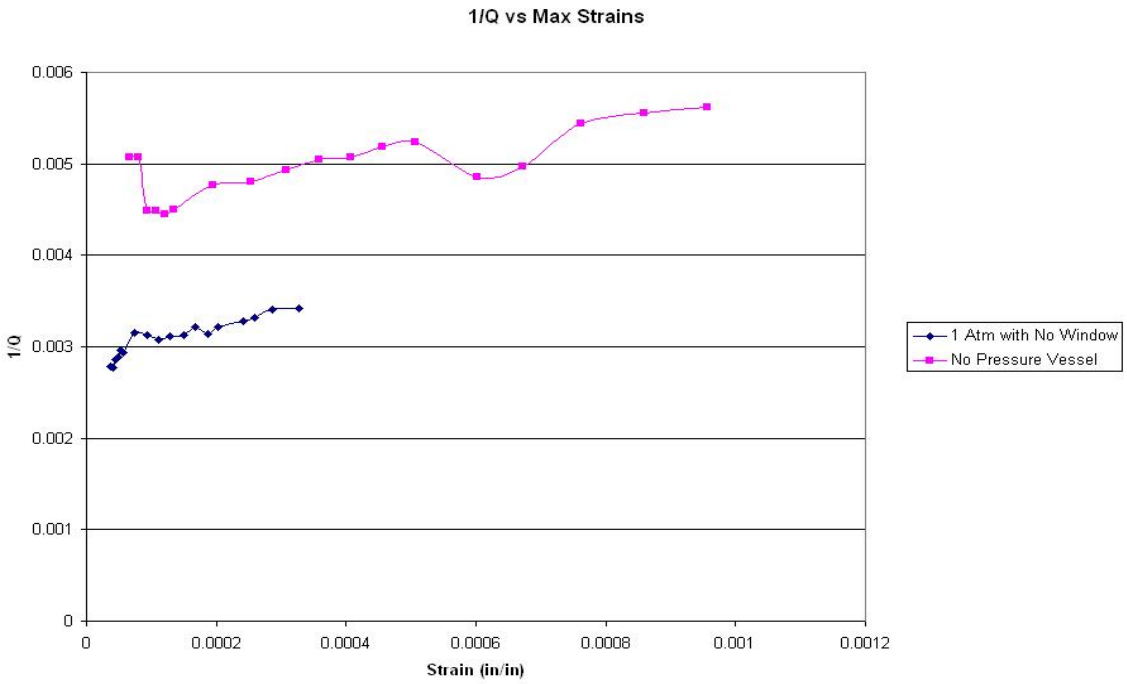

Figure 66. 1/Q vs. Maximum Strain for Atmosphere Testing without Viewing Window, Mode 3

The above figure demonstrates the strain versus damping comparison for mode 3. In both scenarios, the base plate was subjected to the same loading condition. Slight variations in damping occurred within each data set around 100 micro-strain. Certain loading conditions resulted in the same strain, with much lower damping for the vessel without a viewing window scenario. The average difference of 40% may have been caused by some pressure wave interference caused by the reverberation of pressure waves off either the inside of the pressure vessel or off of the base plate. Testing without a pressure vessel allowed for the pressure waves to dissipate into the surrounding medium.

In addition, the general trend of increased damping with increased strain was seen. This testing was performed with a bare specimen. This trend again pointed towards softening of the constraint blocks at higher strain levels.

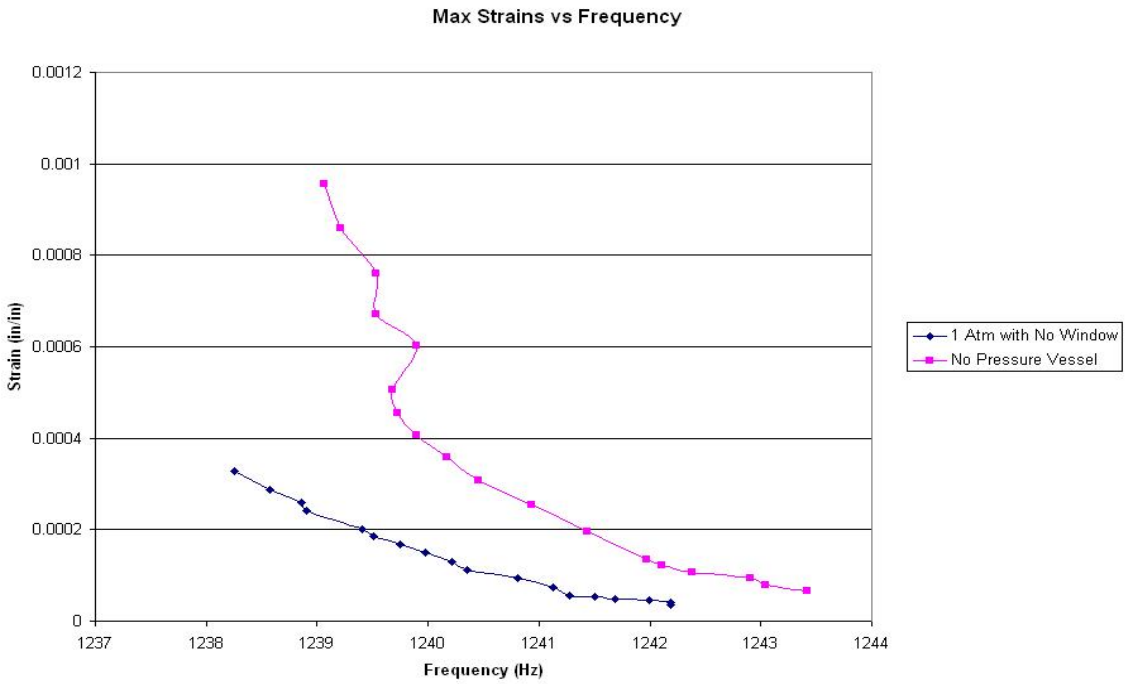

Figure 67. Maximum Strain vs. Frequency for Atmosphere Testing without Viewing Window, Mode 3

The above diagram again shows the trend of peak frequency downshifts with increases in strain. This was true for both testing conditions. The “no window” scenario exhibited the different peak frequency values for a given strain level. There was a downshift in peak frequencies for the “no window” scenario in comparison to the “no pressure vessel” scenario.

Figure 68 and Figure 69 show the same set of testing, but correspond to mode 4 for the bare plate specimen. Again, lower damping was seen for the vessel without a window than for the "no vessel" scenario. The specimen exhibited an average of 37% higher damping level for a given strain level. The damping increased with strain in both situations.

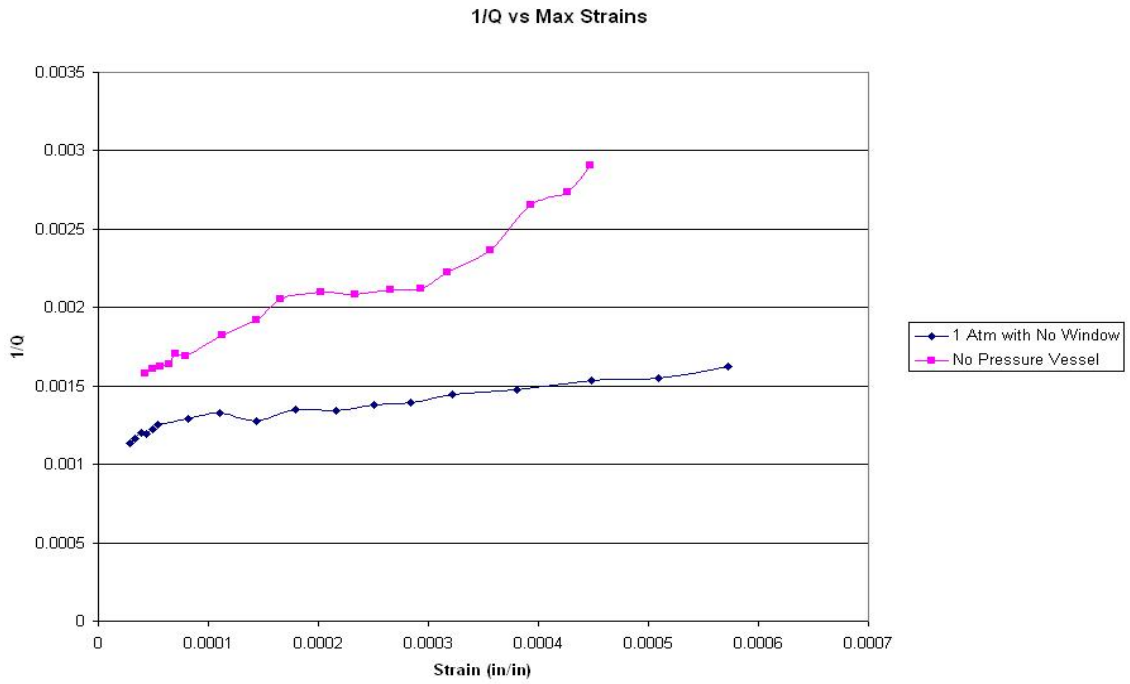

Figure 68. 1/Q vs. Maximum Strain for Atmosphere Testing without Viewing Window, Mode 4

Finally, the peak frequencies for mode 4 matched closer for a given strain level than for mode 3. Contrary to mode 3, the "no vessel" scenario displayed slightly lower peak frequencies for a given strain level. See Figure 69 below.

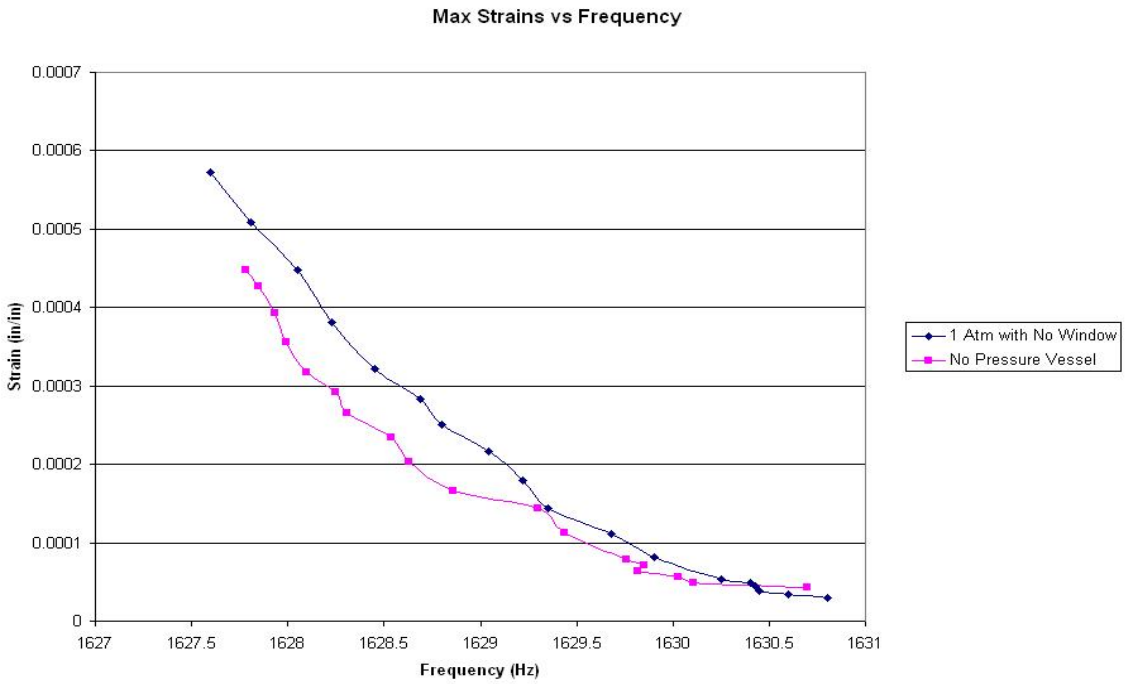

Figure 69. Maximum Strain vs. Frequency for Atmosphere Testing without Viewing Window, Mode 4

Foam testing as described in Chapter III was attempted to demonstrate the effects of the standing wave under the test specimen during oscillation. Unfortunately, a coated specimen was used during this section of testing and there was too much interference with the base plate to make the data valid. Therefore, the results are not listed. Foam testing did not confirm nor discount the standing wave theory.

Stationary Vessel Testing

The results of the stationary pressure vessel testing revealed that under small strain levels, an increase in pressure caused both a slight change in the damping and the modal peak frequencies. Figure 70 below demonstrates the change in Q values for different modes for the 9.5” x 4.5” x 0.125” titanium plate described in Chapter III. These Q and modal frequency values were found using an eigensystem realization

algorithm (5). There were too few data points to use a half-power bandwidth method for determining Q. Using the half-bandwidth method for this section of testing would have caused significant variations in Q, dependent upon data points chosen for analysis.

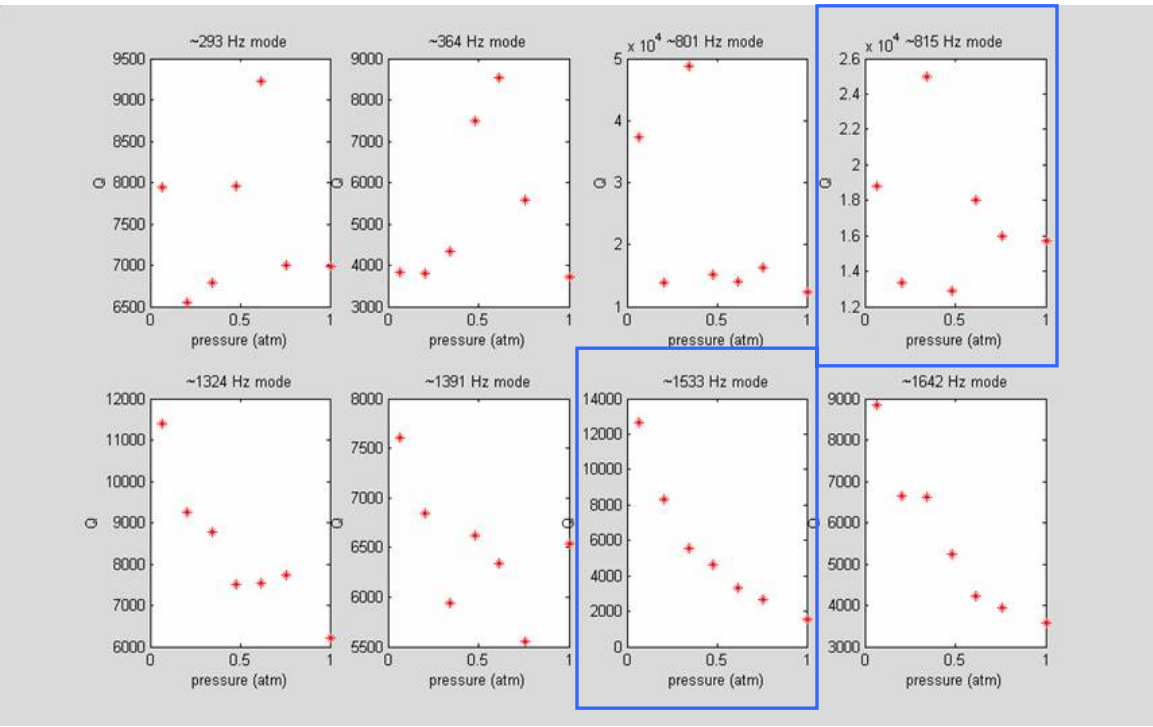

Figure 70. Q Values at Varying Pressures

The two modes of interest were 815 Hz and 1533 Hz. These two modes have similar mode shapes as modes 3 and 4 for the 4.5" x 4.5" x .125" plate. There was not a significant change in Q corresponding to pressure changes for mode 4. Although there were variations in damping at varying atmospheres, the data does not trend in any one direction. No significant conclusions could be drawn about the relationship between pressure and damping for mode 4. The data indicates significantly large Q values of greater than 10,000.

Alternatively, mode 7 showed a nearly linear dependence upon change in pressure. An 85% drop between near vacuum (.04 atm) condition and full atmosphere (.98 atm).

Although it was not of specific interest for this study, mode 5 and 8 also showed damping dependence on pressure. A drop in Q of 67% occurred from the near vacuum condition to .5 atm. Again, the Q values were significantly larger than those found during shaker testing. With a minimum Q value of just less than 2,000, mode 7 revealed Q values significantly less than the mode 4 values which were greater than 10,000.

The Q values of far greater than 1,500 at every pressure, for both modes investigated, were considerably larger than all Q values found during testing performed using the electrodynamic shaker. The free-free-free-free boundary condition during testing eliminated the damping due to the clamp in a clamped-free-free-free condition. The stationary pressure vessel results show that air damping was present, but may have been negligible compared to the other damping mechanisms present in the electrodynamic shaker testing. It should again be noted that the strain levels during this section of testing were significantly smaller than were excited during electrodynamic shaker testing. Magnet excitation limited the feasible strain levels.

Figure 71 below graphs the relationship between peak modal frequency and atmosphere for the 9.5” x 4.5” x 0.125” plate. The modal frequencies changed with respect to pressure for every both mode tested. Specially, both modes 4 and 7 showed a linear dependence upon pressure.

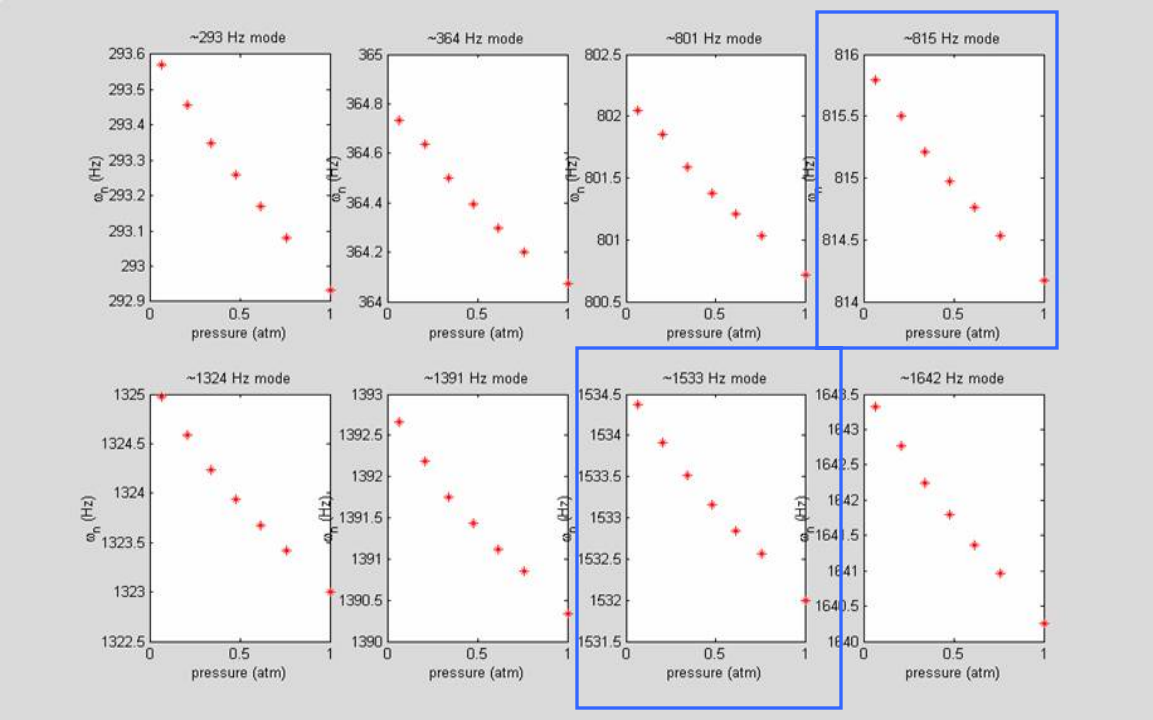

Figure 71. ω_n Values at Varying Pressures

Mode 4 showed a 0.19% downshift in modal frequency (ω_n) from near vacuum to full atmosphere. Mode 7 revealed a 0.17% downshift in frequency from near vacuum to full atmosphere condition.

V: Conclusions and Recommendations

Conclusions

Damping levels for the coated and uncoated 4.5” x 4.5” x 0.125” specimen were initially verified with past values. Mode 3 showed minimal net damping due to the coating. Mode 4 yielded an average difference in damping of 68% between the coated and bare plate. The average net Q value of the mag spinel material for mode 4 was 230. Damping levels for given strains matched closely for both coated and uncoated plates for modes 3 and 4. Expected increases in damping with strain were observed for the coated plate. Peak frequency downshifts were also observed with increases in strain levels in both the coated and uncoated specimen.

Mode 3 (2^{nd} bend), clamped-free-free-free, for the bare titanium specimen yielded the following results during partial pressure testing:

1. No quantifiable trend between increases in damping with increased pressure.
2. A 0.24% average decrease in peak modal frequency between near vacuum and full atmosphere condition.
3. Trend of increased damping with increases in strain.
4. Trend of decreased peak modal frequency with increases in strain.

Mode 4 (two-stripe), clamped-free-free-free, for the bare titanium specimen yielded the following results during partial pressure testing:

1. A 20.1% average increase in damping between near vacuum and full atmosphere condition.
2. A 0.18% average decrease in peak modal frequency between near vacuum and full atmosphere condition.
3. Trend of increased damping with increases in strain.
4. Trend of decreased peak modal frequency with increases in strain.

The 2nd bending mode of the free-free-free-free, for the bare titanium specimen yielded the following results during partial pressure testing at very low strain levels:

1. No quantifiable trend between increases in damping with increased pressure.
2. A 0.19% average decrease in peak modal frequency between near vacuum and full atmosphere condition.

The two-stripe mode of the free-free-free-free, for the bare titanium specimen yielded the following results during partial pressure testing at very low strain levels:

1. A 85% drop in Q between near vacuum and full atmosphere condition.
2. A 0.17% average decrease in peak modal frequency between near vacuum and full atmosphere condition.

During the course of this study, various factors were discovered that could affect the system damping measurement. The following were obstacles that may be of issue in future testing using the electrodynamic shaker for determining material damping in specimens:

1. Modal interference of both the base plate and the pressure vessel and the interaction between the two.

2. The condition of the clamped support and its effect on the measured damping.
3. Possible pressure wave excitation that may lead to interactions between the strain in the specimen and a corresponding value of damping.
4. The temperature of the specimen, which in turn may affect the modulus of elasticity and hence, the modal frequency.

Recommendations

The largest difficulties encountered during this study dealt with the base plate interference in modal frequency for modes 3 and 4 in the electrodynamic shaker testing. There are a multitude of approaches that may surmount these difficulties. Two possible solutions include changing the base plate and altering the specimen size.

The most intuitive solution would be to increase the thickness of the base plate. Thus, the modal frequencies of the base plate would be higher than for the one inch base plate used for this study. Hence, the modal frequencies would be out of the frequency range of interest for modes 3 and 4 of this specimen size. The total weight of the pressure vessel system of less than 80 lbs. did not prove of too great of mass for the 18,000 lb. electrodynamic shaker. Consequently, a thicker base plate would increase the mass of the system. Yet, due to density of aluminum, continuing with the use of an aluminum base plate would most likely keep the mass of the complete system to within reason.

Another option to surmount the troubles with base plate influence would be to alter the specimen thickness. Reducing the specimen thickness to ½ of the current

specimen thickness would yield 2nd bend and two-stripe modal frequencies of less than 1000 Hz.

Finally, there were disagreements in base excitations between data sets. For example, a 5 g base excitation in one test scenario was not necessarily the same as a 5 g base excitation in another scenario. For this reason, the control accelerometer should be moved to the base of the constraint blocks. This would present more problems physically when the control accelerometer is mounted within the pressure vessel. Adjustments to accelerometer would be difficult and timely. However, the acceleration at the base of the specimen would match the acceleration entered in the controller software by the experimenter.

Finally, this investigator feels that there are great difficulties in quantifying air damping when there is significant damping caused by other sources. This is especially true with the influence of the clamped constraints. Exciting titanium specimen in a free-free-free-free condition would alleviate the specimen from this damping source. Testing at higher strain levels in the free-free-free-free condition may provide insight into the damping properties of mag spinel hard coating. Additionally, shaker testing at high strain levels (> 1,000 in/in) in partial pressures may yield greater difference between near vacuum and the full atmosphere condition.

Appendix A: Technical Drawings for Pressure Vessel

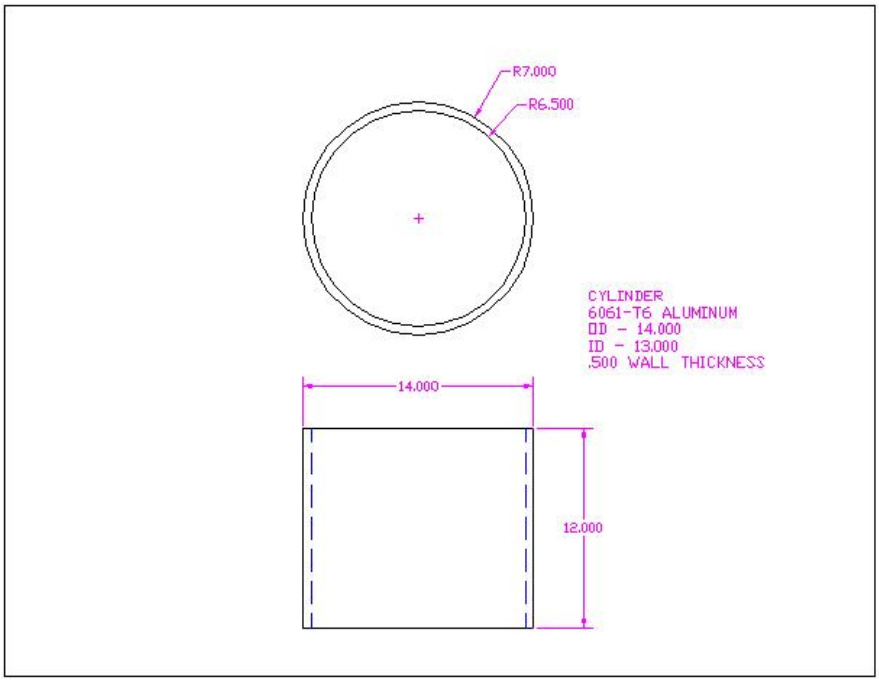

Pressure Vessel Cylinder

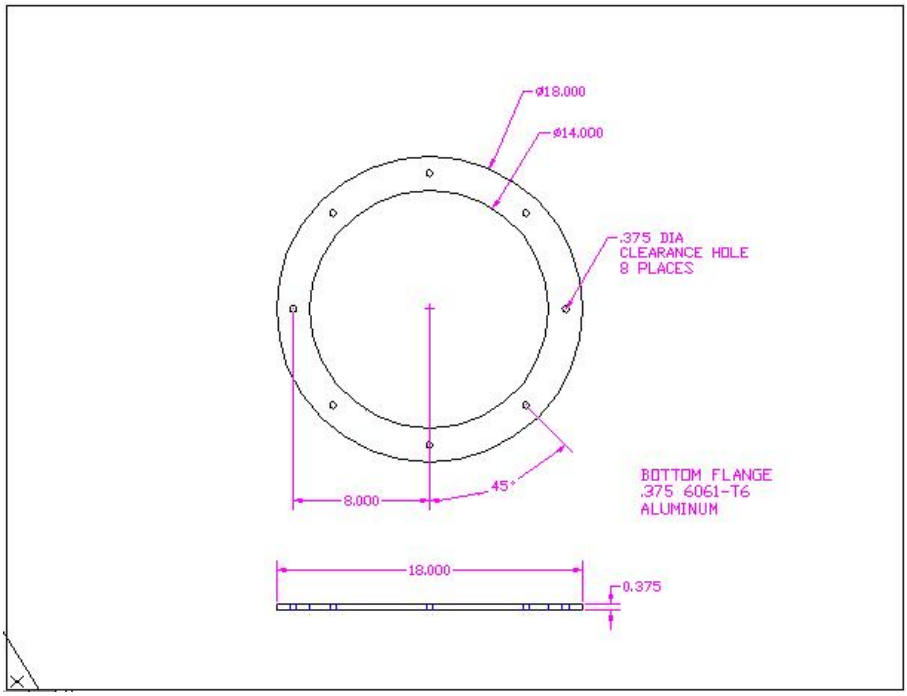

Pressure Vessel Hoop Flange

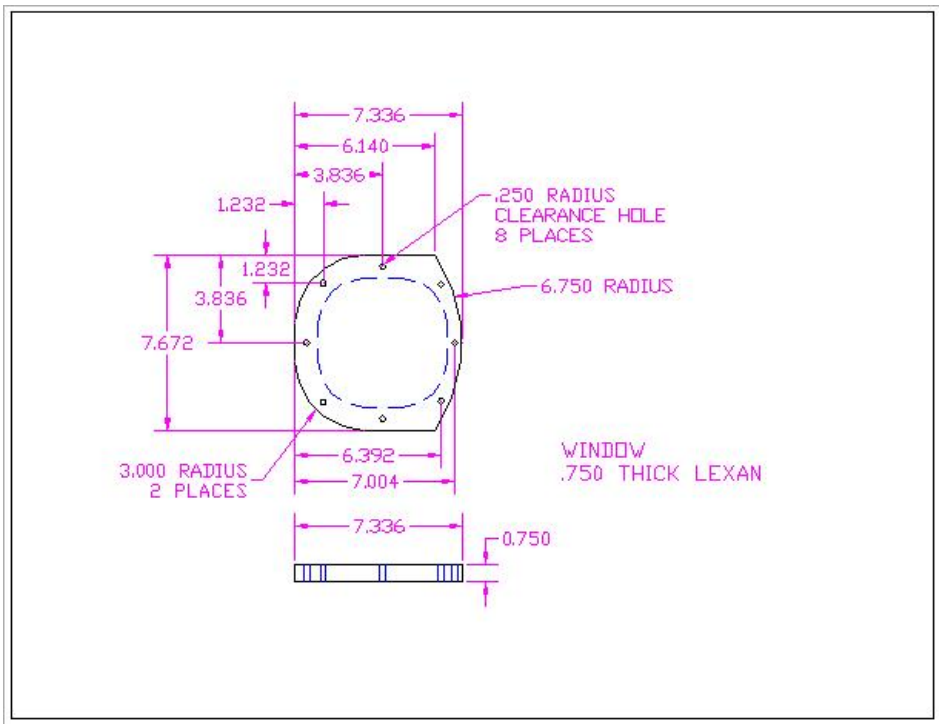

Specimen Viewing Window

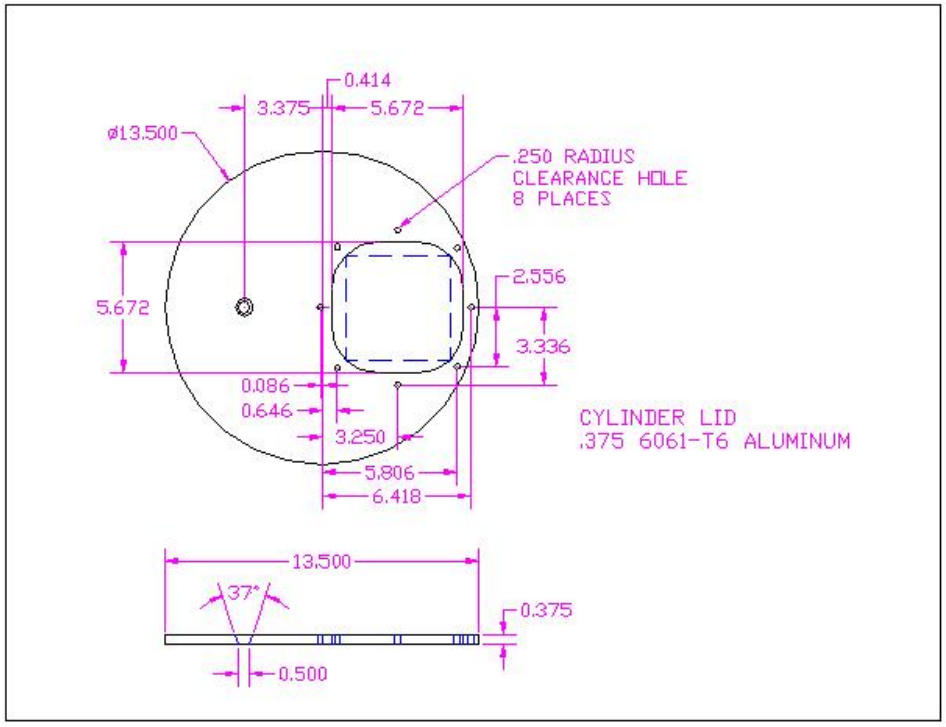

Pressure Vessel Top Lid

Appendix B: Ping Testing Results

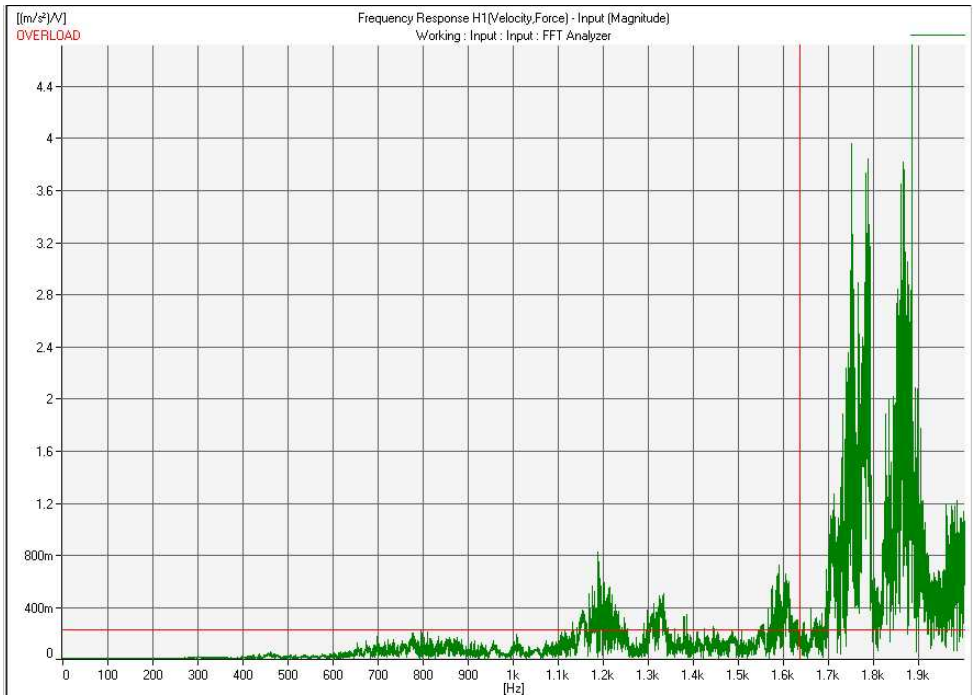

Ping Testing Results with Plate, with Pressure Vessel, and with Bungee Cords

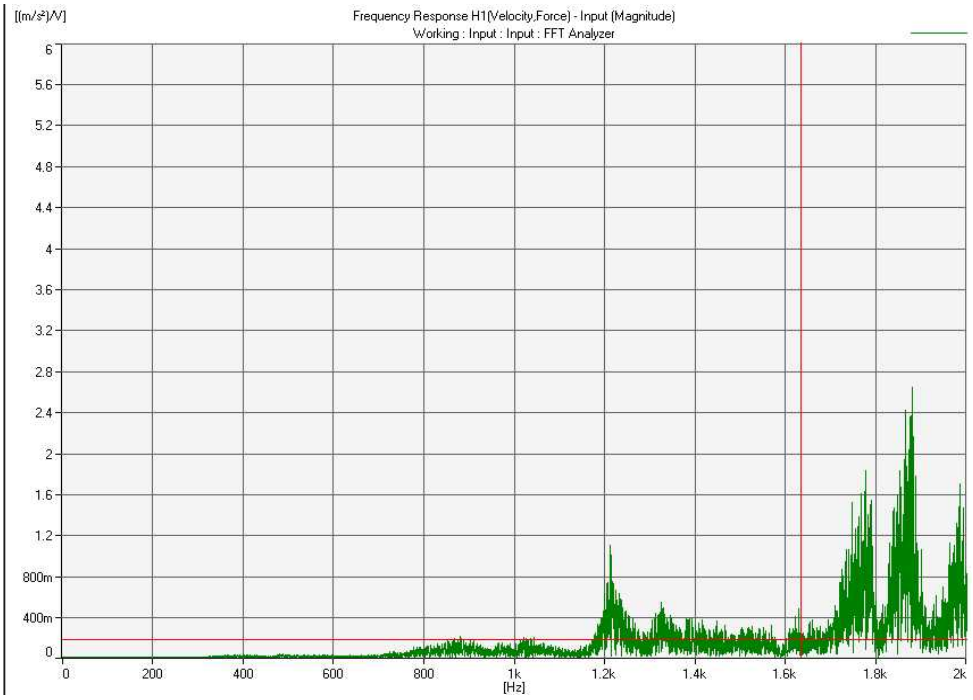

Ping Testing Results with Plate, with Pressure Vessel, and without Bungee Cords

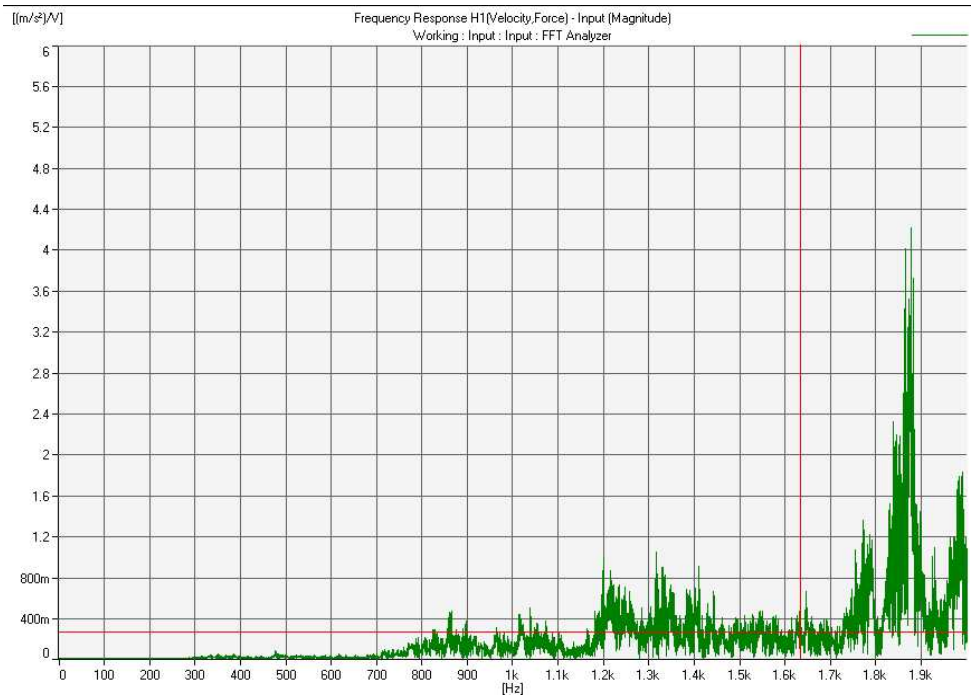

Ping Testing Results without Plate, with Pressure Vessel, and with Bungee Cords

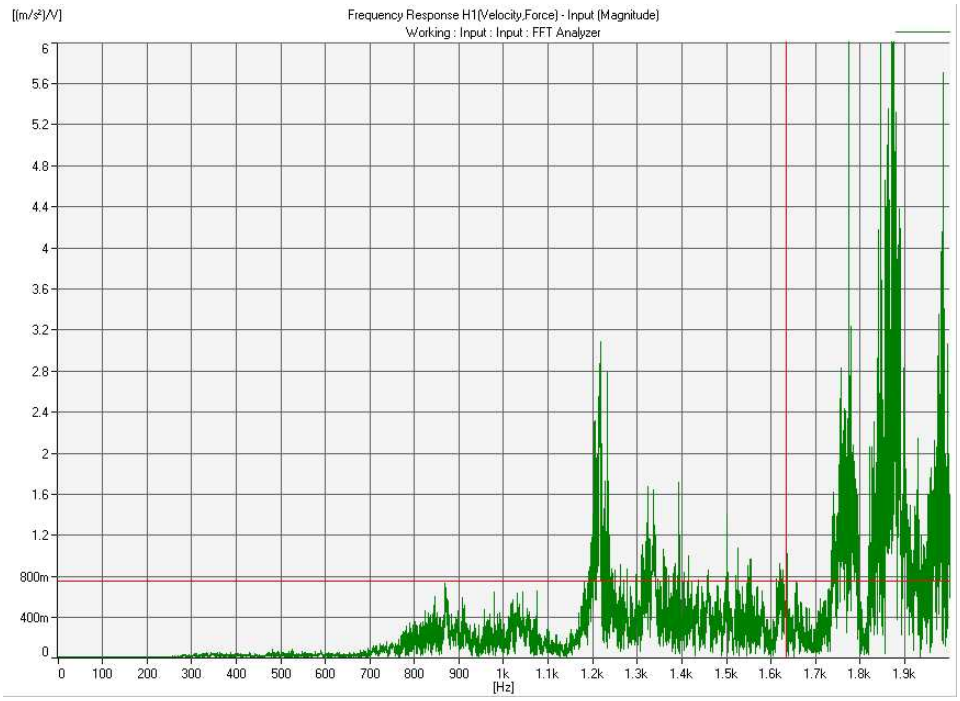

Ping Testing Results without Plate, with Pressure Vessel, and without Bungee Cords

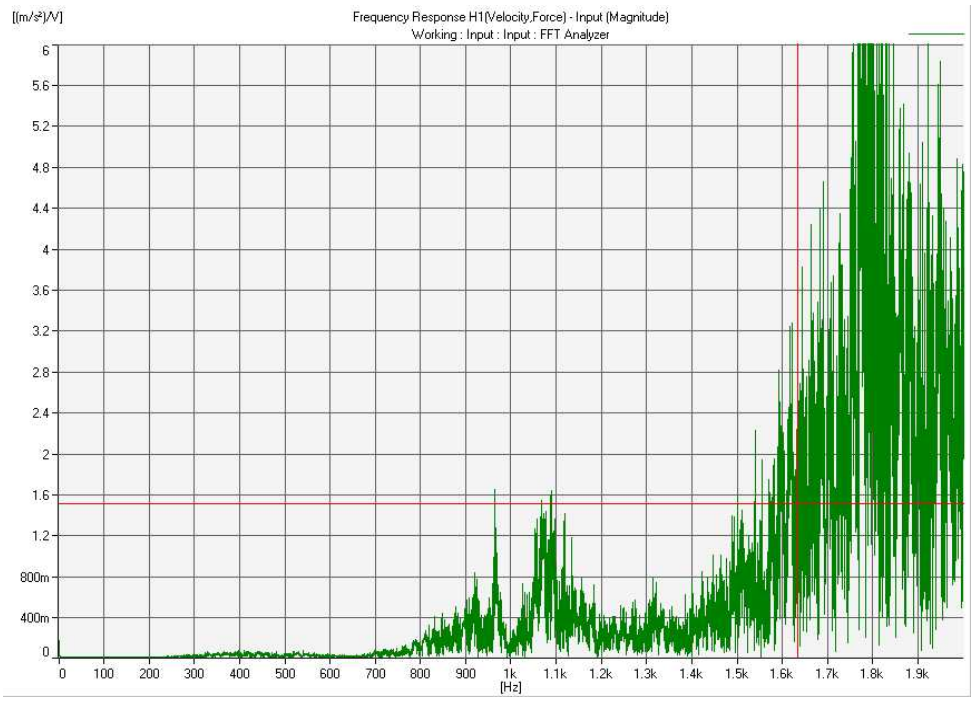

Ping Testing Results without Plate and without Pressure Vessel

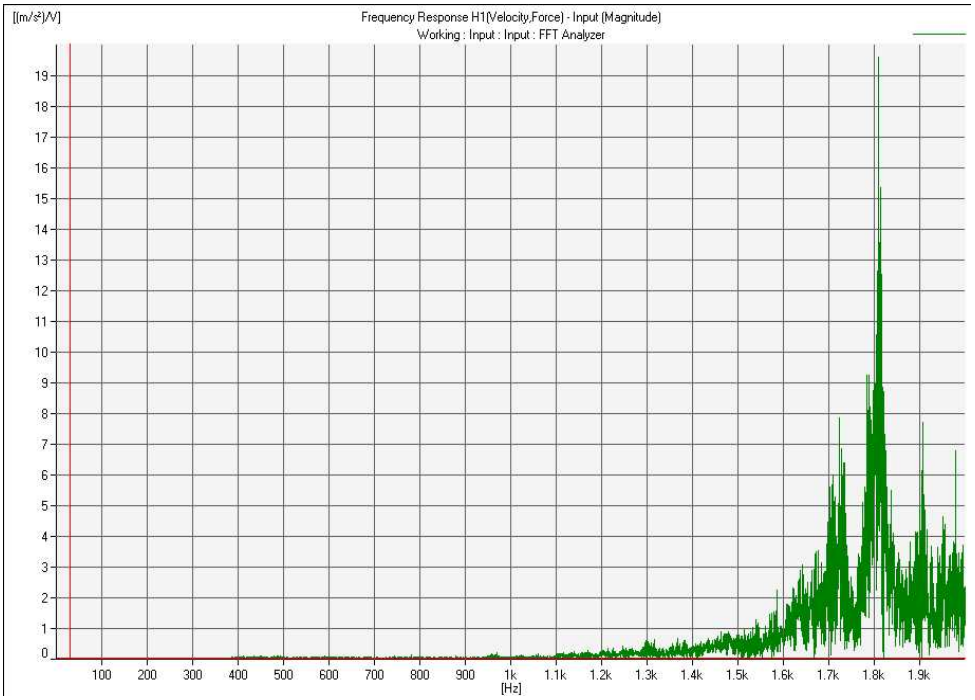

Ping Testing Results with Plate, without Pressure Vessel

Appendix C: Constraint Block Results

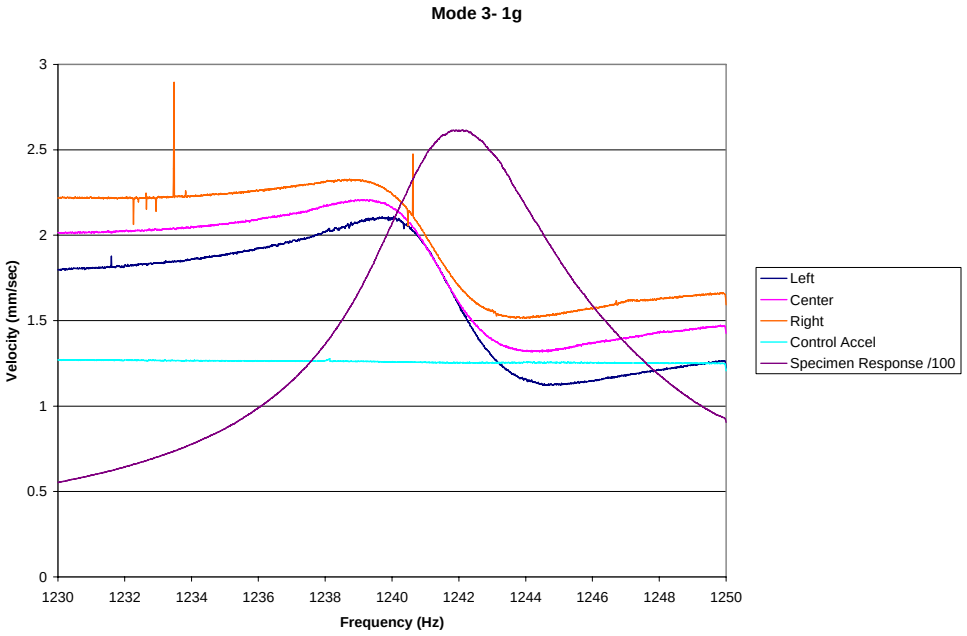

Mode 3, 1g Base Excitation

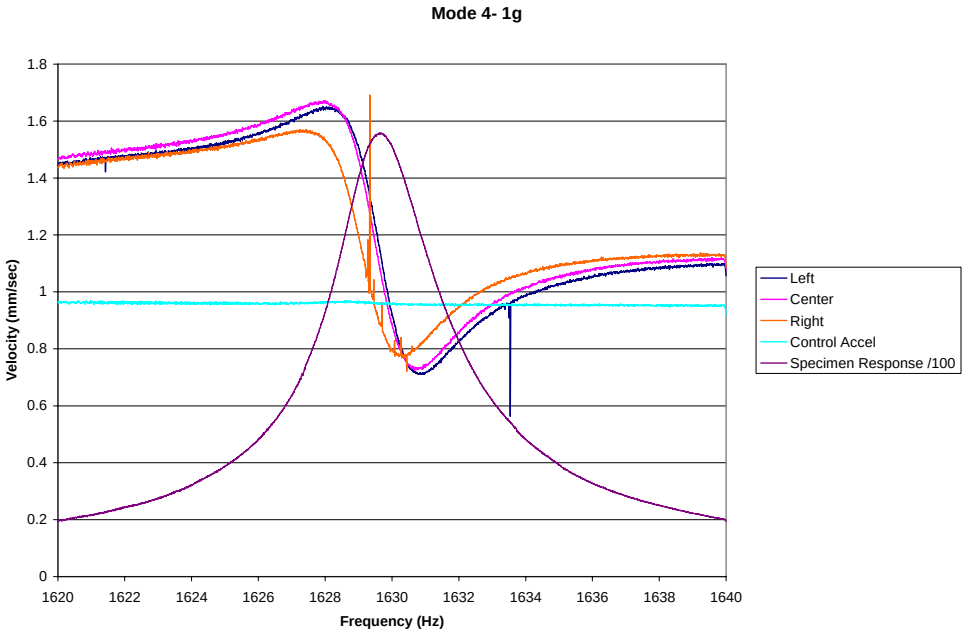

Mode 4, 1g Base Excitation

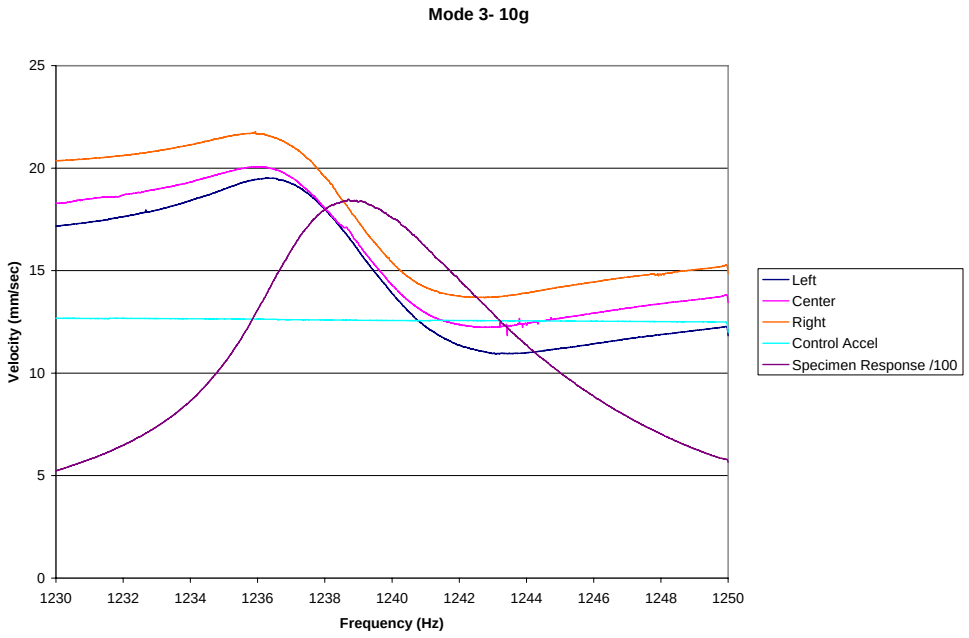

Mode 3, 10g Base Excitation

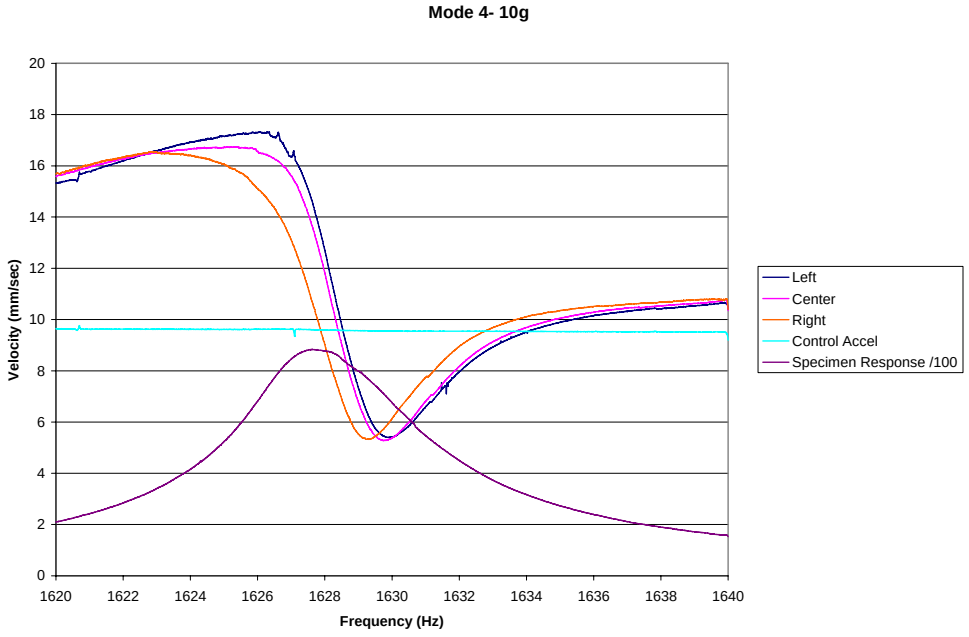

Mode 4, 10g Base Excitation

Appendix D: Frequency Response for Bare Plate, Mode 3 at Varying Pressures

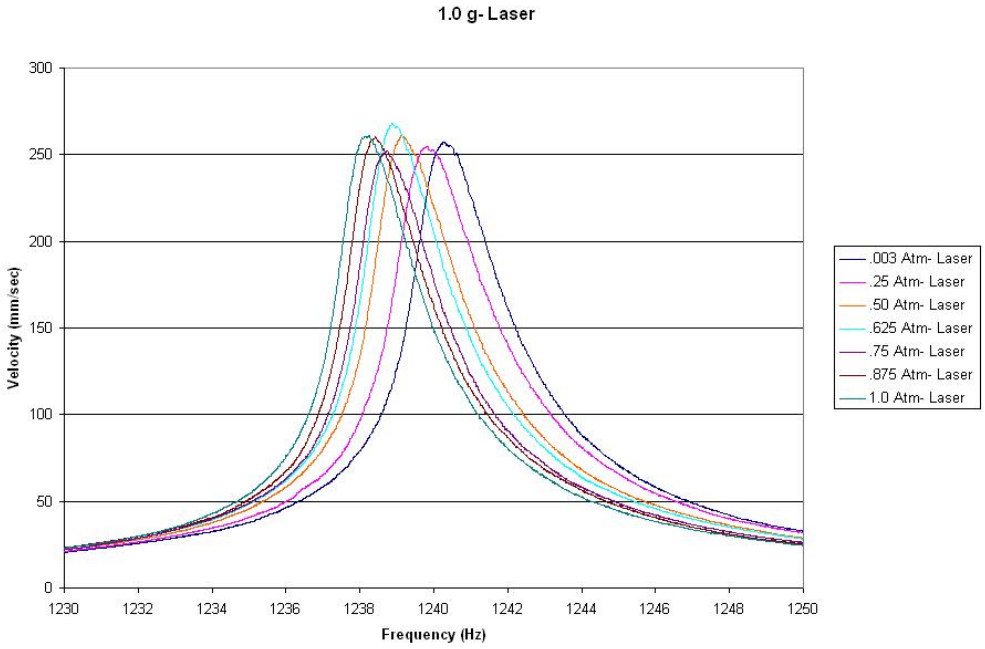

Frequency Response for Bare Plate, Mode 3, 1.0 g at Varying Pressures

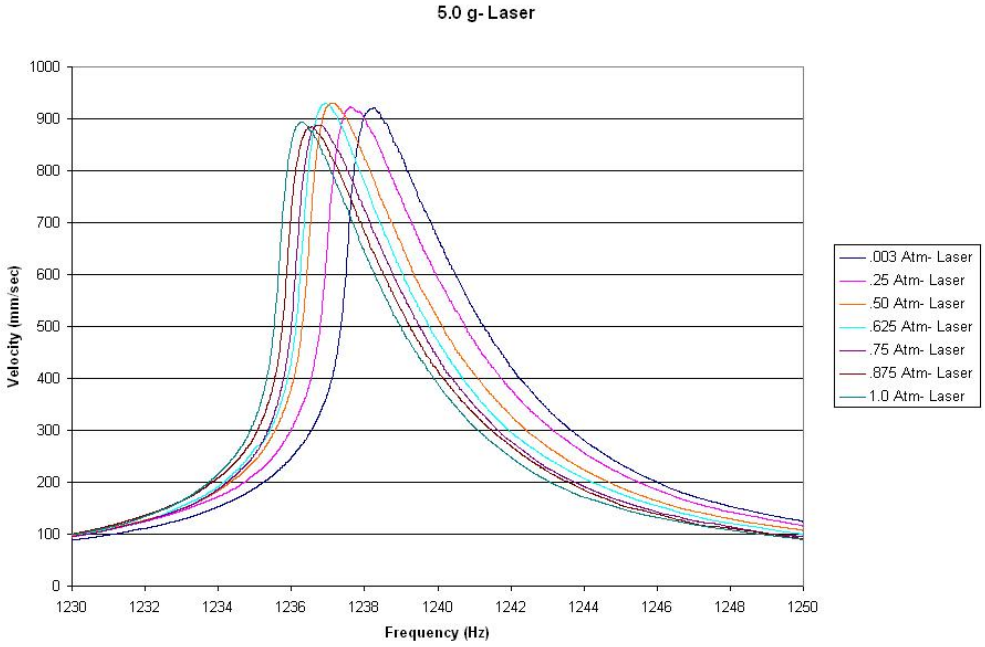

Frequency Response for Bare Plate, Mode 3, 5.0 g at Varying Pressures

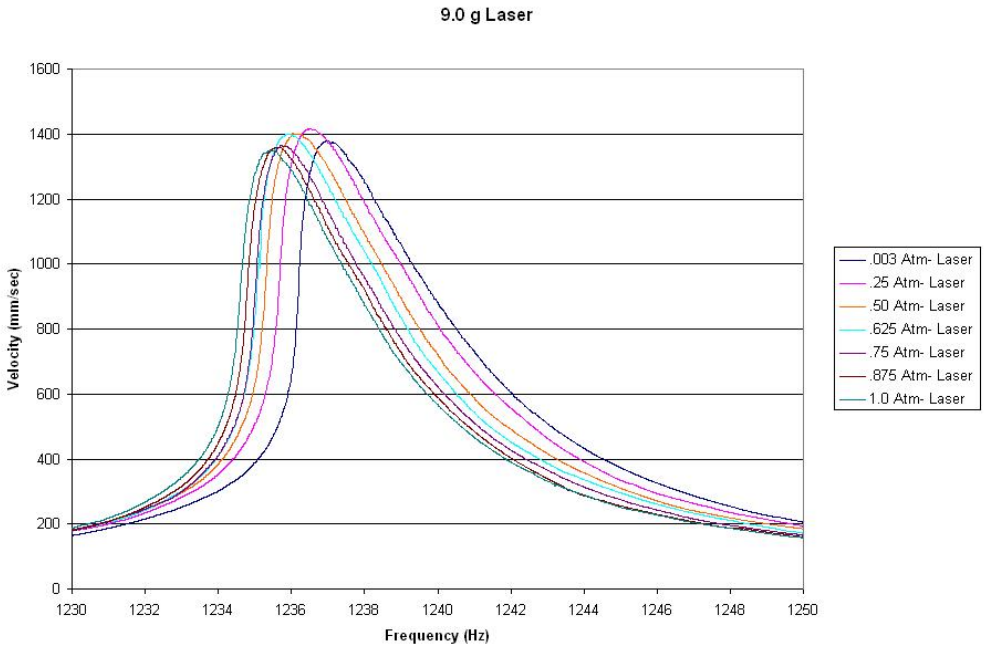

Frequency Response for Bare Plate, Mode 3, 9.0 g at Varying Pressures

Appendix E: Frequency Response for Bare Plate, Mode 4 at Varying Pressures

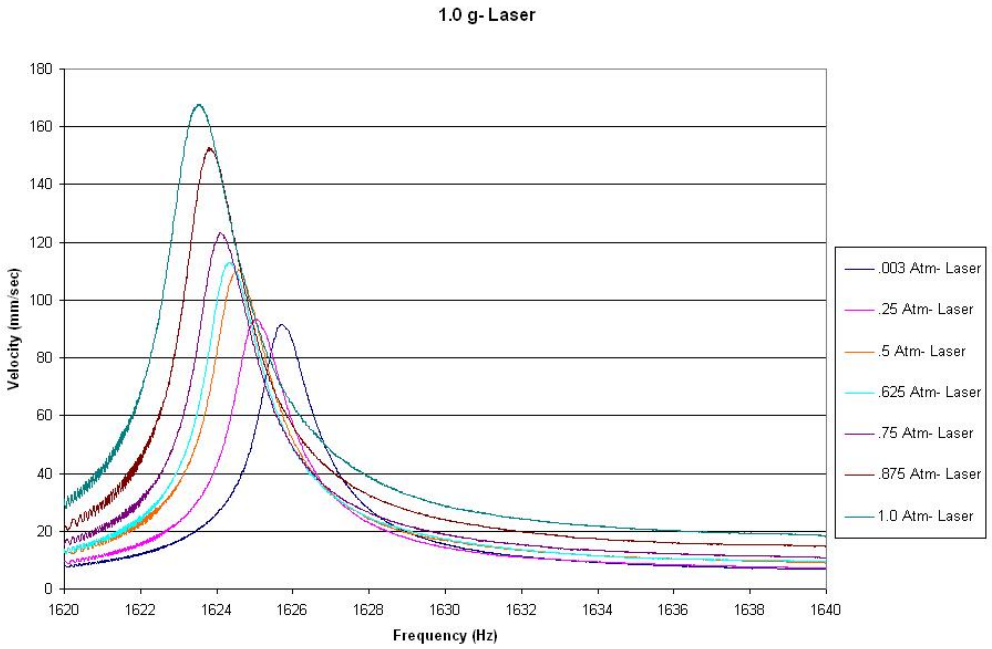

Frequency Response for Bare Plate, Mode 4, 1.0 g at Varying Pressures

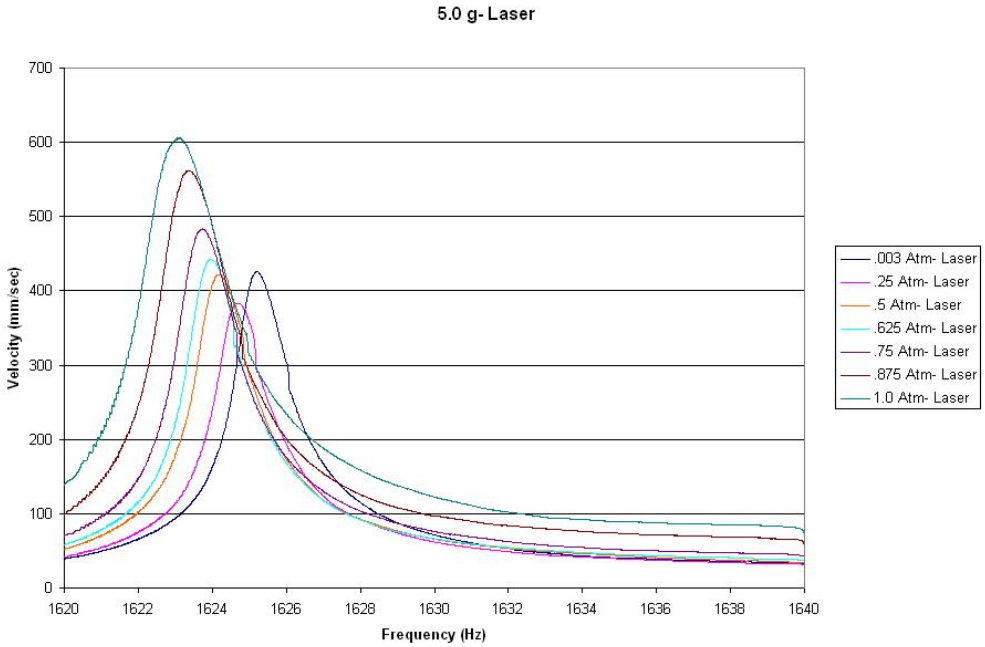

Frequency Response for Bare Plate, Mode 4, 5.0 g at Varying Pressures

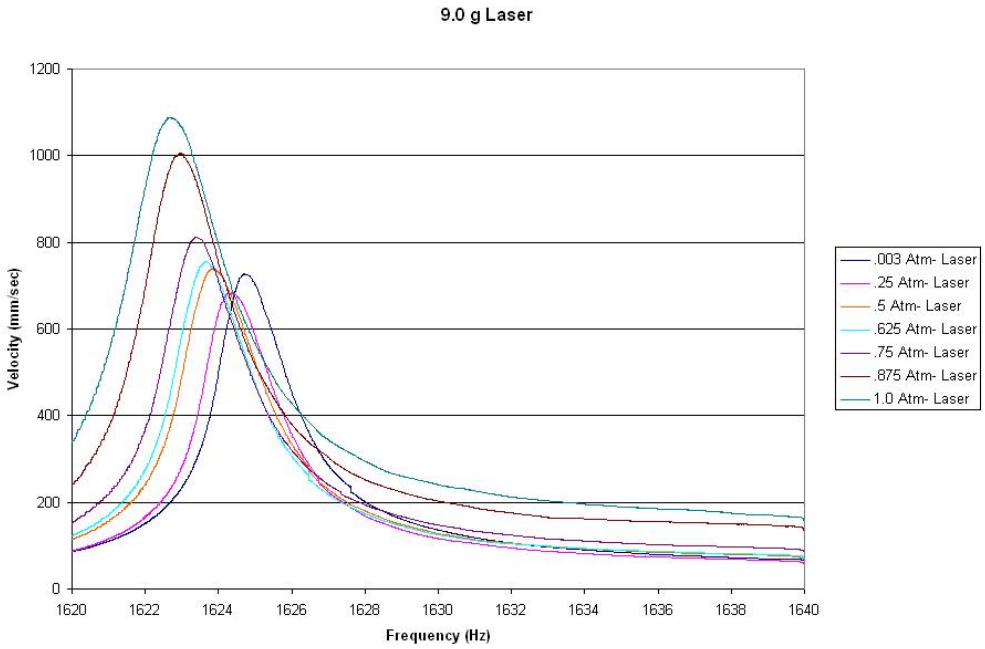

Frequency Response for Bare Plate, Mode 4, 9.0 g at Varying Pressures

Bibliography

1. Baz, A. “Active Damping”, *Encyclopedia of Vibration*, pp. 351-364. San Diego: Academic Press, 2001.

2. Baker, W.E., Woolam W.E., and Young D. “Air and Internal Damping of Thin Cantilever Beams”, *International Journal of Mechanical Sciences*, 9: 743-766 (1967).

3. Beres, W., Li, J., Patnaik, P.C. “Finite Element Based Modeling of the Low Plasticity Burnishing Process for Fatigue Property Enhancement”, 9th National Turbine Engine High Cycle Fatigue Conference, March 2004.

4. Blackwell, C. M. *The Evaluation of the Damping Characteristics of a Hard Coating on Titanium*. MS Thesis, AFIT/GAE/ENY/04-M03. Department of Aeronautics and Astronautics, Air Force Institute of Technology (AU), Wright-Patterson AFB OH, March 2004.

5. Cobb, R. G. *Structural Damage Identification From Limited Measurement Data*. PhD Dissertation, AFIT/DS/ENY/96-3. Department of Aeronautics and Astronautics, Air Force Institute of Technology (AU), Wright-Patterson AFB OH, March 1996.

6. Cowles, B.A. “High Cycle Fatigue in Aircraft Gas Turbines – an Industry Perspective”, *International Journal of Fracture*, 80: 147-163 (1996).

7. Edwins, D.J. “Damping Measurements”, Encyclopedia of Vibration, pp. 332-335. San Diego, CA: Academic Press, 2001.

8. Green, J., and Patsias S. “A Preliminary Approach for the Modeling of a Hard Damping Coating Using Friction Elements”, *Proceedings, 7th National Turbine Engine High Cycle Fatigue Conference*, West Palm Beach, FL, May 2002.

9. Ivansic, F. T. *The Effect of a Hard Coating on the Damping and Fatigue Life of Titanium*. MS Thesis, AFIT/GAE/ENY/03-12. Department of Aeronautics and Astronautics, Air Force Institute of Technology (AU), Wright-Patterson AFB OH, March 2003.

10. Leissa, A. W. *Vibration of Plates*. Washington D.C.: GPO, 1969.

11. "Material Properties", *Matweb, Material Property Data*, October, 2004, www.matweb.com.

12. Meirovitch, L. *Elements of Vibration Analysis*. Boston: McGraw-Hill, 1986.

13. *Metallic Materials and Elements for Aerospace Vehicle Structures, MIL-HDBK-5J*. Department of Defense Handbook, 31 Janurary 2003.

14. Nicholas, T. and J. R. Zuiker. "On the Use of the Goodman Diagram for High Cycle Fatigue Design", *International Journal of Fracture*, 80: 219-235 (1996).

15. Patsias, S., and W. Robin. "Hard Damping Coatings: Material Properties and F.E. Prediction Methods", *Proceedings, 8th National Turbine Engine High Cycle Fatigue Conference*, Monterey, CA, April 2003.

16. Patsias, S., Byrne, A., and Shipton, M. "Hard Damping Coatings: Optimization of Damping Effectiveness by Controlling the Deposition Parameters", *Proceedings, 9th National Turbine Engine High Cycle Fatigue Conference*, Pinehurst, NC, March 2004.

17. Ritchie, R.O., Boyce, B.L., Campbell, J.P., Roder, O., Thompson, A.W., and Mulligan, W.W. "Threshold for High Cycle Fatigue in a Turbine Engine Ti-6Al-4V Alloy", *International Journal of Fatigue*, 21: 653-662 (1999).

18. Shen, M.-H. H. "Development of a Free Layer Damper Using Hard Coatings", *Proceedings, 7th National Turbine Engine High Cycle Fatigue Conference*, West Palm Beach, FL, May 2002.

19. Shipton, M. and S. Patsias. "Hard Damping Coatings: Internal Friction as the damping mechanism", *Proceedings, 8th National Turbine Engine High Cycle Fatigue Conference*, Monterey, CA, April 2003.

20. Stephen, D.G. and Scavullo, M.A. “Investigation of Air Damping of Circular and Rectangular Plates, a Cylinder, and a Sphere”, NASA TN, D-1865, April 1965.

21. Tarnopolsky, A.Z. “Aerodynamic Damping of Randomly Excited Plates in Stationary and Moving Air”, *Journal of Sound and Vibration*, 253: 795-805 (2002).

22. Torvik, P. J., Patsias, S., and Tomlinson G.R. “Characterizing the Behavior of Hard Coatings: Comparisons from Two Methodologies”, *Proceedings, 7th National Turbine Engine High Cycle Fatigue Conference*, West Palm Beach, FL, May 2002.

23. Torvik, P. J. “Determining Material Properties of Nonlinear Damping Materials from System Response Data”, *Proceedings, 8th National Turbine Engine High Cycle Fatigue Conference*, Monterey, CA, April 2003.

24. Torvik, P. J. Air Force Institute of Technology, Personal Correspondence and Computer Files on Air Damping, February 2004.

25. Torvik, P. J. Air Force Institute of Technology, Personal Correspondence and Computer Files on a Coupled Air-Plate System, January 2005.

26. Torvik, P. J. Air Force Institute of Technology, Personal Correspondence and Computer Files on the Influence of Deflection in Shaker Mounting Systems, January 2005.

27. Torvik, P. J. “The Dynamics of the Air Film Damper”, *Proceedings, 9th National Turbine Engine High Cycle Fatigue Conference*, Monterey, CA, April 2003.

28. Ungar, E. E. “Damping Materials”, Encyclopedia of Vibration, pp. 327-331. San Diego, CA: Academic Press, 2001.

29. Ungar, E. E. “Damping of Panels Due to Ambient Air”, *American Society of Mechanical Engineers*, 38: 75-83 (1980).

Vita

Kyle S. Allen was born in Olympia WA. He graduated from Olympia High School in 1997 and progressed to the United States Air Force Academy for his undergraduate degree.

While at the Academy he played defensive tackle for the Fighting Falcons, starting his final two years. He graduated in 2001 with a Bachelors of Science in Engineering Sciences and a commission as a Second Lieutenant in the United States Air Force.

Lt. Allen's first assignment was the 46th Test Squadron at Eglin Air Force Base, Florida. While there, he served as a data-link test engineering. In the fall of 2003, Lt. Allen began his studies at the Air Force Institute of Technology. After graduating in March, 2005, Lt. Allen will move again to Air Force Operational Test and Evaluation Center at Kirtland Air Force Base, New Mexico.

He continues to be active both in community service organizations and various athletic activities. He is continually grateful for the gifts of friends and family that bless him every day.

REPORT DOCUMENTATION PAGE

Form Approved
OMB No. 074-0188

The public reporting burden for this collection of information is estimated to average 1 hour per response, including the time for reviewing instructions, searching existing data sources, gathering and maintaining the data needed, and completing and reviewing the collection of information. Send comments regarding this burden estimate or any other aspect of the collection of information, including suggestions for reducing this burden to Department of Defense, Washington Headquarters Services, Directorate for Information Operations and Reports (0704-0188), 1215 Jefferson Davis Highway, Suite 1204, Arlington, VA 22202-4302. Respondents should be aware that notwithstanding any other provision of law, no person shall be subject to an penalty for failing to comply with a collection of information if it does not display a currently valid OMB control number.
PLEASE DO NOT RETURN YOUR FORM TO THE ABOVE ADDRESS.

1. REPORT DATE *(DD-MM-YYYY)*	2. REPORT TYPE	3. DATES COVERED *(From – To)*
21-03-2005	**Master's Thesis**	Aug 2003 – Mar 2005

4. TITLE AND SUBTITLE

Evaluation Techniques for Determining Damping Mechanisms on Titanium Plates

5a. CONTRACT NUMBER

5b. GRANT NUMBER

5c. PROGRAM ELEMENT NUMBER

6. AUTHOR(S)

Allen, Kyle S., 1st Lieutenant, USAF

5d. PROJECT NUMBER

5e. TASK NUMBER

5f. WORK UNIT NUMBER

7. PERFORMING ORGANIZATION NAMES(S) AND ADDRESS(S)

Air Force Institute of Technology
Graduate School of Engineering and Management (AFIT/EN)
2950 Hobson Way, Building 641
WPAFB OH 45433-7765

8. PERFORMING ORGANIZATION REPORT NUMBER

AFIT/GAE/ENY/05-M01

9. SPONSORING/MONITORING AGENCY NAME(S) AND ADDRESS(ES)

Dr. Charles Cross
AFRL/PRTS
1950 5th Street Bldg. 252 DSN: 656-5530
WPAFB OH 45433-7251

10. SPONSOR/MONITOR'S ACRONYM(S)

11. SPONSOR/MONITOR'S REPORT NUMBER(S)

12. DISTRIBUTION/AVAILABILITY STATEMENT

APPROVED FOR PUBLIC RELEASE; DISTRIBUTION UNLIMITED.

13. SUPPLEMENTARY NOTES

14. ABSTRACT

High cycle fatigue (HCF) is the single largest cause of component failure for all modern military gas turbine engines. Hard coatings, such as magnesium aluminate spinel, have been found to provide significant damping properties. Past studies have had difficulties isolating the contributions of these hard coating damping layers from other damping mechanisms.

This study explored techniques for assessing the contribution of different damping mechanisms on titanium plates during vibration testing. The study investigated 2nd bend and 2-stripe modes. Two different specimen sizes were tested in both a clamped-free-free-free and free-free-free-free condition. Specimens were tested at varying pressures. Increases in pressure caused linear peak modal frequency downshifts for both modes of interest for both specimen sizes, and for both boundary conditions. Increases in damping were also seen with increases in pressure for bare plates for the two-stripe mode for both boundary conditions.

The clamped boundary condition contributions on the system damping were also investigated. Increases in the stiffness of the cantilevered clamp in the clamped-free-free-free condition were shown to have limited affect on plate damping.

15. SUBJECT TERMS

Vibration, High Cycle Fatigue, Damping, Fatigue, Titanium, Magnesium Aluminate Spinel, Resonance, Resonance Frequency, Resonance Mode, Finite Element Analysis, Air Damping

16. SECURITY CLASSIFICATION OF:			17. LIMITATION OF ABSTRACT	18. NUMBER OF PAGES	19a. NAME OF RESPONSIBLE PERSON
a. REPORT	b. ABSTRACT	c. THIS PAGE			Dr. A. N. Palazotto (ENY)
U	U	U	UU	145	19b. TELEPHONE NUMBER *(Include area code)* (937) 255-3636, e-mail: Anthony.Palazotto@afit.edu

Standard Form 298 (Rev. 8-98)
Prescribed by ANSI Std. Z39-18